MICROBIAL ECOLOGY OF A MANMADE OIL SPILL IN THE GULF OF MEXICO AND A NATURAL, HYDROTHERMAL OIL SEEP IN THE GULF OF CALIFORNIA

Luke Justin McKay

A dissertation submitted to the faculty of the University of North Carolina at Chapel Hill in partial fulfillment of the requirements for the degree of Doctor of Philosophy in the Department of Marine Sciences.

Chapel Hill
2014

Approved by:

Andreas Teske

Barbara MacGregor

Carol Arnosti

Marc Alperin

Alexander Loy

ABSTRACT

Luke Justin McKay: Microbial Ecology of a Manmade Oil Spill in the Gulf of Mexico and a Natural, Hydrothermal Oil Seep in the Gulf of California
(Under the direction of Andreas P. Teske)

Members of the *Marinobacter* genus play an important role in hydrocarbon degradation in the ocean – a topic of special significance in light of the recent *Deepwater Horizon* oil spill of 2010. The *Marinobacter* group has thus far lacked a genus level phylogenetic probe that would allow in situ identification of representative members. Here, two new 16S rRNA-targeted oligonucleotide probes (Mrb-0625-a and Mrb-0625-b) were developed to enumerate *Marinobacter* species by fluorescence in situ hybridization (FISH). In silico analysis of this probe set demonstrated 80% coverage of the *Marinobacter* genus. A competitor probe was developed to block hybridization by Mrb-0625-a to six *Halomonas* species with which it shared a one base pair mismatch. The probe set was optimized using pure cultures, and then used in an enrichment experiment with a deep sea oil plume water sample collected from the *Deepwater Horizon* oil spill. *Marinobacter* cells rapidly increased as a significant fraction of total microbial abundance in all incubations of original contaminated seawater as well as those amended with *n*-hexadecane, suggesting this group may be among the first microbial responders to oil pollution in the marine environment. The new probe set will provide a reliable tool for quantifying *Marinobacter* in the marine environment, particularly at contaminated sites where these organisms can play an important role in the biodegradation of oil pollutants.

The next sections of this dissertation focus on the hydrothermally active sediments at Guaymas Basin, which show a wide range of shallow subsurface temperatures: from 3°C to 200°C in the first 45 cm depth. A combination of extreme thermal gradients and compressed geochemical and metabolic zones limits the depth range of microbial colonization in Guaymas sediments. Using stable carbon isotopic values for methane and dissolved inorganic carbon compared to associated temperatures the upper thermal limits for the anaerobic oxidation of methane and organic carbon remineralization in Guaymas sediments are suggested to be 80^{o}C and 100^{o}C, respectively. At higher temperatures the isotopic imprints of these microbially mediated processes cannot be detected. Additionally, 16S rRNA gene clone libraries demonstrate differential biogeographical zonation patterns for archaea versus bacteria, with archaeal community structure being more heavily influenced by hydrothermal regimes. *Chloroflexi* and Deltaproteobacteria dominated the bacterial clone libraries, and anaerobic methane-oxidizing (ANME) archaea represented nearly half of the total archaeal clone library. Thermal zonation of ANME archaeal subgroups is strong: ANME-2c is restricted to low temperature sediments (<25^{o}C), ANME-1 is dominant at warmer temperatures, and the ANME-1 Guaymas archaea appear to have access to the deepest and hottest sediment horizons up to approximately 80^{o}C.

In the last chapter of this dissertation, microbial life at extreme temperatures was investigated further by RNA-based methodologies. Using push core samples collected by the Alvin submarine at four high temperature sites with 40-cmsbf thermal maxima ranging from 100°C to 185°C, the composition of the active microbial community and its possible influence on carbon and sulfur cycling was investigated. Here, evidence is presented indicating that hydrothermal fluctuations are frequent enough to restrict hyperthermophilic life to sediments

with average in situ temperatures between 70°C and 95°C, where temperatures may vary by 25°C in as little as a day. Strong microbially mediated sulfate reduction is implicated by sharp decreases in porewater sulfate within the upper 15 cm of all four high temperature cores, while stable isotopic evidence of methane oxidation is only expressed in a single core. Archaeal sequence recovery was greater than bacterial sequence recovery in six out of eight samples from the four cores, but bacterial sequence recovery was particularly strong for a single core, yielding 35% of the total archaeal and bacterial recovery from all samples. Although putative anaerobic methane oxidizing (ANME) archaea were very common, distinct cores hosted diverse and distinct sequence assemblages, including ANME-1 Guaymas, ANME-2c, and ANME-2d/GoM Arc-1/*Methanoperedenaceae*. Dominant bacterial groups fell within the *Thermodesulfobacteriaceae* family in the *Thermodesulfobacteria* phylum, the *Helicobacteriaceae* family in the subphylum *Epsilonproteobacteria*, or were close relatives of *Desulfocapsa exigens* in the subphylum *Deltaproteobacteria*. The most probable thermo- or hyperthermophilic groups were investigated by co-occurrence of OTUs across the four hottest samples within the sediment cores and appear to be ANME-1 Guaymas and an uncultured representative of the Miscellaneous Crenarchaeotal Group (MCG)-15 for archaea, and members of the *Thermodesulfobacteriaceae* family for bacteria.

This dissertation is dedicated to my three older brothers, Josh, Howard, and Adam.

ACKNOWLEDGEMENTS

I would like to express the utmost gratitude for guidance and support provided by my advisor, Andreas Teske. This work would not have been possible without technical contributions by Vincent Klokman, Tony Gutierrez, Howard Mendlovitz, Barbara MacGregor, Daniel Albert, Daniel Hoer, Andrea Hale, Douglas LaRowe, and Dirk de Beer. Howard Mendlovitz conceptualized and constructed the temperature logging probes, which added a major discussion point to chapter 3. I would also like to thank my advisory committee, Carol Arnosti, Alex Loy, Marc Alperin, and Barbara MacGregor, for advice in the development of experiments and subsequent analyses, and I thank Tingting Yang, Kai Ziervogel, and Samantha Joye for sampling assistance. Funding support for this work comes in part from a graduate fellowship from the Center for Dark Energy Biosphere Investigations, the North Carolina Space Grant, the Gulf of Mexico Research Initiative consortium research support entitled "Ecosystem Impacts of Oil and Gas Inputs to the Gulf (ECOGIG)" administered by the University of Mississippi, an NSF RAPID Response grant (NSF-OCE 1045115) (for chapter 1), and by NSF-OCE 0647633 (for chapters 2 and 3). Lastly, I thank the members and former members of the Teske Lab, Tingting Yang, Zena Cardman, Lisa Nigro, JP Balmonte, Lindsay D'Ambrosio, Frederick Dowell, Sarah Underwood, Vincent Klokman, Charlie Martin, Andrew Hyde, Kelly Speare, Srishti Dasarathy, Karen Lloyd, Mark Lever, Alan Durbin, Jen Biddle, Cassandre Lazar, and Verena Salman for providing an atmosphere of general awesomeness in which to work.

TABLE OF CONTENTS

LIST OF TABLES

Table

LIST OF FIGURES

LIST OF ABBREVIATIONS

FISH – fluorescence in situ hybridization

sp. – species (singular)

spp. – species (plural)

PBS – phosphate buffered saline

PFA – paraformaldehyde

FITC – fluorescein isothiocyanate

TRITC – rhodamine isothiocyanate

CY3 – cyanine 3 dye

6FAM – 6-Carboxyfluorescein

DAPI – 4',6-diamidino-2-phenylindole

cmbsf – centimeters below seafloor

PCR – polymerase chain reaction

RT – reverse transcription

ANME – anaerobic methanotroph

AOM – anaerobic oxidation of methane

OMR – organic matter remineralization

DIC – dissolved inorganic carbon

MCG – miscellaneous Crenarchaeotal group

MBGB – Marine Benthic Group B

MBGD – Marine Benthic Group D

MBGE – Marine Benthic Group E

MG-1 – Marine Group 1

DHVE-6 – Deep Hydrothermal Vent Euryarchaeota Group 6

DSEG – Deep Sea Euryarchaeotal Group

SAGMEG – South African Gold Mine Euryarchaeotal Group

JS1 – Japan Seep 1

WS3 – Wurtsmith Group 3

OP1 – Obsidian Pool Group 1

OTU – operational taxonomic unit

PCA – principle components analysis

CHAPTER 1: DEVELOPMENT OF A GROUP-SPECIFIC 16S rRNA-TARGETED PROBE SET FOR THE IDENTIFICATION OF *MARINOBACTER* BY FLUORESCENCE IN SITU HYBRIDIZATION[1]

Introduction

The ability of marine ecosystems to recuperate from oil pollution is largely dependent on the activities of indigenous communities of hydrocarbon-degrading bacteria, which often varies depending on the ecosystem in question. For example, contaminants from the *Deepwater Horizon* oil spill have affected several marine ecosystems, including the deep water column (Diercks et al., 2010), coastal waters and beaches (Graham et al., 2010; Hayworth et al., 2011), salt marshes (Silliman et al., 2012), and deep sea sediments (Liu et al., 2012). Initial microbial analyses following the Macondo wellhead blowout have shown diverse microbial phylotypes associated with distinct sites of oil contamination. Members of the *Oceanospirillales* and the genus *Halomonas* were dominant in the deep sea hydrocarbon plume (Hazen et al., 2011), Firmicutes and *Alphaproteobacteria* in open ocean surface slicks (Redmond et al., 2011), and *Alcanivorax*, *Marinobacter*, and *Rhodobacteracaeae* spp. were dominant in coastal beaches (Kostka et al., 2011). Detecting and identifying microbial communities across different habitats is integral to the assessment of the microbial degradation of oil contaminants in the marine environment.

[1] This chapter was previously published as an article in *Deep Sea Research Part II: Topical Studies in Oceanography*. The original citation is as follows: McKay L, Gutierrez T, Teske A. "Development of a Group-Specific 16S rRNA-Targeted Probe Set for the Identification of *Marinobacter* by Fluorescence In Situ Hybridization," *Deep Sea Research Part II: Topical Studies in Oceanography* (available online November 2013) DOI: 10.1016/j.dsr2.2013.10.009

Methods to identify and monitor the abundance of hydrocarbon-degrading microorganisms in environmental samples enhance understanding of their natural ecology, their response to oil spills, and their role in degrading the oil (Head et al. 2006). Fluorescence in situ hybridization (FISH) is an effective technique allowing phylogenetic identification, enumeration, and direct spatial visualization of microorganisms in their natural environment. It utilizes 16S rRNA-targeted oligonucleotide probes labeled with, for example, a fluorophore, that bind to the complementary site on the 16S rRNA gene of a target microorganism(s) (Amann et al., 1995). Genus-level oligonucleotide probes were previously developed for *Alcanivorax* (Syutsubo et al., 2001) and *Cycloclasticus* (Maruyama et al., 2003) – organisms which, respectively, have been shown to play an important role in the degradation of aliphatic and aromatic hydrocarbons in oil-polluted seawater (Head et al., 2006). Another important group of oil-degrading bacteria in the ocean is *Marinobacter*, members of which have also been shown to become heavily enriched during oil spills (summarized by Duran, 2010). In addition to hydrocarbon association, several clades of this genus were ubiquitously found in mutual association with dinoflagellates and coccolithophores originating from seas and oceans all over the world (Amin et al. 2009). Despite their ubiquity in marine environments and the important role that these organisms contribute to the degradation of hydrocarbons and other processes, molecular tools to quantify them have had limited coverage. Previously, FISH probes or primer sets were developed targeting 29% (Xiao et al., 2010), 4.2% (Brinkmeyer et al., 2003), and 9.2% (Gray et al., 2011) of the *Marinobacter* genus for specific applications. So far, however, no FISH probe set exists that provides a high level of coverage for this monophyletic group. Here, two probes for FISH were developed and optimized that together could be used to detect up to 80% of the currently established genus, or used in concert with previously published probes to examine environmental compositions and

influences of distinct *Marinobacter* subgroups. These probes were then used to assess the abundance of *Marinobacter* within the overall microbial community over time following an input of hydrocarbon similar to contamination that occurred during the *Deepwater Horizon* oil spill.

Sampling Procedures and Methodology

Oligonucleotide probe design

Group-specific oligonucleotide probes for *Marinobacter* were designed against current 16S rRNA gene sequence databases. Using the Probe Design tool of Arb v104 (Pruesse et al., 2007), probe candidates were selected in August 2011 based on their provision of the greatest possible coverage of 659 sequences representing the genus *Marinobacter*. Probe candidates were analyzed using the probeCheck server (Loy et al., 2008) and the Ribosomal Database Project's Probe Match tool (Cole et al., 2008) to evaluate their in silico specificity and coverage. From this, two probe sequences, Mrb-0625-a (5'-CAG TTC GAA ATG CCG TTC CCA-3'; 21-mer) and Mrb-0625-b (5'-CAG TTC GGA ATG CCG TTC CCA-3'; 21-mer), were selected. Both probes converged over the same position (0625 – 0645) based on the 16S rRNA E. coli gene (Lane, 1991) with one base pair mismatch between them. Probe coverage for Mrb-0625-a was 75% of all sequences comprising the Marinobacter genus, whereas that for Mrb-0625-b was 5% of the remaining 25% of sequences not covered by Mrb-0625-a. Together, both probes covered 80% of the Marinobacter group. Six Halomonas clone sequences sharing one basepair mismatch to probe Mrb-0625-a were also identified. A competitor probe, Hal-0625-a (5'-CAG TTC CAA ATG CCG TTC CCA-3'; 21-mer), was designed to reduce hybridization of Mrb-0625-a to these non-target halomonads. Table 1 summarizes the probes that were developed in this study.

Oligonucleotide probe optimization

Pure cultures of *Marinobacter algicola* (DSM 16394), *Marinobacter flavimarus* (DSM 16070) and *Marinobacter zhanjiangensis* (KCTC 22280) were used in a preliminary test of the FISH probes at 0% and 10% formamide concentrations, and then *M. algicola* and *M. zhanjiangensis* were used in the optimization of formamide stringency. The strains were grown without hydrocarbons on a marine broth (ZM/10) composed of ¾-strength naturally aged seawater, peptone (0.05%), yeast extract (0.01%), and supplemented after steam-sterilization with filter-sterile (0.2 µm) trace elements and vitamins to final concentrations as previously described (Blackburn *et al.*, 1989). For fixation three volumes of 4% (v/v) paraformaldehyde solution in 1x phosphate buffer saline (PBS; 130 mM NaCl, 2 mM NaH_2PO_4, 8 mM Na_2HPO_4, pH 7.4) were mixed with one volume of exponentially-grown cells and incubated for 3 h at 4°C. After three washings with 1x PBS, the samples were stored in a 1:1 (v/v) solution of 1x PBS and ethanol at -20°C.

Initial hybridizations with pure bacterial cultures and the newly-designed probes were performed using formamide (FA) concentrations of 0% and 10% in order to confirm permeability of the cells to the probes and adequate signal intensity. Optimal conditions for hybridization with these probes were determined by multiple hybridizations using increasing FA concentrations from 0% to 70%. Because the two probe sequences differ by only one nucleotide and target the same binding site, they were used simultaneously in competitive hybridization experiments. *M. algicola* was used as the reference strain for Mrb-0625-a and as the single mismatch non-target strain for Mrb-0625-b, whereas *M. zhanjiangensis* was used as the reference strain for Mrb-0625-b and as the single mismatch non-target strain for Mrb-0625-a. Hybridization assays were performed using standard methods (Daims et al., 2005). Samples hybridized with fluorescently-labeled probes were visualized using an Olympus BX51

epifluorescence microscope (Tokyo, Japan) equipped with a Hamamatsu C8484 digital camera (Hamamatsu City, Japan). Probe-conferred signal intensities were quantified with MetaMorph image analysis software version 7.6.0.0 (Sunnyvale, CA, USA).

Sample collection

During a research cruise on the R/V Walton Smith (May 26 to June 8, 2010), seawater samples from 1000-1250 m depth were collected by CTD rosette sampler within 1-7 miles from the Macondo wellhead in the Gulf of Mexico. Some of these CTD deployments recovered samples from a deepwater hydrocarbon plume that had formed early during the spill and was marked by localized oxygen depletion and an increase in colored dissolved organic matter which was indicative of the presence of petrochemical hydrocarbons and elevated microbial activities from hydrocarbon oxidation (Diercks et al., 2010; Joye et al., 2011; Yang et al., 2012—ASLO talk). Upon collection, live plume samples were stored at 4°C for 15 months until they were used as the inoculum for enrichment experiments with and without *n*-hexadecane to evaluate the FISH protocol described below.

Marinobacter enrichment setup

Enrichment cultures were prepared using steam-sterilized screw-capped 100 ml glass vials. Two vials were prepared containing 6 ml of filter-sterilized (0.2 µm) ONR7a marine medium (Dyksterhouse et al., 1995) supplemented with *n*-hexadecane (4% v/v). Two additional vials were prepared in the same way but without *n*-hexadecane. The initial concentration of hydrocarbons in the inoculum prior to addition of *n*-hexadecane was unknown. All four vials were inoculated with 1.2 ml of the plume water sample. An additional vial containing 6 ml of sterile ONR7a and *n*-hexadecane was inoculated with pre-filtered (0.2 µm) and autoclaved plume water to act as the killed control. All vials were incubated in the dark with gentle shaking (60

rpm) at 27°C, which falls within the optimum growth temperature range (25 – 30°C) for most *Marinobacter* (Duran, 2010). Fixation of subsamples (100 µl) was performed by mixing with 300 µl of 4% (v/v) paraformaldehyde and incubating at 4°C for 3 hrs. Cells were collected by centrifugation (15,000 x g; 5 min), mixed with ice-cold 1X PBS and ethanol (1:1), and then stored at -20°C.

FISH analysis of Marinobacter enrichment

Subsamples from the time-series incubation were diluted (500- to 1000-fold) in 1X PBS and then filtered onto 0.22 µm polycarbonate filters (25 mm, Millipore GTTP). FISH was performed directly on filter sections according to previous protocols (Glöckner *et al.,* 1996; Loy *et al*., 2005; Pernthaler *et al.,* 2001). Probe GAM42a was included in some hybridizations to quantify the abundance of *Marinobacter* against all *Gammaproteobacteria*. Since hybridization with GAM42a employs more stringent conditions (i.e. a higher FA concentration) (Manz et al., 1992) than that with Mrb-0625-a, a double hybridization assay was performed with GAM42a first. All hybridizations were counterstained with 4',6-diamidino-2-phenylindole (DAPI) following standard methods (Porter and Feig, 1980) prior to visualization under the epifluorescence microscope. Eight to twelve random fields of view were counted for all time points except time point 1, for which 5 fields of view were counted.

Fluorescently-labeled probes (Mrb-0625-a, Mrb-0625-b, GAM42a), labeled at the 5'-end with 6-carboxyfluorescein (6-FAM) or with the sulfoindocyanine dye CY3, and unlabeled probes Hal-0625-a and BET42a, were obtained from EurofinsMWG Operon (Huntsville, AL, USA). *n*-Hexadecane was obtained from Acros Organics (New Jersey, USA). To distinguish Mrb-0625-a fluorescence from Mrb-0625-b fluorescence, the probes were labeled with 6FAM and CY3, respectively. All other chemicals were of molecular biology or HPLC grade.

Results and Discussion

Marinobacter phylogeny and probe coverage

A phylogenetic tree was constructed that included all currently published type strains of *Marinobacter* and other related organisms to illustrate coverage of the newly-developed probes (Mrb-0625-a and Mrb-0625-b) (Figure 1). The total of *Marinobacter* sequences in the Silva 104 reference database at the time these probes were designed (August 2011) was 659, of which 63% are cultured isolates and the remaining 37% are uncultivated clone sequences. An additional 13% of the *Marinobacter* genus—represented in the tree by *M. maritimus* and *M. psychrophilus* (Figure 1) —is targeted by a complementary, but not yet empirically tested, probe designated Mrb-0625-c (Table 1). The remaining 7% of the genus does not branch together and could not be comprehensively targeted by a single probe.

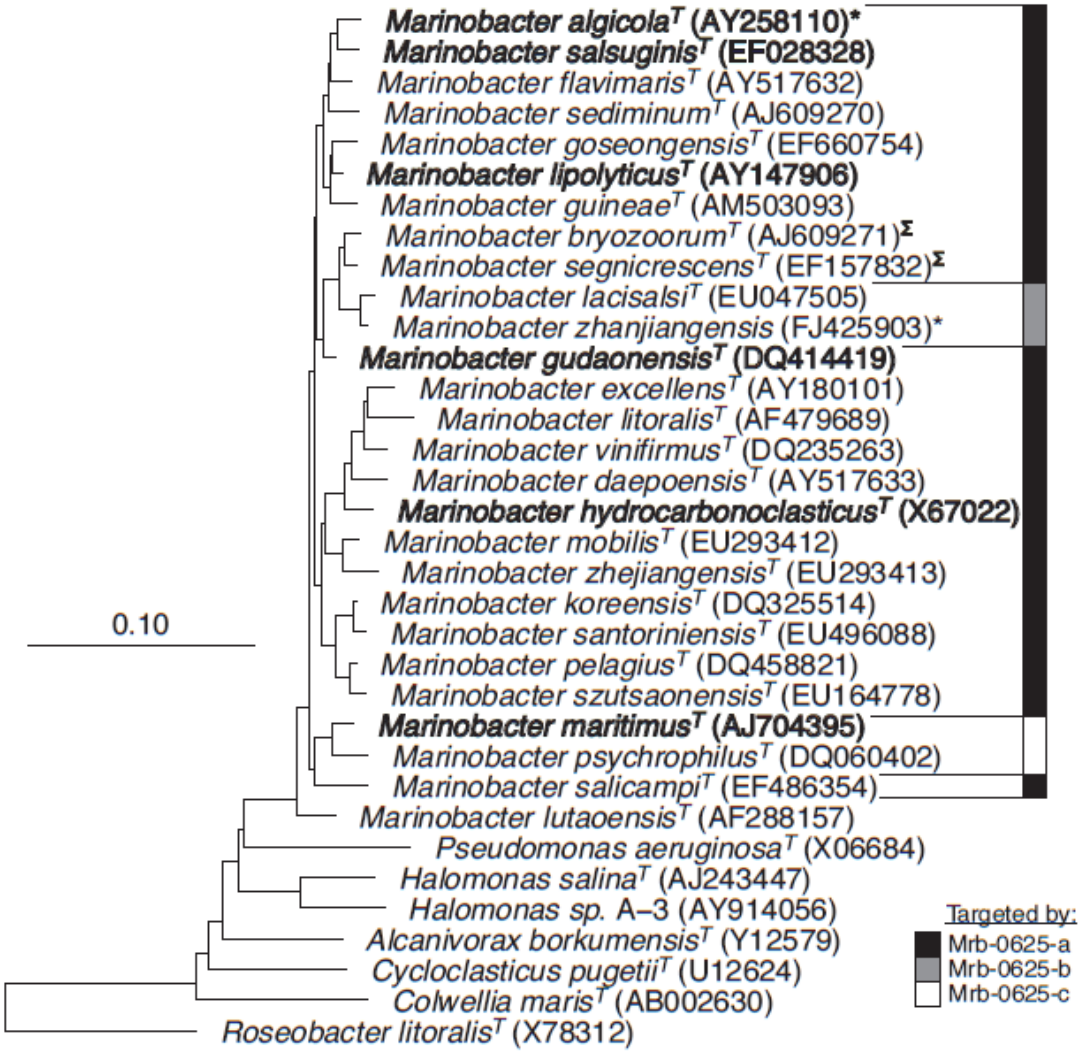
Marinobacter algicola^T (AY258110)*
Marinobacter salsuginis^T (EF028328)
Marinobacter flavimaris^T (AY517632)
Marinobacter sediminum^T (AJ609270)
Marinobacter goseongensis^T (EF660754)
Marinobacter lipolyticus^T (AY147906)
Marinobacter guineae^T (AM503093)
Marinobacter bryozoorum^T (AJ609271)Σ
Marinobacter segnicrescens^T (EF157832)Σ
Marinobacter lacisalsi^T (EU047505)
Marinobacter zhanjiangensis (FJ425903)*
Marinobacter gudaonensis^T (DQ414419)
Marinobacter excellens^T (AY180101)
Marinobacter litoralis^T (AF479689)
Marinobacter vinifirmus^T (DQ235263)
Marinobacter daepoensis^T (AY517633)
Marinobacter hydrocarbonoclasticus^T (X67022)
Marinobacter mobilis^T (EU293412)
Marinobacter zhejiangensis^T (EU293413)
Marinobacter koreensis^T (DQ325514)
Marinobacter santoriniensis^T (EU496088)
Marinobacter pelagius^T (DQ458821)
Marinobacter szutsaonensis^T (EU164778)
Marinobacter maritimus^T (AJ704395)
Marinobacter psychrophilus^T (DQ060402)
Marinobacter salicampi^T (EF486354)
Marinobacter lutaoensis^T (AF288157)
Pseudomonas aeruginosa^T (X06684)
Halomonas salina^T (AJ243447)
Halomonas sp. A–3 (AY914056)
Alcanivorax borkumensis^T (Y12579)
Cycloclasticus pugetii^T (U12624)
Colwellia maris^T (AB002630)
Roseobacter litoralis^T (X78312)
0.10
Targeted by:
Mrb-0625-a
Mrb-0625-b
Mrb-0625-c

Figure 1. Small subunit ribosomal RNA (16S rRNA) phylogeny of members of the gammaproteobacterial marine hydrocarbon-degrading genus *Marinobacter* and six other hydrocarbon-degrading *Gammaproteobacteria*. Of the 659 *Marinobacter* species in the current 16S Silva database, 27 cultured representatives were chosen to demonstrate the overall diversity of the genus as well as approximate percent coverage by the oligonucleotide probes. Type strains are indicated by ^{T}. Strains with known hydrocarbon-degrading capabilities are shown in bold (summarized by Duran, 2010) while species marked with $^{\Sigma}$ were not able to growth on *n*-tetradecane or crude oil (Guo et al., 2007). *Roseobacter litoralis* (X78312) was used as the outgroup. The species used to test and optimize the probes, *Marinobacter algicola* and *Marinobacter zhanjiangensis*, are indicated by asterisks. Mrb-0625-c is a suggested third probe that targets an additional 13% of the Marinobacter group not covered by Mrb-0625-a and Mrb-0625-b, but was not empirically evaluated in this study.

Probe optimization and formamide series

The melting curves for probes Mrb-0625-a and Mrb-0625-b when used in hybridizations with target and non-target reference strains and in the absence and presence of each other are shown in figure 2. In all experiments fluorescence intensity was greater for target strains compared to non-target strains (with a 1-bp mismatch), demonstrating strong probe specificity. Empirically optimized FA concentrations ensured specificity during hybridization with these probes (Table 1). In the case of probe Mrb-0625-a, fluorescence signal intensities decreased significantly at FA concentrations above 20%, indicating that this concentration would be suitable for hybridizations with this probe to specifically detect up to 75% of members that comprise the *Marinobacter* group. With Mrb-0625-b, fluorescence signal intensities did not decrease as sharply at FA concentrations above 20%, though were highest at 20-25% FA concentration and remained distinguishable from non-target signals up to 40% FA concentration. Therefore, when using the probes individually 20-25% FA is the ideal stringency for Mrb-0625-a and 35-40% FA for Mrb-0625-b.

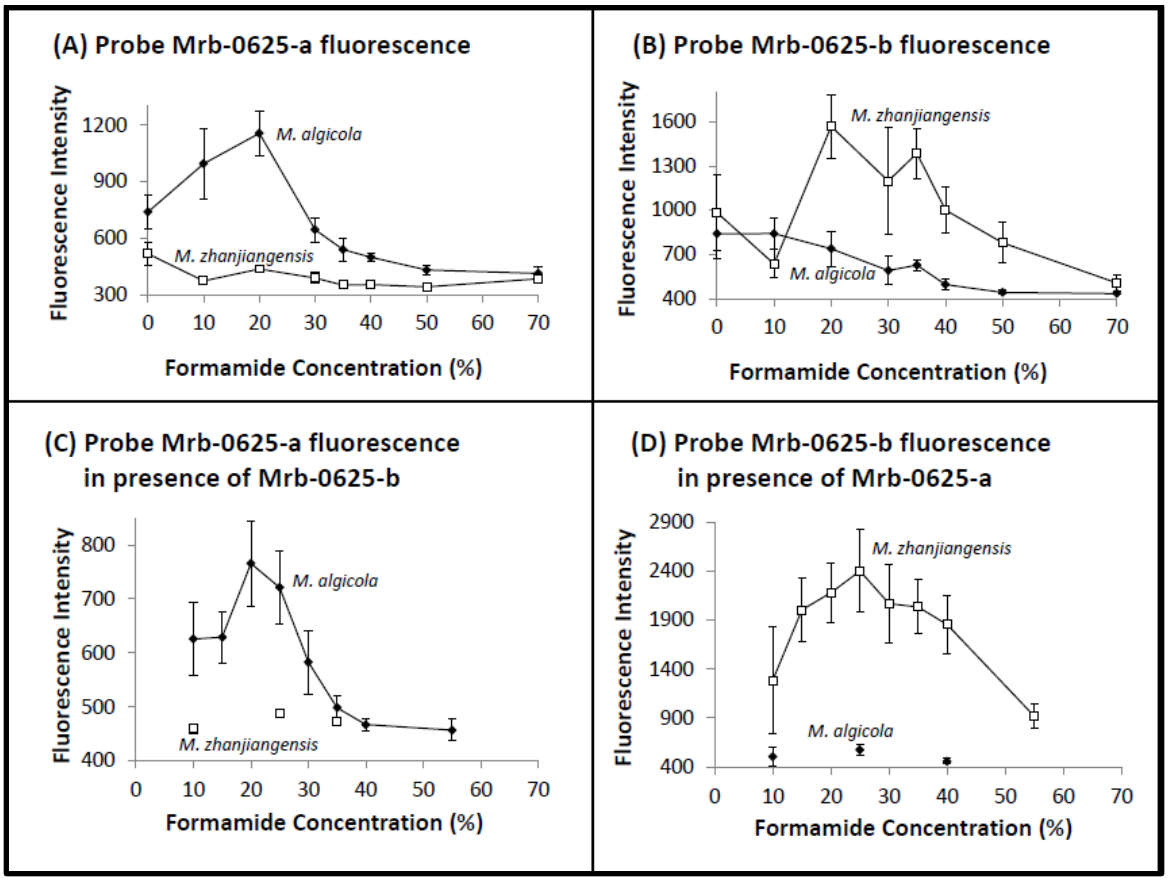
(A) Probe Mrb-0625-a fluorescence
Fluorescence Intensity
1200
900
600
300
M. algicola
M. zhanjiangensis
0 10 20 30 40 50 60 70
Formamide Concentration (%)
(B) Probe Mrb-0625-b fluorescence
Fluorescence Intensity
1600
1300
1000
700
400
M. zhanjiangensis
M. algicola
0 10 20 30 40 50 60 70
Formamide Concentration (%)
(C) Probe Mrb-0625-a fluorescence
in presence of Mrb-0625-b
Fluorescence Intensity
800
700
600
500
400
M. algicola
M. zhanjiangensis
0 10 20 30 40 50 60 70
Formamide Concentration (%)
(D) Probe Mrb-0625-b fluorescence
in presence of Mrb-0625-a
Fluorescence Intensity
2900
2400
1900
1400
900
400
M. zhanjiangensis
M. algicola
0 10 20 30 40 50 60 70
Formamide Concentration (%)

Figure 2. Dissociation profiles of 16S rRNA-targeted FISH probes Mrb-0625-a and Mrb-0625-b evaluated against a perfectly-matching (target) and one basepair-mismatching (non-target) strain. Black diamonds represent hybridization intensities for *M. algicola*; white squares correspond to hybridization intensities for *M. zhangjiangensis*. In two separate experiments Mrb-0625-a was hybridized with its target strain, *M. algicola*, and with its single base pair mismatch strain, *M. zhanjiangensis* (A). In two separate experiments Mrb-0625-b was hybridized with its target strain, *M. zhanjiangensis*, and with its single base pair mismatch strain, *M. algicola* (B). In additional experiments both probes were used together as competitors for the same 16S rRNA motif on both target strains. Dissociation curves are shown for Mrb-0625-a hybridized to its target and non-target strain in the presence of Mrb-0625-b (C), and for Mrb-0625-b hybridized to its target and non-target strain in the presence of Mrb-0625-a (D). Each data point represents the average fluorescence intensity value ± standard deviation from ten randomly-selected fields of view. Mrb-0625-a is labeled with 6FAM, and Mrb-0625-b is labeled with CY3 in all experiments. Linear interpolation was excluded for *M. zhanjiangensis* in C and *M. algicola* in D to denote lower resolution in formamide concentration changes.

Two additional FA series experiments were conducted to optimize using both probes together in the same hybridization. In one of these experiments, 6FAM-labeled Mrb-0625-a and CY3-labeled Mrb-0625-b were applied together with *M. algicola*, while in the other experiment both probes were applied together with *M. zhanjiangensis*. The melting curves for 6FAM-labeled Mrb-0625-a hybridized with target strain *M. algicola* and with non-target strain *M. zhanjiangensis* show that the signal intensity of the *M. algicola* cells at 25% FA concentration is clearly distinguishable from the non-target fluorescence of *M. zhanjiangensis* (Fig. 2C). Conversely, fluorescence during hybridization of CY3-labeled probe Mrb-0625-b to target strain *M. zhanjiangensis* and non-target strain *M. algicola* resulted in distinguishable signals between target and non-target fluorescence within a range from 15% to at least 40% FA, while non-target fluorescence was greatly reduced in the competitive hybridization (Figure 2D). Competitive interference by Mrb-0625-a is not likely beyond 35% FA, since Mrb-0625-a targeted fluorescence is greatly diminished at greater FA concentrations (Figure 2A, C). As a result, Mrb-0625-b shows a gradual decay of fluorescence signal (Figure 2D) not unlike the previous experiment without use of competitive Mrb-0625-a (Figure 2B). When using the two probes

together in the same hybridization reaction, a common stringency of 25% FA is recommended for the simultaneous detection of their target *Marinobacter* species.

The competitive use of alternately labeled Mrb-0625-a and Mrb-0625-b at their empirically-determined optimal FA concentration of 25% was then tested with a mixed population of *M. algicola* and *M. zhanjiangensis* (Figure 3). Consistent with the FA series results from Figure 2, the two *Marinobacter* reference strains could be clearly distinguished from one another. Since an overlay of figures 3A (showing Mrb-0625-a targeted signals) and 3B (showing Mrb-0625-b targeted signals) did not yield any double-labeled cells that were orange or yellow, but rather that were either distinctly green or distinctly red (Figure 3C), non-target binding is interpreted as negligible and the probes appear to be highly specific for their respective target organisms. Further confirmation comes from morphological observations: from previous pure (non-mixed) culture experiments, *M. zhanjiangensis* cells were larger than *M. algicola* cells, and this can be observed in the difference between red and green cell size in Figure 3.

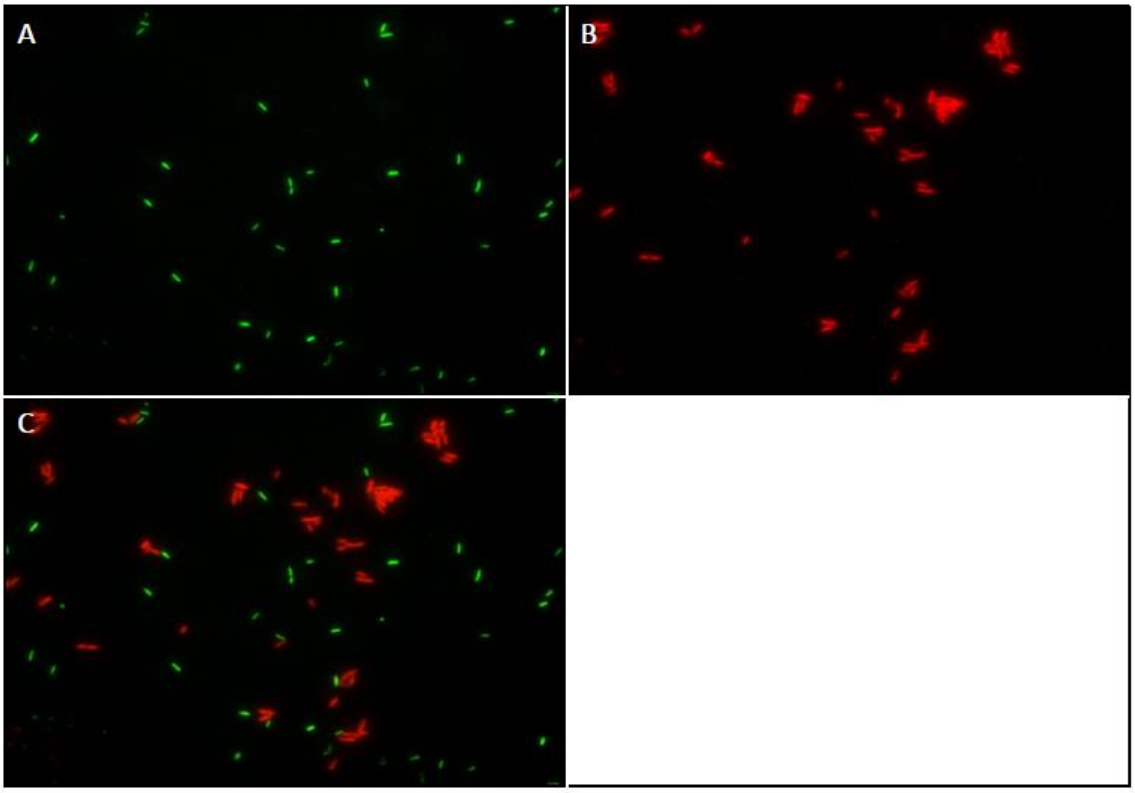

Figure 3. Competitive hybridization experiment showing Mrb-0625-a and Mrb-0625-b fluorescence in a mixed culture of their respective target strains, *M. algicola* and *M. zhanjiangensis*. (A) FITC filtered image of Mrb-0625-a (labeled with 6FAM) targeting *M. algicola*. (B) TRITC filtered image of Mrb-0625-b probe (labeled with CY3) targeting *M. zhanjiangensis*. (C) Overlay of images from A and B, representing the same field of view.

Probe	Genus coverage	Representative strain	Sequence 5' – 3'	Optimal [FA]
S-G-Mrb_0625-a-A-21	75%	*Marinobacter algicola* (AY258110)	CAGTTCGAAATGCCGTTCCCA	20-25%
S-G-Mrb_0625-b-A-21	5%	*Marinobacter zhanjiangensis* (FJ425903)	CAGTTCGGAATGCCGTTCCCA	35%
S-G-Mrb_0625-c-A-21	13%	*Marinobacter maritimus* (AJ704395)	CAGTTCGAAGTGCCGTTCCCA	ND
S-G-Hal_0625-a-A-21	0%	*Halomonas sp. A-3* (AY914056)	CAGTTCCAAATGCCGTTCCCA	ND

Table 1. According to the standard nomenclature for the naming of new probes (Alm et al., 1996), official names of probes Mrb-0625-a, Mrb-0625-b, Mrb-0625-c and Hal-0625-a are S-G-Mrb_0625-a-A-21, S-G-Mrb_0625-b-A-21, S-G-Mrb_0625-c-A-21, and S-G-Hal_0625-a-A-21, respectively. Also indicated are percent genus coverage, representative strains and accession numbers, 5'-3' sequences for each probe, and optimal FA concentrations for hybridization. Sequence mismatches between probes are indicated in white lettering. Mrb-0625-c is a suggested third probe that targets an additional 13% of the Marinobacter group not covered by Mrb-0625-a and Mrb-0625-b is also included in this table, but was not empirically evaluated in this study.

Marinobacter spp. response to oil-contaminated seawater

A microbial enrichment with plume water samples obtained from 1000-1250 m depth in the Gulf of Mexico during the Deepwater Horizon oil spill was characterized with the *Marinobacter* probe set. Since previous work with the plume water samples from the Gulf of Mexico showed that it contained *Marinobacter* species, as revealed in 16S rRNA clone libraries and isolation experiments (Yang et al., in review), it was considered a suitable field sample for application of the *Marinobacter* FISH protocol employing these new probes. *n*-Hexadecane has been used in several studies to enrich for and isolate *Marinobacter* species (Gauthier et al., 1992; Nguyen et al., 1999; Green et al., 2006; McGowan et al., 2004; Abed et al., 2007), and was therefore selected as a model hydrocarbon to enrich for these organisms. At 27°C, the incubation temperature was set within the optimum range for growth of most *Marinobacter*

cultures (25 – 30°C, Duran, 2010). After enrichment with *n*-hexadecane, subsamples taken during this experiment were analyzed using probes Mrb-0625-a and Mrb-0625-b to provide information on the detection and abundance of *Marinobacter*. Hybridizations with 6FAM-labeled Mrb-0625-a revealed that a substantial fraction (e.g., ca. 30% in vial 1, day 3) of the entire DAPI-stained microbial population in the plume water inoculum was composed of *Marinobacter* species (Figure 4A; Table 2). Samples taken from these experiments and hybridized with the Mrb-0625-b probe did not yield any signals (results not shown). Therefore, the *Marinobacter* population in this enrichment was quantified using only the Mrb-0625-a probe (discussed below). Hazen and colleagues (2010) showed that *Halomonas spp*. were significantly enriched in plume waters during the Deepwater Horizon oil spill – by as much as 140% compared to their abundance in non-plume water samples. In order to block false positive Mrb-0625-a hybridization to halomonads, FISH experiments with this probe included the unlabeled Hal-0625-a competitor probe (Table 1) which shares 100% sequence homology to halomonads with a 1 base pair mismatch at the 16S rRNA region targeted by Mrb-0625-a.

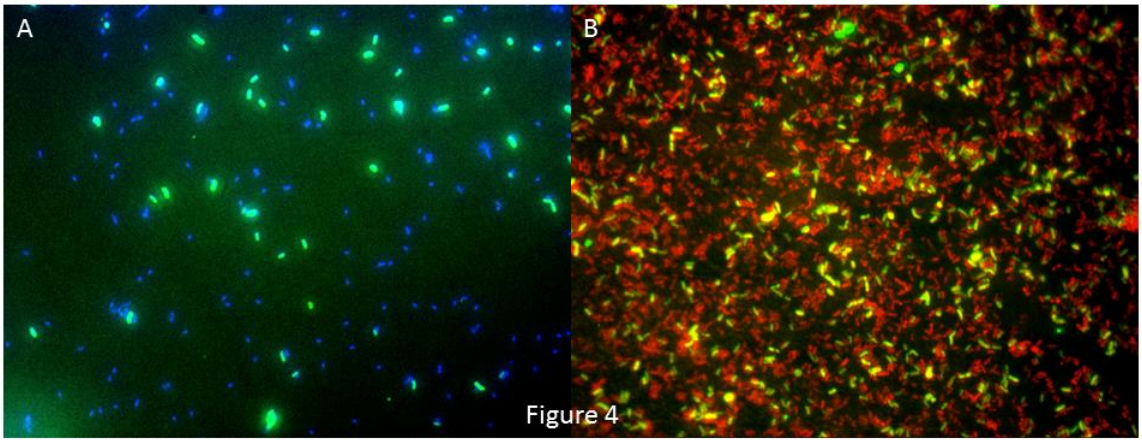

Figure 4. Hybridization of samples from the *n*-hexadecane enrichment experiment with (A) Mrb-0625-a (green) amongst the entire DAPI-stained microbial population (blue) in a sample taken from vial 1 after 3 days, and (B) Mrb-0625-a (yellow-green) amongst the entire GAM42a-targeted gammaproteobacterial population (red) in a sample taken from vial 2 after 4 days incubation.

	Day of Incubation							
	0	**1**	**2**	**3**	**4**	**5**	**10**	**21**
1-6FAM	3.56	29.9	62.0	663	759	413	254	96.2
1-DAPI	12.0	96.9	132 *	2200	2710	2260	2320	3570
2-6FAM	3.56	11.4	56.3	473	384	442	457	496
2-DAPI	12.0	59.9	99.0 *	1650	1710	2020	2170	2480
3-6FAM	3.56	12.5	68.6	61.5	44.2	54.7	31.4	27.4
3-DAPI	12.0	29.4	82.3	74.5	57.5	74.1	109	54.9
4-6FAM	3.56	7.13	35.1	7.83	115	141	9.26	12.1
4-DAPI	12.0	20.7	40.8	20.0	122	153	20.7	30.3

Table 2. Microbial cell counts show changes in total microbial abundance and the corresponding fraction of Marinobacter spp. abundance in each vial over the 21 day time course. Values are in 10^6 cells ml^{-1}. The first row indicates the day of incubation and the first column indicates the vial # and either DAPI, for total microbial community, or 6FAM, for Mrb-0625-a conferred fluorescence. Asterisks demarcate spikes in microbial abundance in vials 1 and 2 between days 2 and 3, concomitant with noticeable changes in turbidity (Supplementary Figure S1). Cell counts from time zero are identical for all vials because they were performed only once on the original inoculum prior to incubation. Vials 1 and 2 were amended with 4% *n*-hexadecane; vials 3 and 4 were not.

It should be noted that the identification of organisms using FISH that employs a probe(s) targeting only a single binding site is not always sufficiently robust. Since no other realistic combination of comprehensive genus-level *Marinobacter* probes could be developed, a double hybridization with the class-level, cy3-labeled GAM42a probe and unlabeled BET42a as competitor (Manz et al., 1992) was performed on selected samples from the plume water enrichment experiment. FISH analysis of a sample taken from vial 2 at day 4 hybridized with 6FAM-labeled Mrb-0625-a and CY3-labeled GAM42a showed that *Marinobacter* cells targeted by Mrb-0625-a represented 30% of the gammaproteobacterial population (Figure 4B). Superimposition of duplicate fields of view under red and green light filters demonstrated

Marinobacter cells in yellow due to Mrb-0265-a fluorescence in green and GAM42a fluorescence in red.

The abundance of *Marinobacter* cells quantified with probe Mrb-0625-a had markedly increased as a result of enrichment with *n*-hexadecane (Figure 5A) compared to the untreated (i.e. no added *n*-hexadecane) controls (Figure 5B). The most dramatic increase (ca. 1 order of magnitude) in abundance occurred between days 2 and 3 and coincided with a significant increase (ca. 1.5 order of magnitude) in the total bacterial population detected by DAPI counts. This was consistent with the observation of an increase in the turbidity of the culture liquid of vials 1 and 2 (amended with *n*-hexadecane) occurring during this time (Supplementary Figure S1). Bacterial abundance remained elevated in the *n*-hexadecane-amended incubations, reaching approximately 3.0×10^9 cells ml^{-1} by the termination of these experiments at day 21. From day 3 to day 21 the *Marinobacter* fraction of the total microbial population had steadily decreased from 30%±5% to 2.7%±0.8% in vial 1, and from 29%±6% to 20%±5% in vial 2. Given the relatively rapid growth of the total microbial community (increase in cell count by a factor of 15) compared to *Marinobacter* spp. (increase by a factor of 8-10) in both hexadecane-amended vials, it appears that *Marinobacter* in the enrichments responds more slowly to a sudden input of hexadecane than the overall microbial population.

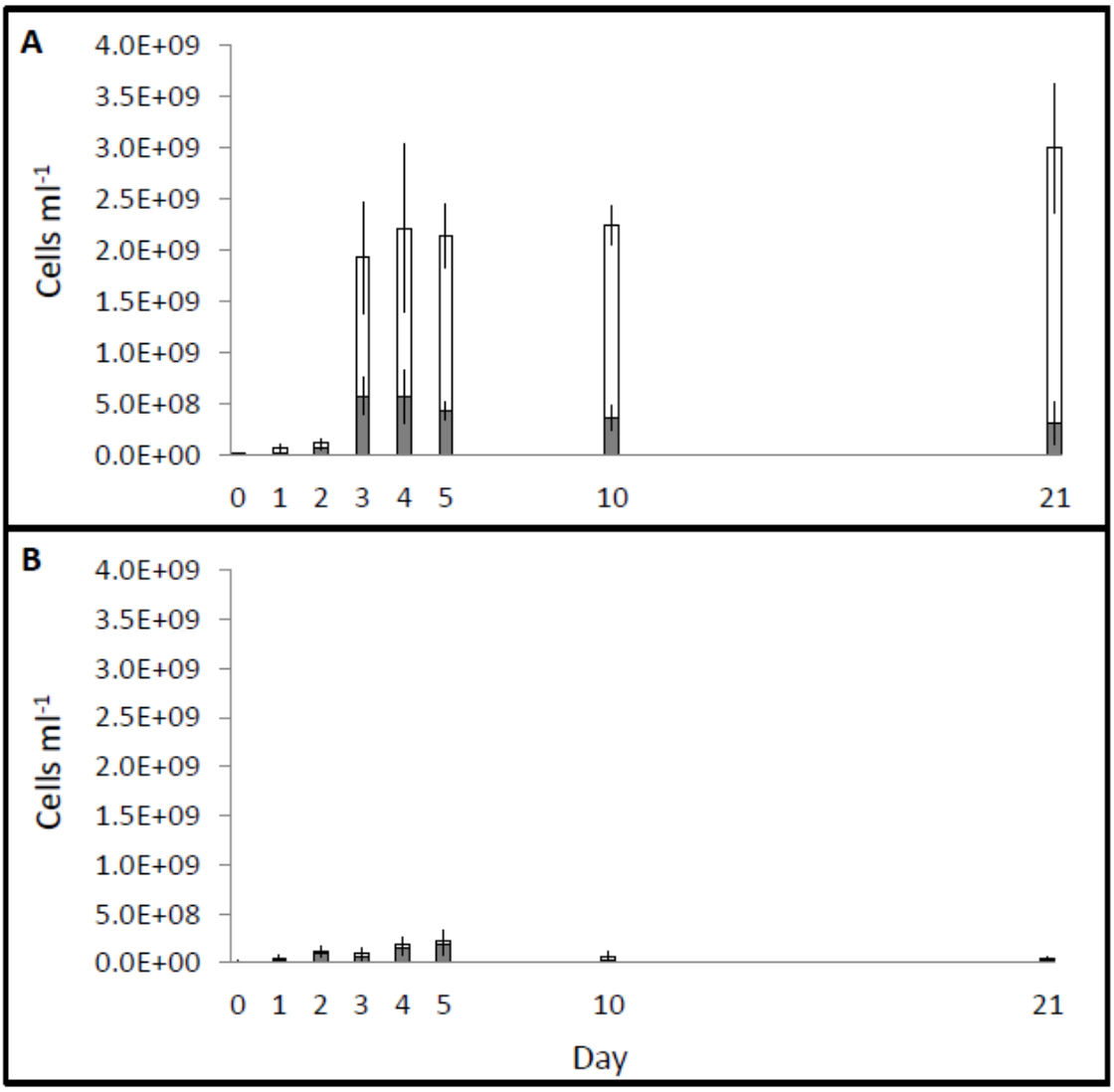
A
4.0E+09
3.5E+09
3.0E+09
2.5E+09
2.0E+09
1.5E+09
1.0E+09
5.0E+08
0.0E+00
Cells ml-1
0 1 2 3 4 5 10 21
B
4.0E+09
3.5E+09
3.0E+09
2.5E+09
2.0E+09
1.5E+09
1.0E+09
5.0E+08
0.0E+00
Cells ml-1
0 1 2 3 4 5 10 21
Day

Figure 5. Absolute DAPI-stained (white and grey) and Mrb-0625-a-targeted (grey only) cell numbers throughout the time course of the enrichment experiment. All experiments were performed in parallel in two sets of duplicate vials (Vials 1 and 2; Vials 3 and 4); DAPI and FISH counts for these duplicated assays are plotted separately in two neighboring columns for all time points to show the variability of the microbial growth and enrichment patterns among replicate vials. (A) Average cell numbers for hexadecane-amended vial 1 (lefthand column) and vial 2 (right-hand column) from days 0, 1, 2, 3, 4, 5, 10, and 21 of the enrichment. (B) Average cell numbers for non-hexadecane-amended vial 3 (left-hand column) and vial 4 (right-hand column) from days 0, 1, 2, 3, 4, 5, 10, and 21 of the enrichment. Error bars represent standard deviation from mean cell counts. The x-axis is abbreviated between days 5 and 10 and between days 10 and 21.

Trophic cascading by marine hydrocarbon degraders

Although the enrichment experiment had the primary objective of testing the newly designed *Marinobacter* probe set, the data offers some insight into the dynamics of marine hydrocarbon degradation. The overall increase in the bacterial population and relative decrease in *Marinobacter* after the observable microbial response to *n*-hexadecane on day three (Fig. 5A) suggests a trophic cascade of distinct microorganisms that participated in the degradation of the *n*-hexadecane, and possibly also of other hydrocarbons that were inherently present in the plume water inoculum. A community-level collaboration and succession of different microbial groups is not atypical following an oil spill in marine waters (Head et al., 2006; Yakimov et al. 2007). Initial degradation of the *n*-hexadecane by *Marinobacter* and other unknown bacteria in these enrichments may have yielded intermediates that fueled the growth of secondary degraders. Such a trophic cascade may in part explain the changes in the microbial community composition of the deep oil plume from the *Deepwater Horizon* spill which have been observed by different researchers (Redmond and Valentine 2012; Kessler et al. 2011; Yang et al., in review).

Vials 3 and 4 (not amended with *n*-hexadecane) also exhibit overall increases in DAPI-stained microbial cell counts up until day 10 for vial 3 and day 5 for vial 4, but these numbers are approximately 2 orders of magnitude lower compared to those from the *n*-hexadecane-amended

vials (Table 2; Supplementary Figure S2). Interestingly, *Marinobacter* appeared to represent the dominant fraction of the lower-density total microbial community in non-amended incubations – ca. 40% by day 1, then peaking at 83%±9% in vial 3 and 94%±6% in vial 4 by days 2 and 4 before dropping back down to ca. 40-50% by day 21. This is not implausible when considering that C16 hydrocarbons (like hexadecane) were found to constitute a significant fraction (2^{nd} and 4^{th} highest) of the total C10 to C35 presence in two deep sea plume water samples (Wade et al., 2011). Hence, low-density pre-enrichment of *Marinobacter* in the deep water plume inoculum was likely attributed to the endogenous presence of these types of hydrocarbons and to *Marinobacter* seed populations that responded well to sample containment. Prolonged bottle storage for 15 months might also have had an effect; bottle incubation of marine water samples resulted in elevated transcription within the Alteromonadales order, which includes the *Marinobacter* genus (Stewart et al., 2012).

Conclusion

16S rRNA oligonucleotide probes targeting an important group of hydrocarbon-degrading and micro-algal associated bacteria, the *Marinobacter*, provide a useful tool with which to study the occurrence and ecological response of these organisms during major perturbations in the marine environment. The newly developed FISH probe set (Mrb-0625-a + Mrb-0625-b + competitor Hal-0625-a) was developed to target up to 80% of species comprising the *Marinobacter* genus, and tested empirically for hybridization stringency. The observations of the *Marinobacter* and total microbial community response to oil contamination indicate that *Marinobacter* spp. may be among the first responders to the presence of hydrocarbons in marine systems. Combining the newly developed probe set with previously published *Marinobacter* probes MB-IC022 (Brinkmeyer et al., 2003) and MB115 (Xiao et al., 2010) could provide more

detailed analysis on the dynamics of *Marinobacter* subgroups in the environment. Furthermore, the new probe set provides a useful expansion to the current collection of oligonucleotide probes by allowing in situ identification of microbial groups contributing to important metabolic processes, such as the breakdown of hydrocarbons.

CHAPTER 2: THERMAL AND GEOCHEMICAL ZONATION OF MICROBIAL BIOGEOGRAPHY IN GUAYMAS BASIN HYDROTHERMAL SEDIMENTS

Introduction

The Gulf of California is a young, expanding ocean as the North American and Pacific plates diverge via a system of narrow spreading zones interspersed by extended transform faults (Lizarralde et al., 2007). At a depth of 2000 m in the center of this Gulf lies Guaymas Basin, where a hydrothermal spreading center is buried by up to 400 meters of organic-rich sediments. Fresh magmatic sills intrude into the thick sediment layer squeezing hot, chemically altered fluids through fissures upwards toward the seafloor (Einsele et al., 1980). Thermocatalytic transformation of freshly deposited organic matter results in a hydrocarbon-rich sedimentary environment. From above, the cold, oxygenated bottom water mixes and circulates with arriving hydrothermal fluids, creating steep physicochemical gradients in the surficial sediments (Gundersen et al. 1992). The shallow subsurface microbial community at Guaymas Basin takes advantage of this wide thermal and substrate diversity, and similarly diverse microbial processes characterize the upper sediments, including microbial methanogenesis, anaerobic methane oxidation, sulfate reduction and sulfide oxidation (Teske et al., 2003).

The anaerobic oxidation of methane (AOM) was first implicated in Guaymas Basin by the presence of 16S rRNA genes and ^{13}C-depleted archaeal lipids of anaerobic methane-oxidizing (ANME) archaea (Teske et al. 2002, Schouten et al. 2003), and has since become recognized as a dominant microbial process in these sediments. Ex situ AOM rates were determined in high temperature and high pressure laboratory incubations (Kallmeyer and Boetius, 2004). More recently evidence has been provided for specialized thermophilic or at

least thermotolerant ANME archaea at Guaymas Basin (Holler et al., 2011; Biddle et al., 2012). In the absence of a pure culture of ANME archaea, the possibility of in situ thermal structuring of ANME subgroups was explored. Particular focus was given to the influence of temperature and chemistry on local microbial biogeography, with an emphasis on microorganisms involved in sulfate reduction and AOM.

Methods

Temperature measurements

Shallow subsurface temperature profiles were acquired from the upper 40 to 50 cm of sediment at 113 distinct sites by high temperature and heat flow probes operated by HOV Alvin as described previously (McKay et al., 2012).

Sediment sampling and site locations

Guaymas Basin sediment was retrieved in 30 to 45 cm push cores by the Alvin submersible on RV Atlantis cruises AT15-40 and AT15-56 in November and December of 2008 and 2009, respectively. Upon arrival to the ship push core sediment was sectioned in 3-cm intervals and aliquots from each layer were reserved for downstream geochemical and molecular biological analyses. Three cores were taken in transect across a *Beggiatoa* mat (27°00.9087N, 111° 22.7932W), from the center where orange *Beggiatoa* spp. cover sediments that harbor the steepest thermal gradient (core 4569-9), to the periphery where white *Beggiatoa* spp. grow over less hot sediments (core 4569-2), to cooler, bare sediments adjacent to the mat (4569-4). Like 4569-2, core 4571-4 was also retrieved from the white section of a *Beggiatoa* mat, but at a different site 664 m away (27° 01.1032N, 111° 22.8128W). Because of the similarities in temperature structure and differences in porewater geochemistry, 4569-2 and 4571-4 were chosen as thermal replicates and geochemical variants. As a background core, 4567-28 was

retrieved from a site with no visible hydrothermal activity located at 27° 00.542063N, 111° 24.488767W.

Porewater geochemistry

Sediment samples were taken for methane measurements by adding 5.0 ml of sediment from each depth horizon into a 30 ml serum vial, adding 2.0 ml of NaOH, mixing well, and storing upside down at -20°C until laboratory analysis at the University of North Carolina at Chapel Hill. For DIC, sulfate, and sulfide analysis, porewater was extracted from the remaining sediment by centrifugation in 50 ml conical tubes and subsequent filtration through 0.45 µm nylon syringe tip filters. DIC samples were taken as 2.0-3.0 ml aliquots in 30 ml serum vials and stored upside down at -20°C until analysis at UNC. Concentration and stable isotopic values of DIC and methane were measured at UNC by a Hewlett Packard 5890 Gas Chromatograph coupled to a Finnigan Mat 252 Isotope Ratio Mass Spectrometer. Sulfate measurements were performed shipboard by acidifying 1.0 ml porewater samples with 50% HCl, bubbling with nitrogen for four minutes, and running the samples through a 2010i Dionex ion chromatograph (Sunnyvale, CA), as described previously (Martens et al., 1999). Spectrophotometric analysis of porewater for sulfide concentrations was performed shipboard (Cline, 1969). It should be noted that sediment samples were not retrieved in pressurized vessels, and outgassing of CH_4, DIC, and ΣH_2S was possible.

16S rRNA gene sequencing and analysis

Total DNA was extracted from two to three selected depth intervals for five cores using the MoBio Powersoil DNA extraction kit (Carlsbad, CA). Using the Takara Speed Star HS DNA polymerase kit (Mountain View, CA), PCR amplification of the full length 16S rRNA gene was performed separately for Archaea with primers ARC8F-ARC1492R (Teske et al., 2002) and

for Bacteria with primers BAC8F-BAC1492R (Teske et al., 2002). The PCR amplification was checked by gel electrophoresis on 1.5% agarose gel, and bands of amplified DNA were extracted from the gel using the Wizard SV Gel and PCR Cleanup System (Madison, WI). Following gel cleanup, amplified DNA was transformed into vectors and cloned in *E. coli* cells using the TOPO TA cloning kit from Invitrogen (Carlsbad, CA). Successful colonies were picked and sent to GeneWiz (South Plainfield, New Jersey) for Sanger sequencing. Sequences were cleaned up and assembled using Sequencher software by Gene Codes Corporation (Ann Arbor, MI) and preliminary alignments were made using the Online Aligner with the Silva v105 database (Pruesse et al., 2007). The ARB software package (Ludwig et al., 2004) was used for further, manual sequence aligning and phylogenetic tree building and trees were converted to figures using Adobe Illustrator (Mountain View, CA). Additionally, web-based UniFrac software (Lozupone and Knight, 2005; Lozupone et al., 2006) was implemented to create principle components analysis (PCA) plots comparing the ARB generated phylogeny for archaea and bacteria to environmental sample information. Duplicate clone sequences were assigned using the de novo OTU picking function (≥ 97% similarity) built in to Qiime software (Caporaso et al., 2010). Qiime software was also used for rarefaction analysis of observed OTUs for each sample (Supplementary Figure S6)

Calculations of thermodynamic potential of the anaerobic oxidation of methane

Gibbs energies, ΔG_r, for the anaerobic oxidation of methane with sulfate to CO_2

$$CH_{4(aq)} + SO_4^{2-} + 2H^+ \rightarrow CO_{2(aq)} + H_2S_{(aq)} + 2H_2O$$

were calculated for five separate cores using the equations, software and thermodynamic data summarized in work by LaRowe and colleagues (2008). Calculations were carried out using measured values of CH_4, $SO_4^{=}$, DIC, ΣH_2S, and temperature under two different pH scenarios.

First, values of ΔG_r were calculated at low pH values extrapolated from temperature correlations of pH measurements from other sites in Guaymas Basin (measured by Dirk De Beer). Secondly, calculations were made using a constant pH value of 5.9 taken from previous measurements of Guaymas Basin vent fluids (Von Damm et al., 1985). The speciation of DIC and ΣH_2S as a function of pH was taken into account.

Results

Bulk comparisons of temperature and porewater carbon chemistry

Guaymas Basin sediments with no hydrothermal activity retain bottom water temperatures of 3°C downcore, while active hydrothermal seepage causes sedimentary temperatures to increase from 3°C to as much as 200°C by 40cm depth (Figure 6).

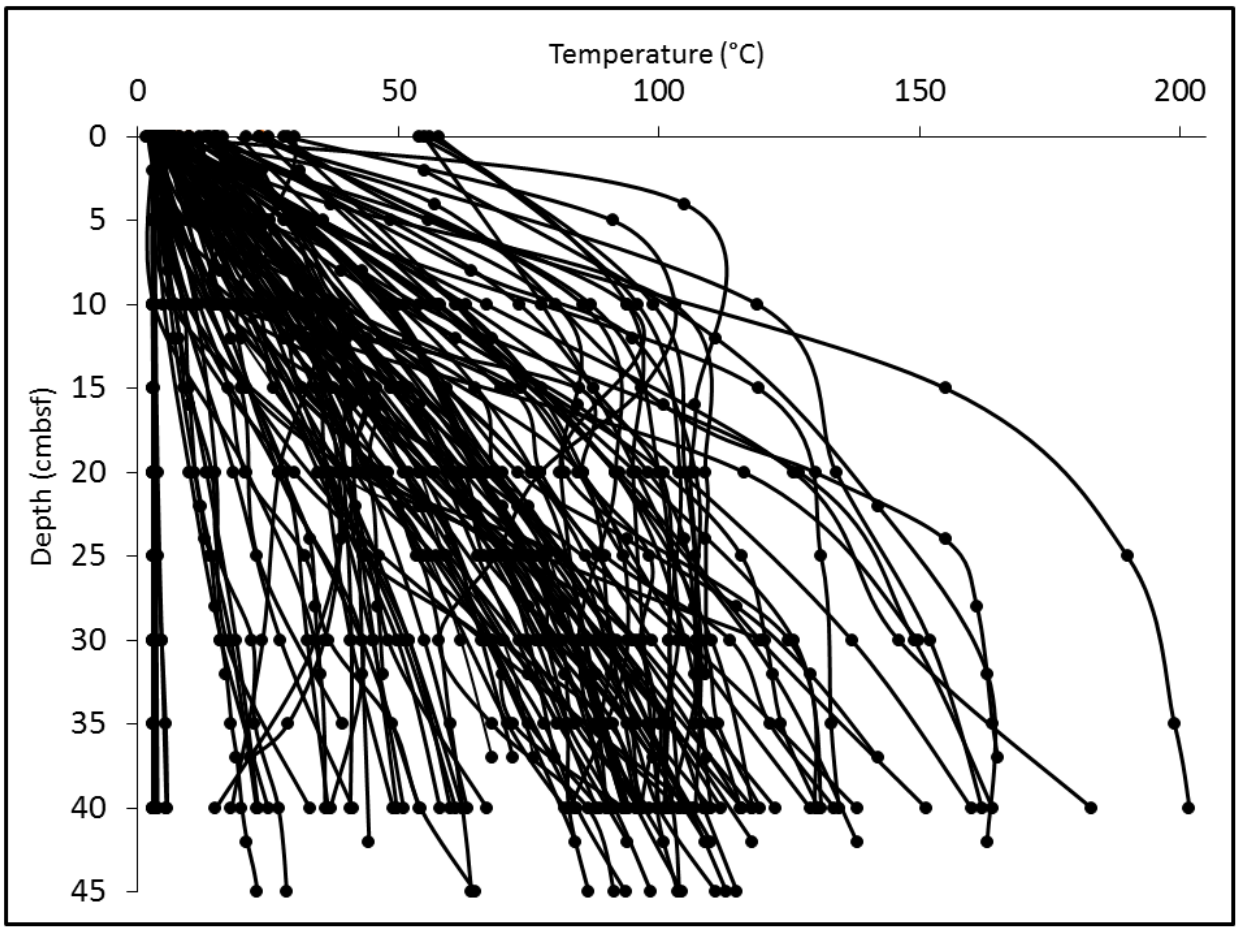

Figure 6. Shallow subsurface temperature profiles from 113 sites at Guaymas Basin indicate the thermal range of different microenvironments within the upper 45 cm of sediment. This figure was modified from McKay et al., 2012.

Temperature profiles from 113 probe measurements spanned the range between these two extremes and typically exhibited an increase in temperature with depth. To investigate a possible correlation between hydrothermal activity and substrate availability comparisons were made for ex situ porewater methane and DIC concentrations and stable isotope profiles with corresponding temperatures from 38 sediment cores sampled in 2008 and 2009 (Figure 7A,B).

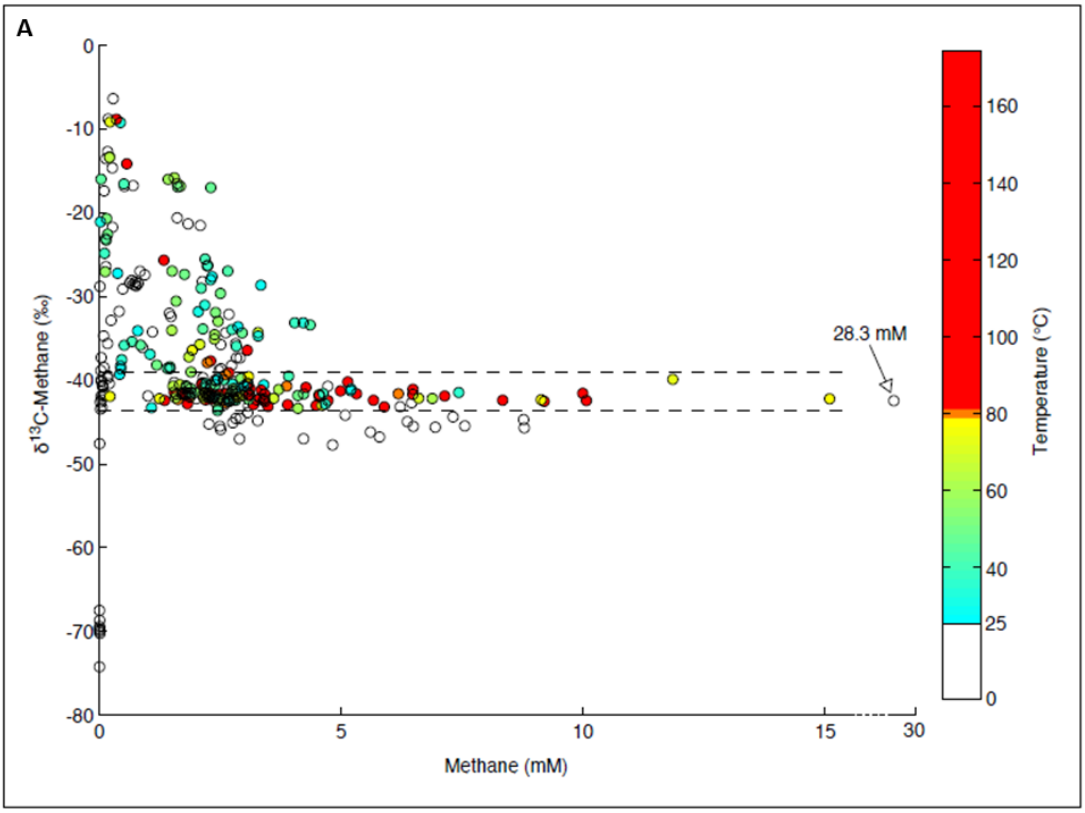
A
0
-10
-20
-30
-40
-50
-60
-70
-80
δ13C-Methane (‰)
28.3 mM
0
5
10
15
30
Methane (mM)
160
140
120
100
80
60
40
25
0
Temperature (°C)

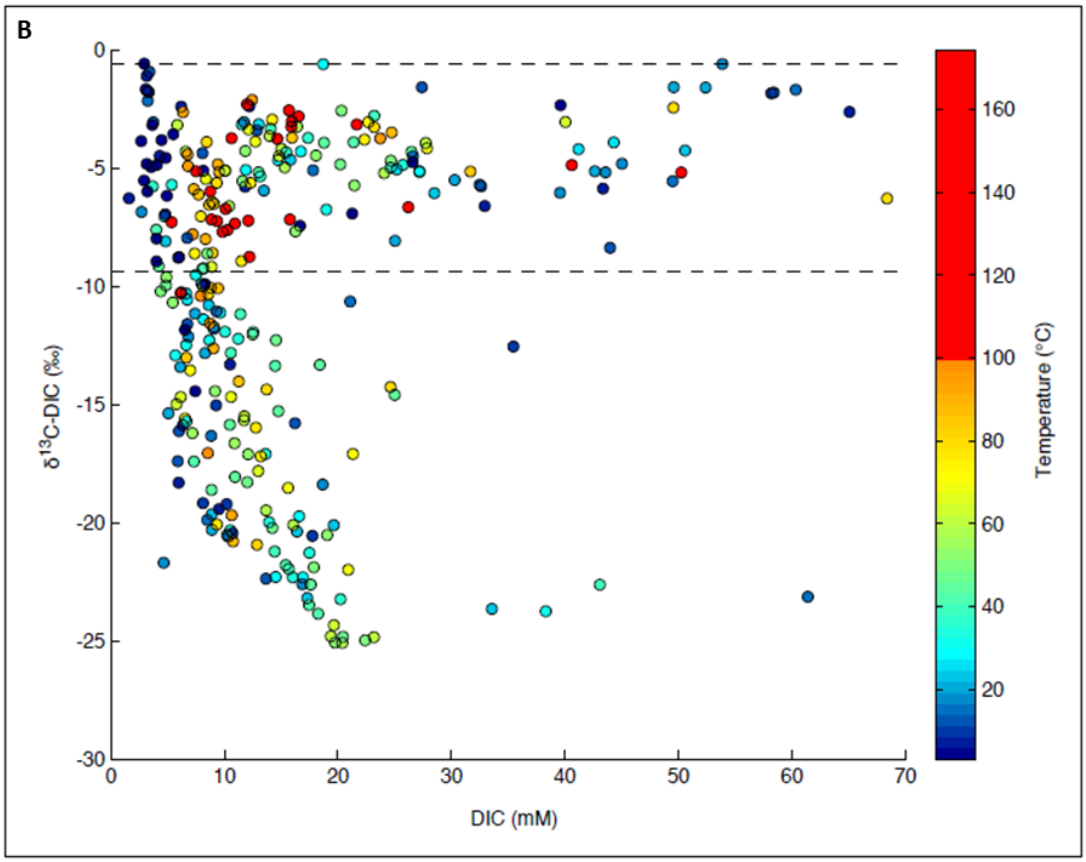
B
0
-5
-10
-15
-20
-25
-30
δ13C-DIC (‰)
0
10
20
30
40
50
60
70
DIC (mM)
160
140
120
100
80
60
40
20
Temperature (°C)

Figure 7. Concentration and stable isotope measurements for methane (A) and DIC (B) with corresponding temperature data. Measurements come from discrete depths of 39 sediment cores. **A)** White circles indicate methane concentration-isotope measurements where in situ temperatures were less than 25°C while colored circles correspond to in situ temperatures indicated by the color bar legend with all temperatures above 80°C in red. Methane concentrations may be under- or over-estimated due to methane bubble formation and/or gas loss during core recovery and sample processing. The x axis was shortened between 15 and 30 mM to include a single data point of 28.3 mM. Dashed lines define the range of thermocatalytically derived methane according to measurements made at presumably unlivable in situ temperatures above 150°C, which is supported by literature values of hydrothermally derived methane at temperatures above 300°C (Welhan and Lupton, 1987; Pearson et al., 2005). **2B)** DIC concentration and stable isotope data corresponding to in situ temperatures above 100°C are indicated by red circles while all other temperatures are represented by the color range indicated by the legend. Dashed lines define the range of high temperature DIC values according to measurements made above 150°C, which is similar to literature values of DIC from hydrothermal fluids with temperatures above 300°C (Seewald et al., 1998; Pearson et al., 2005).

Methane concentrations range between 0 mM and 28.3 mM with an average concentration of 2.56 mM. A methane concentration greater than 1.5 mM represents a methane partial pressure of > 1 atm at the surface temperature. As sediment cores were not pressurized, the degree to which measured methane concentrations reflect in situ values is not known. Stable carbon isotope values from bulk methane data range between $\delta^{13}C$ values from -74.24 ‰ to -6.35 ‰ with an average value of -37.92 ‰, while the range of $\delta^{13}C$ values collected from sediments where temperatures are >25°C, is -43.73 ‰ to -8.82 ‰. More than half of all stable isotopic values for methane (n=191/373) cluster within the range of -43 ‰ to -39 ‰. About 87% of $\delta^{13}C$-methane values from sediments warmer than 80°C fall within this range (Figure 7A). Porewater DIC concentrations range from 1.58 mM to 68.4 mM with an average of 16.03 mM, and $\delta^{13}C$-DIC values range from -25.08 ‰ to -0.58 ‰. With one exception, all $\delta^{13}C$-DIC values associated with temperatures greater than 100°C fall within the relatively ^{13}C-enriched range of $\delta^{13}C$-DIC values within the abiotic range, which was defined by the range of isotopic values from high temperatures sediments above 150°C (Figure 7B). By contrast, lighter $\delta^{13}C$-DIC values outside this range are associated with temperatures below 100°C. While some low temperature $\delta^{13}C$-

DIC values also fall within the abiotic range, only one high temperature δ^{13}C-DIC value is more ^{13}C-depleted than the abiotic range.

Physicochemical descriptions of individual cores

Porewater geochemical profiles, including methane concentrations and stable carbon isotope values, DIC concentrations and stable carbon isotope values, and sulfate and sulfide concentrations are compared to temperature profiles for five individual cores (Figure 8). The data for cores 4569-9, 4569-2, and 4569-4 were previously published (McKay et al., 2012) and are plotted again here for comparison with two additional cores.

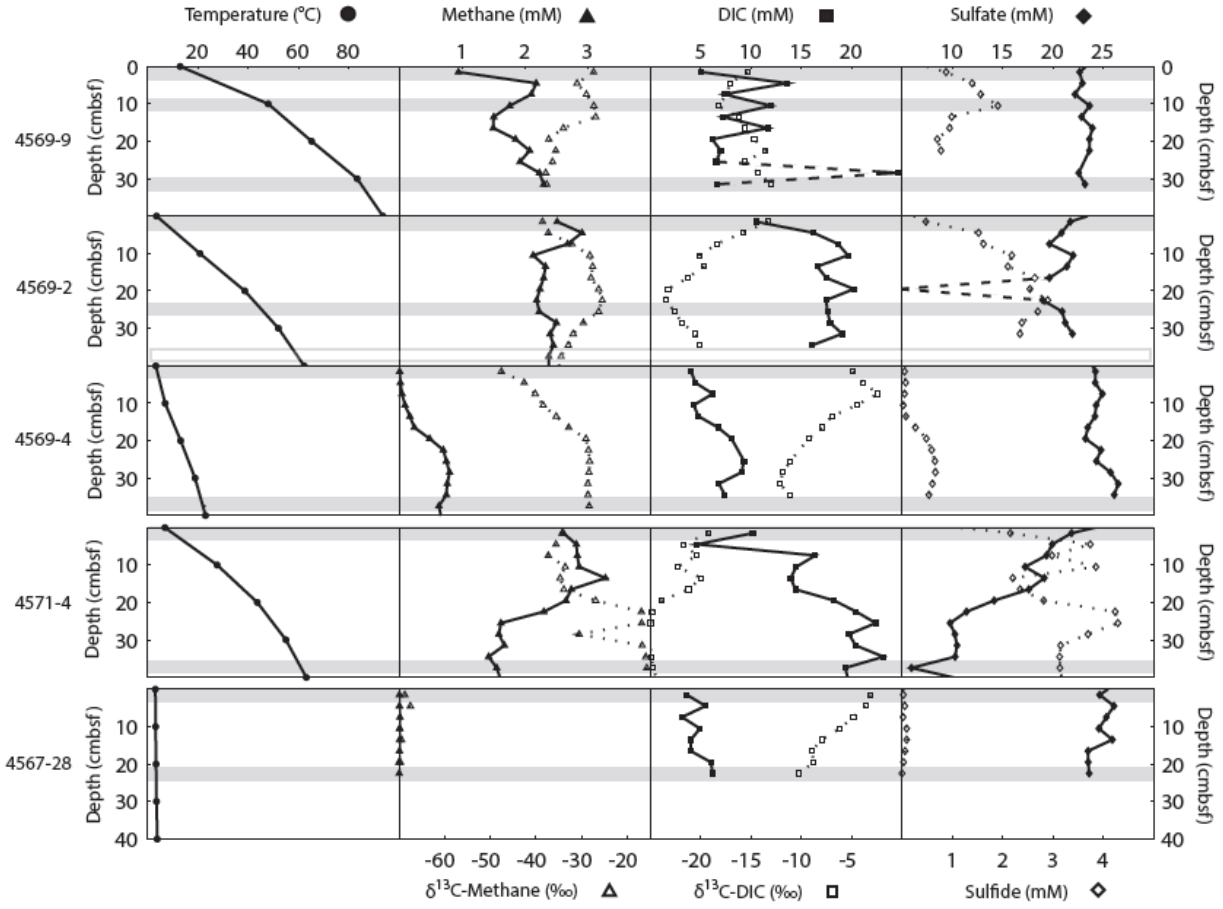

Figure 8. Temperature and geochemical profiles for five individual cores. Shallow 40-cm subsurface profiles for temperature, cell concentration, methane concentrations and isotopes, DIC concentrations and isotopes, and sulfate and sulfide concentrations are given for three cores in transect across a *Beggiatoa* mat (4569-9, 4569-2, and 4569-4), another core from a different *Beggiatoa* mat (4571-4), and a background core with no hydrothermal activity (4567-28). Filled in shapes correspond to the top axes and open shapes correspond to the bottom axes. Grey bands indicate sample depths for archaeal and bacterial clone libraries.

Sediment core 4569-9

4569-9 is the first core in a 3-core transect across a *Beggiatoa* mat, and centrally located over the hydrothermal maximum as indicated by the steepest subsurface temperature gradient measured in the mat. Temperatures increase from 13°C at the surface of the mat to 94°C at 40 cmbsf. Methane concentrations are lowest at the surface (0.95 mM) and remain between 1.5 mM and 2.3 mM throughout the rest of the core. Methane is ^{13}C-enriched at the surface (-27.41 ‰) and becomes lighter downcore, reaching -37.69 ‰ at the last depth sampled where the interpolated temperature from in situ measurements was 83.6°C. DIC concentrations fluctuate considerably between 5 mM and 25 mM while δ^{13}C-DIC values are fluctuating between -12 ‰ and -18 ‰ but remain lighter than the δ^{13}C-DIC values reported previously from Guaymas Basin hydrothermal fluids (-9.4‰) and bottom water (-0.6‰) (Pearson et al. 2005). Sulfide concentrations at the top and bottom of the core are approximately 0.9 mM, with a peak concentration of 1.9 mM at 9-12 cmbsf. No significant sulfate depletion is observed and sulfate concentrations vacillate across a range of 1.4 mM throughout the core.

Sediment core 4569-2

4569-2 is the second core in the 3-core transect and was retrieved from sediment covered by white *Beggiatoa* living around the outside of the central orange region. The temperature profile for this core demonstrates a weaker gradient than that of core 4569-9, increasing from 3°C at the surface to 63.2°C at 40 cmbsf. Methane concentrations range from 2.1 mM to 2.9

mM throughout the core and methane becomes most ^{13}C-enriched (-25.52 ‰) midcore at a depth of 21-24 cmbsf and temperature of ca. 41.5°C. DIC concentrations increase with depth to 10 cmbsf, after which the concentrations show strong oscillations over a range of 5 mM. δ^{13}C-DIC becomes more negative with depth to about 20 cm, and then reverses slope to become more positive with depth. The sulfate concentration profile is highly variable (with a single outlier of 4.8 mM) but with similar concentrations in the surface and deepest sample. In contrast, sulfide accumulation downcore is relatively smooth to a depth of 21 – 24 cmbsf and temperature of 41.5°C, after which sulfide begins to decrease with depth.

Sediment core 4569-4

Core 4569-4 is the third core in the 3-core transect and was retrieved from the bare sediments beyond the edge of the orange and white *Beggiatoa* mat. The corresponding temperature profile for this core increases from 3.3°C at the sediment-water interface to 23.1°C at a depth of 40 cmbsf. Methane accumulation occurs with depth but remains less than 1 mM, while methane steadily becomes more ^{13}C-enriched from -47.58 ‰ at the surface to ca. -28 ‰ at a depth of 21 – 24 cmbsf with a corresponding temperature of 14.4°C. The DIC concentration oscillates but the general trend is an increase from 4.1 mM at the surface to a maximum of 9.3 mM at a depth of 24 – 33 cmbsf where temperatures range between 15°C and 19°C. DIC is ^{13}C-enriched between the surface and 9 cm, and then 13C-depleted down to -12.13 ‰ at 30 cm. Like methane, sulfide accumulates to 1 mM, while the sulfate profile oscillates and increases from 23.7 mM at the surface to 26.1 mM at depth.

Sediment core 4571-4

Core 4571-4 was taken in a different white *Beggiatoa* mat 664 m away from the transect mat. The temperature profile taken next to core 4571-4 closely mimics that of the other core

from the white section of a *Beggiatoa* mat, 4569-2, and increases from 6.9°C at the surface to 63.2°C at 40 cmbsf. Methane concentration and stable isotope profiles from core 4571-4 mirror each other: concentrations decrease from ca. 3 mM at the surface to ca. 1.5 mM at depth, and ^{13}C-enrichment of methane increases from -35 ‰ at the surface to -16 ‰ at 24 – 27 cmbsf (T = 50.6°C). Porewater DIC concentrations increase from 4.6 mM near the surface to 22.4 mM at 24 – 27 cmbsf, while δ^{13}C-DIC decreases from -19.2 ‰ at the surface to -24.97 ‰ at 24 – 27 cmbsf. Finally, sulfide peaks at 4 mM and sulfate is depleted to 4.5 mM near the bottom of the core where temperatures are greater than 50°C.

Sediment core 4567-28

Core 4567-28 was selected as a background core and retrieved from a site with no observable signs of hydrothermal activity. Temperatures associated with these sediments increase very slightly from 3.1°C at the surface to 4.1°C at 40 cmbsf. Methane concentrations here are the lowest compared to all cores measured (≤0.01 mM throughout) and stable isotopic values for methane are extremely ^{13}C-depleted, ranging between -67 ‰ and -75 ‰. DIC concentrations fluctuate between 3 mM and 7 mM and are highest at the deepest depth sampled, 21 – 24 cmbsf, while δ^{13}C-DIC becomes moderately ^{13}C-depleted downcore, reaching -10.25 ‰ at the same depth. Sulfide concentrations remain very low (≤0.1 mM) and sulfate concentrations fluctuate between 23 mM and 26 mM.

16S rRNA gene clone library data

For analysis of 16S rRNA gene based community structure the tops and bottoms of each of the five cores were sampled, as well as an additional mid-section sample for the hottest core, 4569-9. Phylogenetic relationships of total 16S rRNA gene clones recovered from these core sections are reported in neighbor-joining trees separately for archaea and bacteria (Figure S3A,

B). The Guaymas clones were assigned to monophyletic groups—21 within the *Archaea* and 20 within the *Bacteria*—according to relatedness to previously recovered OTUs and cultured isolates. The composition of the archaeal bacterial clone libraries distribution is plotted for each location and depth layer in bar diagrams (Figure 9A, B).

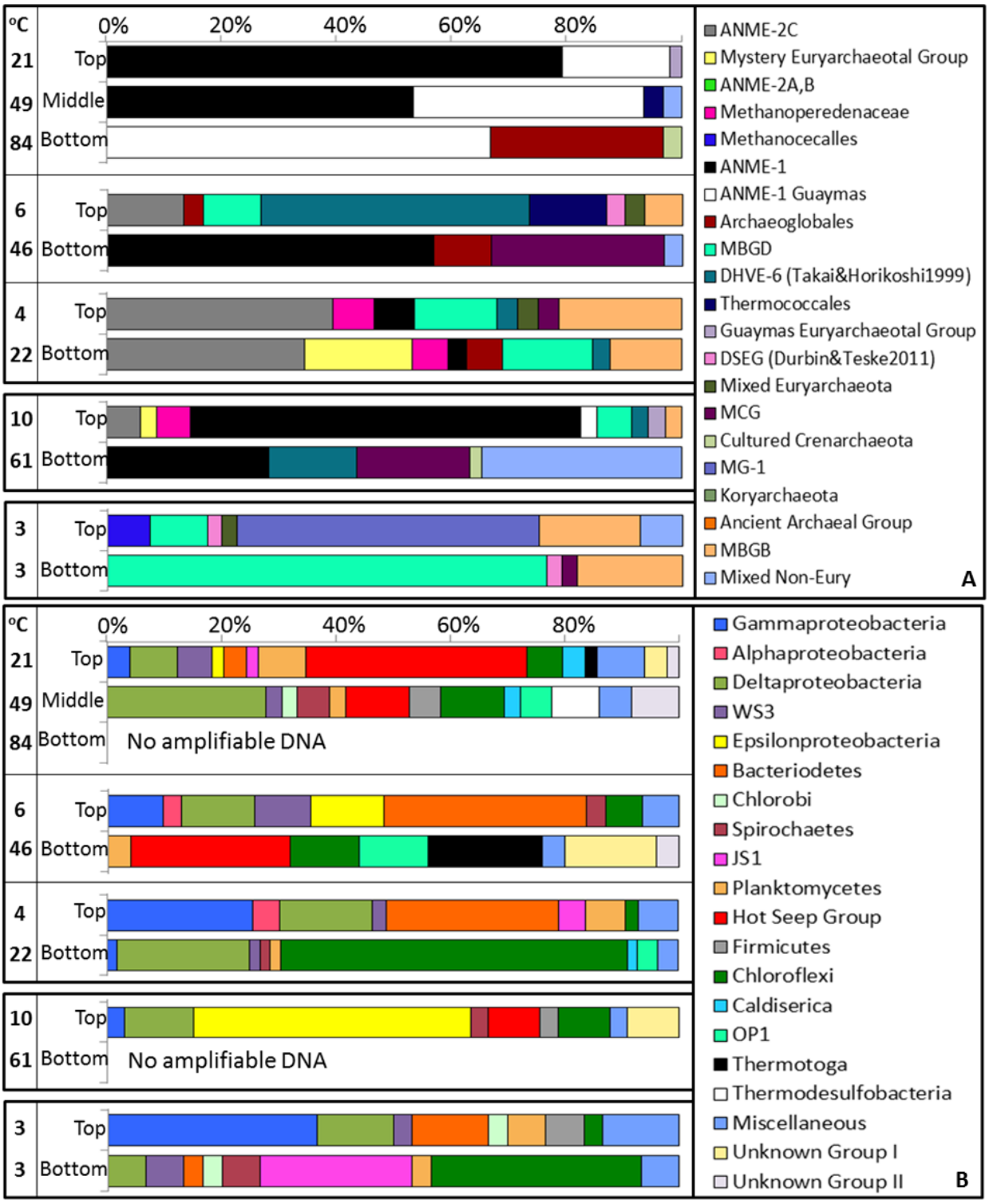
°C
0%
20%
40%
60%
80%
21 Top
49 Middle
84 Bottom
6 Top
46 Bottom
4 Top
22 Bottom
10 Top
61 Bottom
3 Top
3 Bottom
ANME-2C
Mystery Euryarchaeotal Group
ANME-2A,B
Methanoperedenaceae
Methanocecalles
ANME-1
ANME-1 Guaymas
Archaeoglobales
MBGD
DHVE-6 (Takai&Horikoshi1999)
Thermococcales
Guaymas Euryarchaeotal Group
DSEG (Durbin&Teske2011)
Mixed Euryarchaeota
MCG
Cultured Crenarchaeota
MG-1
Koryarchaeota
Ancient Archaeal Group
MBGB
Mixed Non-Eury
A
°C
0%
20%
40%
60%
80%
21 Top
49 Middle
84 Bottom
No amplifiable DNA
6 Top
46 Bottom
4 Top
22 Bottom
10 Top
61 Bottom
No amplifiable DNA
3 Top
3 Bottom
Gammaproteobacteria
Alphaproteobacteria
Deltaproteobacteria
WS3
Epsilonproteobacteria
Bacteriodetes
Chlorobi
Spirochaetes
JS1
Planktomycetes
Hot Seep Group
Firmicutes
Chloroflexi
Caldiserica
OP1
Thermotoga
Thermodesulfobacteria
Miscellaneous
Unknown Group I
Unknown Group II
B

Figure 9. Clone distribution bar graphs for 16S rRNA gene libraries. Relative distributions of clone recovery are presented at the phylum-to-class level for the five cores studied for archaea (A) and bacteria (B). Each bar represents a sampled section of one of the five cores which are indicated further by the grey shaded areas in Figure 8. Three sections were sampled for the hottest core in the microbial mat transect (4569-9) while only two sections, the top and the bottom, were sampled from the other cores. In situ temperatures for each section are listed on the far left. Sequence recovery for each sample is here reported first for archaea and then for bacteria: 4569-9 T (48, 49), 4569-9 M (30, 36), 4569-9 B (30, 0), 4569-2 T (30, 31), 4569-2 B (30, 25), 4569-4 T (28, 43), 4569-4 B (33, 56), 4571-4 T (34, 33), 4571-4 B (46, 0), 4567-28 T (40, 30), and 4567-28 B (48, 30).

The ten groups with the highest number of representatives from the archaeal clone library, in order from highest to lowest, are ANME-1, Marine Benthic Group D (MBG-D, Vetriani et al., 1999), ANME-1 Guaymas (Biddle et al., 2012), ANME-2c (Orphan et al. 2001), Marine Benthic Group B (MBG-B, Vetriani et al., 1999), Deep-sea Hydrothermal Vent Euryarchaeota Group 6 (DHVE-6, Takai and Horikoshi, 1999), Marine Group 1 (MG-1, DeLong 1992), Miscellaneous Crenarchaeotal Group (MCG, Inagaki et al., 2003), Archaeoglobales, and Mystery Euryarchaeotal Group (this study). For Bacteria the ten most abundant groups are *Chloroflexi*, *Deltaproteobacteria*, Hot Seep 1 group (Holler et al., 2011), *Bacteriodetes*, *Gammaproteobacteria*, *Epsilonproteobacteria*, *Planktomycetales*, WS3 (Dojka et al., 1998), Japan Sea Group 1 (JS1, Webster et al., 2004), and Unknown Group I (this study), which is related to the *Planktomycetales-Verrucomicrobia-Chlamydiae* super phylum (Fuerst and Sagulenko, 2011). Phylogenetic relationships within the ANME-related archaea (ANME-1, ANME-1 Guaymas, ANME- 2c, *Methanoperedenaceae*), which make up 48% of total Archaeal 16S rRNA gene recovery (186 of 387 clones), are examined at higher resolution in an ANME-specific phylogenetic tree (Figure 10a). Due to the physiological association between the processes of anaerobic methane oxidation and sulfate reduction, a phylogenetic tree that includes the *Deltaproteobacteria* and the Hot Seep 1 group is also examined at higher resolution (Figure 10b). Together the *Deltaproteobacteria* and the Hot Seep 1 group account for 24% of

the total 16S rRNA gene recovery within the bacterial clone library. Potential paraphyly between the *Deltaproteobacteria* and the Hot Seep 1 group was examined by additional phylogenetic analyses (Supplementary Figure S5).


AJ579316, uncultured archaeon, HMMVPog–34, Loesekann
AY714860, uncultured archaeon GZfos34G5, GZfos34G5, Hallam S.J
AF354157, uncultured archaeon, 1447, Orphan V.J
AJ578123, uncultured archaeon, BS–K–411, Knittel K.
AJ578120, uncultured archaeon, HydCal52, Knittel K.
AY760932, uncultured archaeon, LC1133a–9, Kelley D.S
ANME–1B
FR682489, uncultured archaeon, GUAY_50enr_Arch1, Holler T.;
AF419625, uncultured archaeon, Teske A.;
AF419624, uncultured archaeon, Teske A.;
AB019758, unidentified archaeon, pISA16, Takai K.;
ANME–1A Guaymas I
(Holler et al., 2011; Biddle et al., 2012)
ARB_E1151E1, 4569–9_ARC_9–12_37 (3 clones)
ARB_1808699E, 4569–9_ARC_9–12_30 (2 clones)
ARB_C2DE6022, 4569–9_ARC_0–3_39 (2 clones)
ARB_1D6D446C, 4571–4_ARC_0–3_28 (2 clones)
ARB_21B8944C, 4569–9_ARC_9–12_02 (6 clones)
ARB_A7273FF0, 4569–9_ARC_0–3_41 (19 clones)
AF356644, uncultured archaeon, G72_C59, Longnecker
AF356640, uncultured archaeon, G72_C2, Longnecker
FR682490, uncultured archaeon, GUAY_50enr_Arch41, Holler T.;
ARB_DFE4D9CF, 4569–4_ARC_36–39_32
ARB_CED5E43F, 4569–9_ARC_9–12_36
ARB_463B8C9F, 4569–2_ARC_24–27_21
ARB_B2E613E1, 4571–4_ARC_0–3_04b (2 clones)
ARB_944A504E, 4571–4_ARC_0–3_11 (4 clones)
ARB_69078F4E, 4569–9_ARC_9–12_18a
ARB_B0AE3FB9, 4569–9_ARC_0–3_43 (2 clones)
ARB_B462A1C3, 4569–9_ARC_0–3_47 (3 clones)
ARB_2E4616CC, 4571–4_ARC_36–39_62
ARB_7F7BD70B, 4571–4_ARC_36–39_69 (2 clones)
ARB_3CCFBDBA, 4571–4_ARC_36–39_58
ARB_66AE4090, 4571–4_ARC_36–39_46 (7 clones
ARB_4125A662, 4571–4_ARC_36–39_04 (2 clones)
ARB_71635583, 4569–2_ARC_24–27_20 (14 clones)
ARB_720AB1C9, 4569–9_ARC_0–3_52 (3 clones)
ARB_31E361F3, 4569–9_ARC_0–3_58 (2 clones)
AF419649, uncultured archaeon, Teske A.;
ARB_163F2FEE, 4571–4_ARC_0–3_19
AF419626, uncultured archaeon, Teske A.;
ARB_D7DF7FAF, 4569–9_ARC_0–3_53
ARB_E307C8B, 4571–4_ARC_0–3_41 (2 clones)
ARB_73292513, 4569–2_ARC_24–27_41
ARB_FBDBE8C4, 4571–4_ARC_0–3_29
FR682491, uncultured archaeon, GUAY_50enr_Arch79, Holler T.;
AF419654, uncultured archaeon, Teske A.;
ARB_7846FDFD, 4569–9_ARC_0–3_17
ARB_78989BD6, 4571–4_ARC_0–3_17
ARB_3D840BCE, 4571–4_ARC_0–3_43
ARB_65313EEE, 4569–9_ARC_0–3_03 (2 clones)
ARB_919CE7CB, 4571–4_ARC_0–3_02
ARB_CA4471B4, 4571–4_ARC_0–3_37 (3 clones)
ARB_107B10E3, 4571–4_ARC_0–3_50
ARB_9A7E2972, 4569–9_ARC_0–3_07
ARB_5FE265E2, 4569–4_ARC_0–3_01a
ARB_A9BA3A37, 4569–4_ARC_0–3_12b
ARB_517BDDD5, 4569–9_ARC_0–3_51
ARB_8A1C014A, 4571–4_ARC_0–3_47a (2 clones)
ARB_4235AB10, 4569–9_ARC_0–3_29
ANME–1A Guaymas II (Holler et al., 2011; Biddle et al., 2012)
ARB_A13D6FE7, 4569–9_ARC_9–12_28
ARB_D690166D, 4569–9_ARC_9–12_32
ARB_D4A94471, 4569–9_ARC_9–12_42
ARB_FE27B682, 4571–4_ARC_0–3_05a (2 clones)
ARB_B25B9381, 4569–2_ARC_24–27_50
AF419627, uncultured archaeon, Teske A.;
ANME–1A Guaymas III (here proposed)
ARB_BD3722D9, 4569–9_ARC_0–3_12 (9 clones)
AF419630, uncultured archaeon, Teske A.;
ARB_6B3FC0E, 4569–9_ARC_9–12_11 (9 clones)
AF419655, uncultured archaeon, Teske A.;
ARB_16016121, 4569–9_ARC_9–12_35
ARB_294FA185, 4569–9_ARC_9–12_07a
ARB_728B32CE, 4569–9_ARC_30–33_72
ARB_7A459EB6, 4569–9_ARC_30–33_53 (7 clones)
ARB_E4951CAC, 4569–9_ARC_30–33_69
ARB_F145E327, 4571–4_ARC_0–3_39a
ARB_E981BFC6, 4569–9_ARC_9–12_27a
ARB_9A2F233, 4569–9_ARC_30–33_66
ARB_D2724FE9, 4569–9_ARC_30–33_78 (9 clones)
ARB_2C2FE809, 4569–9_ARC_30–33_61
AF419631, uncultured archaeon, Teske A.;
AF419632, uncultured archaeon, Teske A.;
ANME–1 Guaymas (Biddle et al., 2012)
ARB_FAAD2AA4, 4569–4_ARC_36–39_51
ARB_1DBBA0FC, 4569–4_ARC_36–39_55
ARB_F8FB9AC0, 4569–4_ARC_36–39_53 (4 clones)
ARB_1DF47E9F, 4571–4_ARC_0–3_34a
ARB_8E0DD243, 4569–4_ARC_0–3_58
AF419638, uncultured archaeon, Teske A.;
AF419635, uncultured archaeon, Teske A.;
ARB_C7A3E6ED, 4569–2_ARC_0–3_46 (2 clones)
AF354133, uncultured archaeon, 1439, Orphan V.J
AF354131, uncultured archaeon, 1438, Orphan V.J
AJ890142, uncultured archaeon, fos0626f11, Meyerdierk
ARB_C110744D, 4569–4_ARC_0–3_52 (8 clones)
ARB_E4F91B1D, 4569–4_ARC_36–39_33 (5 clones)
ARB_17E38AB1, 4569–4_ARC_36–39_46
FJ712362, uncultured archaeon, KZNMV–0–A18, Pachiadaki
FJ404024, uncultured archaeon, 40H–260S–3, Zhang L.;
ARB_BFBDA37F, 4569–4_ARC_0–3_50
ARB_C8BB6E6, 4569–4_ARC_36–39_15 (3 clones)
ARB_7BFBDE4D, 4569–4_ARC_36–39_10
HQ588676, uncultured archaeon, AMSMV–25–A2, Pachiadaki
AJ578115, uncultured archaeon, HydBeg125, Knittel K.
AF354129, uncultured archaeon, 1447, Orphan V.J
ARB_E185DF94, 4571–4_ARC_0–3_33 (2 clones)
AF419650, uncultured archaeon, Teske A.;
ARB_AA2BC3BD, 4569–2_ARC_0–3_10
ARB_82A627EA, 4569–4_ARC_36–39_40
ARB_C4C1E69F, 4569–4_ARC_0–3_39b
AF419644, uncultured archaeon, Teske A.;
ANME–2C
ARB_D69AF094, 4569–2_ARC_0–3_15
U20151, Methanosarcina mazei, Boone D.;
AF262036, Methanosarcina mazei, Lai M.C.;
M59137, Methanosarcina acetivorans, Rouviere P
M59140, Methanosarcina thermophila, Rouviere P
AJ012094, Methanosarcina barkeri, von Wintzi
AY196682, Methanosarcina barkeri, Wright A.D
AF432127, Methanosarcina lacustris, Simankova
AB370245, Methanolobus profundi, Mochimaru
U20155, Methanolobus vulcani, Boone D.;
U20152, Methanolobus oregonensis, Boone D.
M59133, Methanohalophilus mahii, Rouviere P
X65537, Methanococcoides burtonii, Franzmann
AF120163, Methanomethylovorans hollandica, Lomans B.P
AJ238002, Methanimicrococcus blatticola, Sprenger W
ANME–2A,B
X16932, Methanosaeta concilii, Eggen R.I.
AB071701, Methanosaeta thermophila PT, Kamagata Y
AY817738, Methanosaeta harundinacea, Ma K.; Liu J.
ARB_6B354E33, 4569–4_ARC_0–3_37a (2 clones)
FJ712371, uncultured archaeon, KZNMV–5–A21, Pachiadaki
ARB_FF529BB1, 4569–4_ARC_36–39_58 (2 clones)
FR682483, uncultured archaeon, GUAY_37enr_Arch23, Holler T.;
DQ521782, uncultured archaeon, SM1–GC205–Arc66, Lloyd K.G.
ARB_6B7FD2C4, 4571–4_ARC_0–3_09 (2 clones)
AF356643, uncultured archaeon, G72_C12, Longnecker
ARB_89A0DB55, 2515322110 16S rRNA Archaeal SSU [Methanoperedens
AF293017, uncultured Green Bay ferromanganous micronodule ar, ARC3, Stein L.Y.
AY835420, uncultured archaeon, 7A08, Dhillon A.
AY835419, uncultured archaeon, 4A08, Dhillon A.
DQ787474, Methermicoccus shengliensis, Cheng L.;
ARB_2CFA0042, 4567–28_ARC_0–3_124 (2 clones)
ARB_165103DF, 4567–28_ARC_0–3_022
AJ578125, uncultured archaeon, BS–K–E9, Knittel K.
AB196288, Methanocella paludicola SANAE, Sakai S.;
Archaeoglobales
Methanomicrobiales
X00662, Halococcus morrhuae, Leffers H.
D11107, Haloferax mediterranei, Kamekura M
Methanobacteriales
Methanococcales
0.10

Figure 10. 16S rRNA gene phylogeny for ANME Archaea (A) and Deltaproteobacteria/Hot Seep Group (B). Phylogenetic trees are based on gene sequences for the 16S small ribosomal RNA subunit from environmental clones from Guaymas Basin sediments. Neighbor joining trees were constructed in ARB with a Jukes-Cantor correction and bootstrap values are based off of 500 iterations of each tree.

Discussion

Thermal variability is extreme in the shallow subsurface sediments of Guaymas Basin. Most surface layer sediments (0-3 cmbsf) retain bottom water temperatures of approximately 3°C, while at a depth of just 40 cmbsf temperatures range from 3°C in hydrothermal inactive sediments to 200°C in sediments with extreme hydrothermal activity (n=113; Figure 6). Sedimentation from high primary production in the water column increases organic matter load in near-shore seafloor environments (Premuzic et al., 1982); however, variation in hydrothermal

activity translates to varied levels of pyrolized and hydrothermally altered organic material, and variable delivery of hydrothermally derived electron donors. Indeed, DIC and methane porewater concentrations (compared to temperature profiles) show high variability, with concentrations ranging from zero to almost 30 mM methane and from zero to 70 mM DIC (Figure 7A, B). It should be noted that the methane concentrations were measured ex-situ and are probably underestimates (or in some cases overestimates) due to outgassing during retrieval (or collection of methane in gas pockets). The variability in methane and DIC concentrations does not correlate well with thermal conditions; increasing methane concentration and increasing temperature, and decreasing DIC concentration and increasing temperature show no significant correlation ($r^2 = 0.06$ and $r^2 = 0.02$, respectively). Multiple factors may control the isotopic composition of a chemical species at a certain depth, including molecular diffusion, transport processes, differential fractionation by microorganisms, and local activity of microorganisms. To investigate the latter of these factors within the framework of a hydrothermal regime, stable isotopic values for methane and DIC were compared with their corresponding temperatures (Supplementary Figure S4). It should be noted, though, that the extent to which other factors influences isotopic composition was not investigated but could play a significant role. If the highly conservative assumption that microorganisms are not viable and show no activity at temperatures above 150°C is made (the actual microbial survival limit may be near 122°C; Takai et al., 2008), then the range of $\delta^{13}C\text{-}CH_4$ values that correspond to temperatures above 150°C—in this dataset, -39.09 ‰ to -43.18 ‰—would represent the range of thermocatalytically-derived methane that is not biologically altered. Oxidation of methane by microorganisms would cause the remaining methane pool to become ^{13}C-enriched as compared to this thermocatalytic range, i.e., resulting in values > -39.09 ‰, which only occurs below a temperature threshold of

approximately 80°C (Supp. Fig. S4C). While the stable carbon isotopic values of methane at other hydrothermal sites are heavier—e.g., -15 ‰ at 21°N on the East Pacific Rise (Welhan, 1988), between -14 ‰ and -7 ‰ at the Lost City serpentinite hydrothermal system (Kelley et al., 2005), between -20 ‰ and -30 ‰ in Yellowstone hot springs (Welhan, 1988)—hydrothermal methane at Guaymas Basin is relatively light, ranging between -43 ‰ and -51 ‰ (Welhan, 1988). The thermocatalytic range of $\delta^{13}C\text{-}CH_4$ from the highest temperature sediments in this study (dashed lines, Figure 7a) is consistent with previous measurements of the isotopic signature of methane from Guaymas Basin hydrothermal fluids above 300°C, for which 3 out of 4 measurements were approximately -43 ‰ (Welhan and Lupton, 1987; Pearson et al., 2005). With the exception of a single sediment core, all cores sampled in 2008 and 2009 indicate that ^{13}C-enriched methane ($\delta^{13}C\text{-}CH_4 > -39.09$ ‰,) is not detected above 80°C; this temperature is therefore a strong candidate for the upper thermal limit of microbial AOM in Guaymas sediments, as far as this process can be isotopically traced.

It should be noted that stable carbon isotope values for methane may be under the dual influence of biological methanogenesis, which results in depleted $\delta^{13}C\text{-}CH_4$ values, and biological methane oxidation, which leads to enriched $\delta^{13}C\text{-}CH_4$ values. Methane concentrations may be low because an active microbial population is efficiently consuming methane or because there is no methane accumulation in that particular zone. Conversely, high methane concentrations could indicate a newly developed hydrothermal source of hydrocarbons to which the methane oxidizing community has not fully responded or cannot keep up with, or large-scale biogenic methane production. Methane concentrations were plotted against corresponding methane isotopic values to elucidate zones of microbial methane production versus consumption (Figure 7A). Data points with corresponding temperatures greater than 25°C (n=216) never

become more ^{13}C-depleted than -43 ‰; stronger ^{13}C-CH_4 depletion indicative of biogenic methane formation is found only at temperatures below 25°C. This is interpreted to indicate that ~ 25°C represents a threshold temperature: at lower temperatures, the contribution of isotopically light biogenic methane can be detected since the hydrothermal methane component is sufficiently attenuated; above 25°C, hydrothermal methane (^{13}C-CH_4 near -43 ‰) and its microbial oxidation – reflected in heavier ^{13}C-CH_4 values within the 25°C to 60°C thermal range – predominates, and may drown out the signal of high-temperature biogenic methanogenesis by hyperthermophilic methanogens isolated from Guaymas Basin (Jones et al., 1983; Kurr et al., 1991).

Similarly, δ^{13}C-DIC values can demonstrate thermal constraints on the microbial process of organic matter remineralization (OMR). In Guaymas Basin, the δ^{13}C-DIC values prior to sedimentary microbial processing range from -0.6 ‰ in bottom water (Pearson et al., 2005) to -9.4 ‰ in hydrothermal fluids (Seewald et al., 1998) (dashed lines, Figure 7B). From this study, δ^{13}C-DIC porewater measurements from high temperature sediments in abiotic temperature regimes above 150°C fall within this range, between -4.87‰ and -8.75‰ (Supplementary Figure S4D). More strongly ^{13}C-depleted values, below -9.4 ‰, likely indicate microbially mediated OMR, and are found only up to approximately 100°C. The resulting 80°C and 100°C estimates for the upper thermal limits of microbial AOM and OMR, have to be qualified twofold. First, abundant hydrothermal methane or non-biogenic DIC could buffer and attenuate the isotopic signatures of microbial AOM and OMR at high temperatures; second, biotic isotopic fractionation could collapse at extremely high temperatures and in situ pressure as has been shown previously for a hyperthermophilic methanogen (Takai et al., 2008). Localized deviations in porewater geochemical profiles must be examined from an individual core perspective to

confirm observations from bulk stable carbon isotope data. Lastly, the lack of heavy methane above 80°C and light DIC above 100°C are observations that cannot themselves be used to conclude the thermal limits AOM and OMR, but rather suggest a starting point for further investigation.

All individual cores examined except the background core (4567-28) and the surface layer of the bare sediment core (4569-4) have $\delta^{13}C\text{-}CH_4$ values more enriched than -39‰, suggesting the prevalence of microbially mediated AOM in hydrothermally active sediments. The in situ temperature range of these sediment cores (up to 83.6°C) is consistent with the previously suggested upper thermal limit for AOM. The $\delta^{13}C\text{-}CH_4$ signal is decreasing downcore, towards -39‰ at the bottom of the high temperature core (4569-9). A notable difference between the two thermally similar cores, 4569-2 and 4571-4 is apparent in the $\delta^{13}C\text{-}CH_4$ profiles. In core 4569-2 the strongest ^{13}C-enrichment of methane (indicative of methane oxidation) appears midcore, near 21 cmbsf and a temperature of ca. 40°C, while in core 4571-4 methane becomes increasingly ^{13}C-enriched all the way downcore towards a temperature of ca. 60°C. This difference suggests that additional factors, for example lateral advection and inmixing of different porewater and methane pools in the hydrothermally flushed Guaymas sediments, may disconnect locally observed isotopic signatures from microbial processes at the same site. The cold background core presents $\delta^{13}C\text{-}CH_4$ values indicative of biological methanogenesis producing methane (at low concentrations) with extremely ^{13}C-depleted values around -70‰.

Calculations of the Gibbs energy of the suggested reaction for sulfate dependent AOM had previously shown that this process remains feasible at increasing temperatures (LaRowe et al., 2008). The Gibbs energy of this reaction is strongly dependent on the in situ methane

concentrations and temperature, but also on pH, which was not measured in situ. Two scenarios were therefore considered—very low-pH conditions extrapolated from temperature-correlated pH gradients from another Guaymas Basin dataset (personal communication with Dirk de Beer) (Figure 11A), and a pH of 5.9, previously published for Guaymas Basin hydrothermal fluids (Von Damm et al., 1985). Compared to the low-pH regime, the moderate pH conditions reduce the Gibbs energy of sulfate dependent AOM, but higher temperatures increase ΔG_r in both cases (Figure 11B). Regardless of which pH model is used in the calculations, it is apparent that sulfate dependent AOM is favorable, and more so with increasing temperature and depth. It should be mentioned that the recently elucidated reaction mechanism for AOM coupled to sulfur disproportionation, with a combined steady state ΔG of -39.2 kJ mol-1 CH_4 for the two half reactions (Milucka et al., 2012), would alter the profiles in Figure 11, which represent AOM coupled to sulfate reduction (steady state ΔG = -34 kJ mol-1 CH_4). However, both processes are stoichiometrically equivalent and would therefore retain the same general trend of increasing favorability with depth and temperature. Favorability, though, must be considered in light of maintenance energy. The benefit of increased thermodynamic potential for sulfate dependent AOM in deeper, hotter, and more acidic sediments is likely overshadowed by the increase in maintenance energy requirements under harsher conditions. While an increase in temperature by 20°C increases the Gibbs energy yield by approximately 10 kJ/mol CH_4 (Figure 11A; 8 e^- transferred per mole CH_4 oxidized), this same change in temperature increases the power requirement of maintenance energy by an order of magnitude (Tijhuis et al., 1993). The shifting balance between AOM energy yield and maintenance energy of thermally stressed cells is likely to limit the temperature range of AOM.

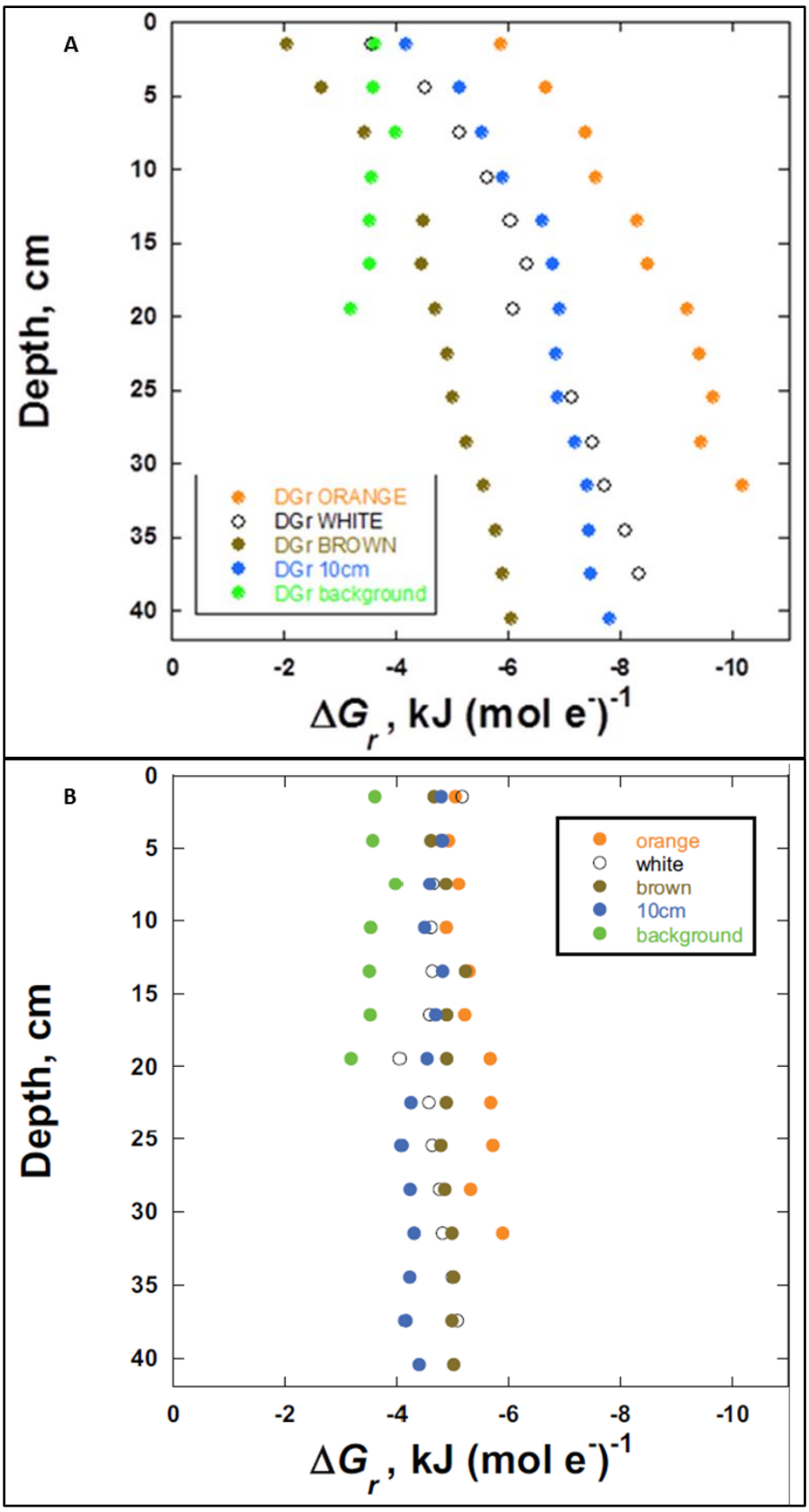
A
Depth, cm
0
5
10
15
20
25
30
35
40
0
-2
-4
-6
-8
-10
ΔG_r , kJ (mol e-)-1
DGr ORANGE
DGr WHITE
DGr BROWN
DGr 10cm
DGr background
B
Depth, cm
orange
white
brown
10cm
background
ΔG_r , kJ (mol e-)-1

Figure 11. Gibbs energy, ΔG_r, of AOM with sulfate in five individual cores. A) Calculations are based on dynamic pH values extrapolated from measured temperature-pH curves at distinct Guaymas sites to the samples from this study. At higher temperatures pH becomes very low (ca. 2) thereby increasing the favorability of the reaction. B) Calculations are based on a fixed pH value of 5.9 taken from the literature (Von Damm et al., 1985). More detailed information can be found in the supplementary text.

In the following section, I will use clone distributions from different depths of the five examined cores to assess the biogeography of microbes in Guaymas Basin hydrothermal sediments. I will discuss microbial distributions in terms of temperature regime, however, geochemical conditions (e.g., electron donors, electron acceptors, and pH) vary along with temperature. Therefore, a group of organisms that appears to favor a given temperature regime, may in fact be constrained by some environmental variable other than temperature.

Clone recovery of 16S rRNA genes shows downcore zonation patterns of archaeal and bacterial communities towards increasing temperatures in the shallow subsurface sediments (Figure 9). Members of the MG-1 archaea are only detected in surficial sediments of the background core. These potentially oxygenated, non-hydrothermal sediments match the habitat requirements of MG-1 phylotypes that predominate in cold, oxic marine surface sediments (Durbin and Teske, 2010). Similarly, MBGD and MBGB archaea also occur in colder sediments, primarily in the background and non-mat cores. Unlike the MG-1 archaea, MBGB and MBGD inhabit deeper, anoxic sediments as well as the upper oxygenated layers. The MBGD archaea increase in clone library representation with depth in the coldest core, consistent with their role in the degradation of detrital proteins in cold, anoxic sediments (Lloyd et al., 2013). Conversely, MBGB archaea make up approximately 20% of the recovered clones in the surficial and deep layers of the background core, which fits well with their wide-ranging habitat preferences including surficial and anoxic sediments (Teske and Sørensen, 2008). 16S rRNA

gene recovery was high for members of the MCG in the deepest depth interval of cores 4569-2 and 4571-4, with in situ temperatures of approximately 46°C and 61°C, respectively. Based on single cell genomic analysis (Lloyd et al., 2013), gene expression analyses (Meng et al. 2014), and stable isotope probing (Seyler et al., 2014), the MCG archaea are generally regarded to be anaerobic heterotrophs, which is consistent with their prominence in the deeper layers of these cores. MCG clones recovered from this study belong to subgroups MCG-7, -13, -3, -8, -15, and -16 of this phylum, as defined previously (Kubo et al., 2012). Representatives of the DHVE-6 group were most prominent in the surface layer of 4569-2 at a temperature of 6.1°C and at depth in core 4571-4 where the temperature is 61°C. These two sediment layers are very distinct from one another both thermally and geochemically, possibly indicating the versatility of DHVE-6 archaea or the accumulation of relict DHVE-6 DNA in deeper layers of core 4571-4. Of the five cores examined, these two have the highest total sulfide content, which is consistent with the occurrence of DHVE-6 OTUs in hydrothermal sediments in Iheya Basin characterized by disseminated sulfides (Takai and Horikoshi, 1999). Members related to the genus *Archaeoglobus* are present in all three of the *Beggiatoa* mat transect cores and appear to be somewhat enriched in deeper, hotter sediment layers (Supplementary Figure S3B). Most of the clones are related to three species of hyperthermophilic sulfate or sulfite reducers (*A. profundus*, Burggraf et al., 1990; *A. veneficus*, Huber et al., 1997; *A. fulgidus*, Beeder et al., 1994), consistent with their sulfidic sediment habitat (Figure 8). Some *Archaeoglobales* clones are related to *Ferroglobus placidus*, a nitrate-reducing iron oxidizer (Hafenbradl et al., 1996) indicating that the role of Guaymas *Archaeoglobales* may not be restricted to sulfur cycling.

Making up 48% of the total archaeal 16S gene recovery, the ANME archaea represent the largest fraction of the total archaeal clone library. All ANME OTUs were related to the ANME-

1 and ANME-2c archaea; they were exclusively recovered from sites associated with hydrothermal activity (Figure 11a). The background core, with negligible methane concentrations (≤0.01mM), did not yield any ANME phylotypes. ANME-2c archaea are prevalent in Guaymas sediments but also appear to be thermally/geochemically restricted; 16S rRNA gene recovery demonstrates ANME-2c presence only in the cool core (4569-4) and the cool surface layers of the two warm cores (4569-2, 4571-4). ANME-1 archaeal phylotypes were present in the cool, warm, and hot cores in both the surface and deep sediment layers. Investigation of the ANME-1 group at higher resolution permits parsing out thermally structured subgroups. The ANME-1 Guaymas group, a separate ANME-1 lineage that is distinct from the widely distributed ANME-1a Guaymas and ANME-1b groups (Biddle et al., 2012; Merkel et al., 2013), appears to be enriched in clone libraries as temperatures increase in the hottest core (4569-9), dominating clone library recovery in the deepest layer at 84°C. ANME-1 Guaymas archaea are a group of putatively thermophilic anaerobic methane oxidizers that are consistently recovered from hot Guaymas sediments (Teske et al., 2002; Biddle et al., 2012; Merkel et al., 2013). In consideration of the previous conclusion that 80°C represents an approximate upper thermal limit for the process of AOM, these occurrence patterns suggest that the ANME-1 Guaymas archaea are the anaerobic methane oxidizers that persist at geochemical conditions near the upper temperature limit of this process, either as a result of high temperature specialization, or due to a wide temperature range combined with high temperature tolerance of ANME-1 Guaymas archaea or some other controlling variable such as pH. All other ANME-1 Archaea demonstrate the opposite trend with increasing temperatures, becoming less dominant as a fraction of the Archaeal clone library. Small-scale phylogenetic clusters within ANME-1 account for previously named Guaymas groups (ANME-1a Guaymas I and II, Biddle et al. 2012)

as well as the here proposed ANME-1a Guaymas III, which is represented by seven clones from high temperature sediments (Figure 10). From the clone library sequences it appears that ANME-2c Archaea are associated with cooler sediments (<20°C), most ANME-1 Archaea tolerate warmer sediments, and the ANME-1 Guaymas group may be specialized thermophiles that can access the methane pool residing at higher temperatures.

Bacterial 16S rRNA gene clones were recovered from all samples except the two hottest depths (4569-9B and 4571-4B). Members of the phylum *Chloroflexi* were the most abundant bacterial clones and were found in nearly every sample. However, while most *Chloroflexi* do not show a specific habitat preference among the Guaymas sediment cores, a specific *Chloroflexi* cluster occurred primarily in the deepest, presumably anoxic sediments of the two coldest cores—4567-28 and 4569-4 (n=39 out of 41 clones; Supplementary Figure S3B). The latter includes *Dehalococcoides ethenogenes* (AF004928) and its close relative *Dehalogenimonas lykanthroporepellens*, anaerobic bacteria most notably capable of reductive dehalogenation of groundwater pollutants (Moe et al., 2009). *Gammaproteobacteria* were a dominant group in surface sediments that are influenced by oxygenated, cool bottom water. Although three of the five cores were retrieved from active *Beggiatoa* mats, only one gammaproteobacterial clone was a member of the candidate group *Maribeggiatoa*, consistent with the requirement to remove bacterial epibionts and contaminants before PCR amplification of these large bacterial filaments (Teske et al., 1999; McKay et al., 2012). Similar to the *Gammaproteobacteria*, members of the phylum *Bacteriodetes* were also dominant in surface sediment samples and only a single clone was recovered from a deeper layer. Although these heterotrophic bacteria occupy very diverse marine sedimentary habitats worldwide (Kirchman, 2002), they are limited to the cool surficial layer of Guaymas hydrothermal sediments. Clone recovery for *Epsilonproteobacteria* was

strong for the surface sediments of three hottest cores, all of which were characterized by *Beggiatoa* mat cover, while no clones were recovered from the background sediment and from cool cores without microbial mat cover. *Epsilonproteobacteria* dominate many microbial mats and/or sulfur oxidizing communities (Engel et al., 2003; Moussard et al., 2006; Sievert et al., 2008) due to their physiological capacity to use multiple electron acceptors including oxygen, nitrate, sulfite, and elemental sulfur (Campbell et al., 2006). This suggests that Guaymas *Epsilonproteobacteria* may require direct or indirect hydrothermal energy sources but are thermally/geochemically restricted to the cool surface layers of active hydrothermal sediments. The next most abundant group falls within the WS3 cluster for which 12 clones were recovered, thus expanding the previously sparse sequence database for WS3 bacteria (Dojka et al., 1998). The WS3 bacteria occur in different sediment samples and may have broad habitat compatibility; however, the WS3 bacteria that exclusively colonize surficial sediments differ phylogenetically from those that are less discriminate (Supplementary Figure S3b). The detection of WS3 clones in surficial sediments does not establish aerobic metabolism—a 0-3cm section of mud from a Guaymas Basin microbial mat likely crosses the anoxic boundary (see Gunderson et al., 1992)—and there is no demonstrated preference for hydrothermally affected versus inactive sediments. Thus, the WS3 cluster that associates with surficial sediments may be controlled by electron acceptor availability, but the preferred electron acceptor remains unclear. Other notable bacterial groups represented in the clone library were Planktomycetales, the JS1 group, and an unknown monophyletic group, accounting for 13, 11 and 9 of 310 clones, respectively. Clones from Planktomycetales were most common in surficial layers in hydrothermally active as well as inactive sediments, JS1 clones were mostly associated with the deepest layer of the inactive background core, and *Spirochaetes* were present in nearly every sample type. The remaining

clones belonged to the following groups: OP1 (7/310), *Thermotoga* (6/310), *Thermodesulfobacteria* (3/310), *Caldiserica* (4/310), *Firmicutes* (5/310), *Chlorobi* (3/310), and *Alphaproteobacteria* (3/310), while 21 of 333 clones were not identifiable.

The second and third most abundant bacterial groups were the *Deltaproteobacteria* and the Hot Seep 1 group (Figure 10B), respectively, both of which are often associated with sulfate reduction (Muyzer and Stams, 2008; Holler et al., 2011). The prevalence of sulfate reduction as a key physiology in Guaymas sediments is supported by several lines of evidence: the common recovery of *Deltaproteobacteria* and Hot Seep 1 16S rRNA or dissimilatory sulfite reduction gene clones from Guaymas sediments (Holler et al., 2011; Biddle et al., 2012), sulfate reduction rate measurements (Meyer et al., 2013; Weber and Jørgensen, 2002), and the strong sulfide accumulation observed in all hydrothermally affected cores. An investigation of bacterial phylum-level phylogeny shows that, contrary to previous assumptions, the Hot Seep 1 group and the *Hippea-Desulfurella* cluster are deeply-branching lineages that cannot be included in the *Deltaproteobacteria* (Supplementary Figure S5). Closer examination of *Deltaproteobacteria* and Hot Seep 1 clones at the family to genus level reveals that the aptly named Hot Seep 1 bacteria (Holler et al., 2011) were recovered exclusively from the three hottest cores (Figure 10B). Sulfate is plentiful and there is evidence of sulfide accumulation at these depth horizons, supporting the putative association of the Hot Seep 1 group with the process of sulfate reduction in hydrothermal sediments. *Desulfosarcina*-related clones were recovered from a wide range of habitat types including the middle depth of the hottest core (4569-9 M), the top layer of the cool core adjacent to the mat (4569-4 T), and the deepest layer of the non-hydrothermal background core (4567-28 B) (Figure 11B). The genus *Desulfosarcina* is a frequently detected marine sulfate reducer (Ravenschlag et al., 2000; Mußmann et al., 2005; Muyzer and Stams, 2008), and

the detection of *Desulfosarcina*-related phylotypes supports the assertion that sulfate reduction is a pervasive process throughout the physicochemically variegated microenvironments of Guaymas Basin. Recovery of 16S rRNA gene clones related to Deep Seep 1 Deltaproteobacteria was greatest in the deepest section of the cool core with no microbial mat cover. Previously Deep Seep 1 clones have been recovered from gas/oil seep and hydrate sediments in the Gulf of Mexico (AY211659, Mills et al., 2005; AM746084, FN421248, Orcutt et al., 2010), which is consistent with their presence in 4569-4 B that has methane concentrations in the mM range. Sulfide and DIC accumulation at this sediment layer indicates the possibility that Deep Seep 1 bacteria here might be participating in sulfate reduction similar to other deltaproteobacterial genera. Another notable deltaproteobacterial group implicated by clone recovery in Guaymas sediments is Eel-2 (Orphan et al., 2001). Presence of this group is strongest in the middle sediment layer of the hottest core (4569-9 M) where a peak in sulfide accumulation coincides with isotopically light DIC and isotopically heavy methane. Consistent with this occurrence, Eel-2 was previously discovered to be the dominant bacterial group in the surface and shallow subsurface of a microbial mat covered hydrothermal seep in the Gulf of Mexico (Lloyd et al., 2010). The presence of Eel-2 bacteria in these warm, sulfide-rich sediments fits nicely with the recent description of *Dissulfuribacter thermophilus*, an elemental sulfur-reducing and thermophilic member of the Eel-2 cluster (Slobodkin et al., 2013).

To assess which factors impart the strongest influence on biogeographical zonation of microbial groups, PCA was performed on the sequence data categorized by environmental sample (Figure 12). For archaea, and not bacteria, environmental samples cluster in accordance with variability in hydrothermal activity. In other words, the most hydrothermally influenced five samples (dashed circle) are characterized by similar archaeal diversity, while the less

hydrothermally influenced samples (dotted circle) group within the lower left quadrant, and the two non-hydrothermal samples fall within the upper left quadrant. Interestingly, bacterial clones present no such hydrothermal-affiliated diversity. Previous analyses also indicated that bacterial diversity was similar regardless of influences by Guaymas sediment temperatures (Meyer et al., 2013). It should be noted, however, that since no bacterial clones were recovered from the two hottest samples, environmental sample clustering is restricted to a lower temperature range for bacteria than for archaea and it is possible that hydrothermal influences cannot be as clearly elucidated. Even the non-hydrothermally active samples, though, are not distinguishable from hydrothermal seep samples according to bacterial diversity, as they are for archaeal diversity.

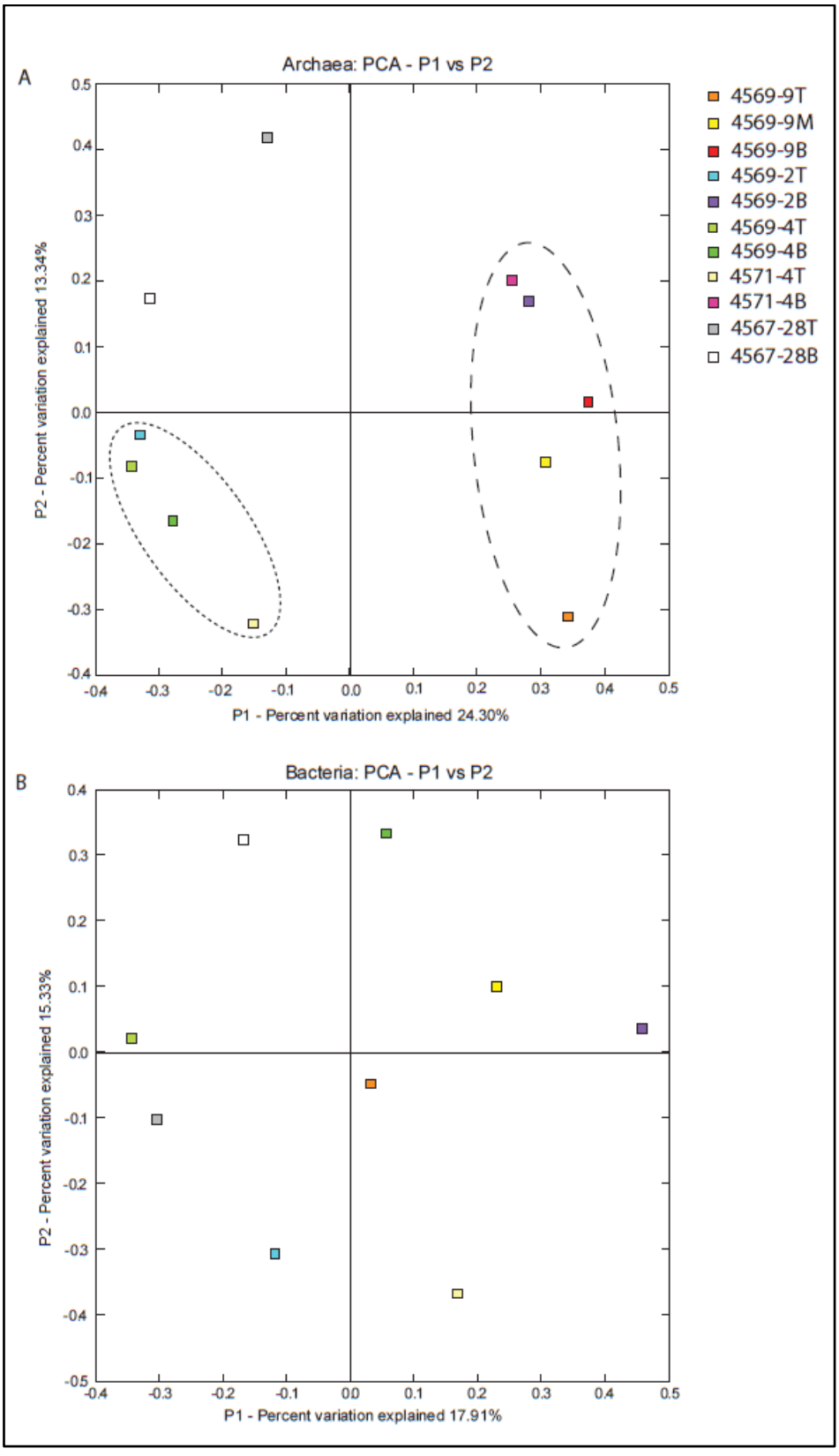
A
Archaea: PCA - P1 vs P2
P2 - Percent variation explained 13.34%
P1 - Percent variation explained 24.30%
4569-9T
4569-9M
4569-9B
4569-2T
4569-2B
4569-4T
4569-4B
4571-4T
4571-4B
4567-28T
4567-28B
B
Bacteria: PCA - P1 vs P2
P2 - Percent variation explained 15.33%
P1 - Percent variation explained 17.91%

Figure 12. Principal components analyses of the microbial diversity according to environmental sample. 16S rRNA gene derived phylogeny, based on a 3% OTU designation, and corresponding sampling locations demonstrate differential clustering patterns for microbial diversity. A) Clustering of similar environmental samples is maintained by the first two principle components, representing 24.30% and 13.34% of the total variance in archaeal diversity. Samples cluster into three main groups including high hydrothermal activity (dashed circle), low-to-medium hydrothermal activity (dotted circle), and no hydrothermal activity (upper left quadrant). B) Bacterial diversity imparts no clustering pattern on environmental samples. When plotted against the first two principle components representing 17.91% and 15.33% of the total variance in bacterial diversity, samples appear randomly distributed.

Synthesis and Conclusions

Shallow subsurface temperatures can reach extreme levels in just 40 cm depth in Guaymas Basin sediments, limiting microbial colonization to thermally tolerable surface sediments. Although the thermodynamic potential for AOM increases with increasing depth and temperature, at temperatures beyond approximately 80°C and 100°C, the ^{13}C-isotopic signatures of microbial anaerobic oxidation of methane and organic matter remineralization appear to be thermally restricted towards the values previously reported for methane and DIC in hydrothermal endmember fluids. Candidates for biogenic signatures of anaerobic oxidation of methane and organic matter remineralization to DIC appear below these temperature limits. This observation should not be interpreted as a definitive conclusion of the thermal constraints on AOM and OMR, but rather the statement of an observed correlation that needs further investigation. Putative methane consuming archaea dominate the archaeal clone library and sulfur cycling bacteria dominate the bacterial clone library, consistent with the porewater geochemical evidence of these physiological modes and their previously suggested association across multiple habitat types (Boetius et al., 2001; Knittel and Boetius, 2009). Archaeal clone library data suggest that the ANME-1 Guaymas archaea tolerate high in situ temperatures up to approximately 80°C, thereby gaining an advantage in access to the geothermal methane pool in hot Guaymas Basin

sediments. Lastly, the results indicate that in situ thermal and/or geochemical gradients structure archaeal community composition and biogeography more than bacterial biogeography.

CHAPTER 3: ACTIVE MICROBIAL LIFE IN HIGH TEMPERATURE GUAYMAS BASIN SEDIMENTS

Introduction

At 2000 m water depth in the Sea of Cortez, Guaymas Basin is a 3.5Mya hydrothermally active spreading center characterized by abundant sources of carbon and energy. A mixture of productive surface waters and terrestrial runoff coats the basalt crust of Guaymas Basin with a 300-400m thick layer of organic rich sediments, which are heated directly or indirectly by magmatic intrusions embedded within the sediment layers (Einsele et al., 1980). Hydrothermally active sites of varying intensities are distributed along the spreading center (Lonsdale and Becker, 1985); in many areas the seafloor sediments appear no different from cold open ocean regions while in others thick and colorful *Beggiatoa* mats indicate hydrothermal seepage and circulation through the sediment-water interface (Jannasch et al., 1989; Gunderson et al., 1992). Active seeps are rich in carbon and energy sources and fuel a diverse subsurface microbial community primarily made up of methanotrophic, methanogenic, and sulfate reducing archaea and bacteria (Teske et al., 2003). Bottom water at Guaymas Basin has a temperature of approximately 3°C, and, in especially active sediments, temperatures can increase up to 200°C in the first 40 cm (McKay et al., 2012). Thus, the abundant carbon and energy sources at Guaymas Basin come with the microbial cost of tolerating high and/or fluctuating temperatures. Here, the activity of microbial communities in four very hot subsurface environments is investigated by pyrosequencing of reverse-transcribed RNA from archaea and bacteria.

This study focuses on sequencing 16S ribosomal RNA (rRNA) instead of rDNA (16S rRNA genes) under the assumption that RNA is less stable extracellularly than DNA and is thus

more representative of the living microbial community. RNA also reflects gene expression and thus microbial activity more directly than DNA, which may indicate the presence of cells or cellular genomes. It has been reported that extracellular DNA may account for up to 90% of total DNA in the upper 10 cm of oceanic sediments (Dell'Anno and Danovaro, 2005), and DNA-based studies of community composition may thus yield misleading results. However, although RNA degrades relatively rapidly and is a better indicator of both life and activity than DNA, microorganisms have multiple intracellular copies of rRNA which are not always uniformly expressed across diverse species. For instance, expression of rRNA may change according to cell mass (Gausing, 1977) due to differential regulatory mechanisms inherent to diverse microorganisms (Wagner, 1994). To this end, abundant sequence recovery from an rRNA starting point may indicate an especially active microbial group, or a group that requires a relatively large pool of rRNA for cellular maintenance. Regardless, analyzing rRNA instead of rRNA genes provides an additional safeguard to avoid false positive sequence-based detection of microbial life, which is especially important in this investigation of the high temperature fringe of viability.

Remarkably, very few studies have investigated high temperature life in the natural environment via RNA-based techniques, and virtually none have examined detailed phylogeny from RNA sequence recovery. To my knowledge, the highest temperature at which RNA has been successfully extracted from a natural sample is 82°C; the RNA extract was used to quantify relative abundance of archaea and bacteria by rRNA slot blotting in a shallow-water hydrothermal seep in the Mediterranean Sea (Sievert et al., 2000). Although the currently established high temperature limit for laboratory-grown life is 122°C (Takai et al., 2008), this temperature extreme may be unsustainable in the environment, where energy and substrate

limitations may translate into more moderate thermal limits of life for microorganisms in situ. The following investigation examines the thermal and geochemical conditions of high temperature microbial life in the hydrothermal sediments of Guaymas Basin and provides a detailed examination of phylogenetic diversity based on reverse-transcribed rRNA.

Materials and Methods

Core and temperature sampling

Using the *Alvin* submarine's heat flow temperature probe 40 cm temperature profiles were measured at sites of hydrothermal activity, as indicated by the presence of microbial mats. During dives 4562, 4565, 4572, and 4573, 3-inch diameter push cores containing around 35-40 cm of sediment were taken adjacent to temperature probe measurements at four very hot sites with subsurface temperatures at 30 to 40 cm depth up to ca. 175°C. Following retrieval from Guaymas sediments the cores were exposed to ex situ low temperatures during the 2-hr ascent and prior to sectioning for a maximum of 8 hours. Aboard the *RV Atlantis* the cores were sectioned in 3-cm intervals and each layer was split into two subsamples for geochemical and molecular biological analyses. Subsamples for molecular biological analyses were frozen immediately after sectioning in liquid nitrogen and stored at -80°C until processing in Chapel Hill. Cores 4573-16 and 4572-18 retrieved sediments adjacent to temperature logging probes that recorded in situ temperatures every five minutes for eight days prior to coring. It is important to note, however, pushcores were taken by the Alvin submersible as close as possible to the temperature logging probes but may have been 10cm away, and considerable changes in the temperature regime may occur within this lateral shift.

Sample preparation and measurement of carbon and sulfur geochemistry

For methane, 5.0 ml of sediment from each section was mixed with 2.0 ml 1M NaOH in a 30 ml serum vial, sealed, mixed well, and stored at -20°C until laboratory analysis in Chapel Hill. All remaining geochemical measurements were measured from porewater, which was obtained by centrifugation of sediments in 50-ml Falcon tubes at 3000 rpm for 15 min. The supernatant from each sediment horizon was subsequently filtered through 0.22 µm polycarbonate filters and divided into aliquots for DIC, sulfate, and sulfide measurements. For DIC, 2.0 ml of porewater was injected into evacuated 30-ml serum vials and stored upside down at -20°C until laboratory analysis. Stable isotopic values and concentrations of methane (measured directly from whole sediment samples) and DIC (from porewater) were measured with a Hewlett Packard 5890 Gas Chromatograph coupled with a Finnegan Mat 252 Isotope Ratio Mass Spectrometer at the University of North Carolina at Chapel Hill. For sulfide quantification, 1.0 ml of porewater was mixed with 0.1M zinc acetate in a 2-ml microcentrifuge tube and stored at 4°C until shipboard spectrophotometric analysis as previously described (Cline 1969). For sulfate 1.0 ml of porewater was mixed with 50 µl of 50% HCl in a 2-ml microcentrifuge tube, bubbled with nitrogen gas for four minutes and stored at 4°C until shipboard analysis. Sulfate concentrations were analyzed shipboard by a 2010i Dionex ion chromatograph (Sunnyvale, CA) as previously described (Martens et al., 1999).

RNA extraction, processing, and reverse transcription PCR (rtPCR)

Selected sediment layers were thawed in trichloroacetic acid (TCA) lysis buffer, bead beaten, and then nucleic acids were precipitated by the addition of 0.6 volume isopropanol overnight at -20°C (McIlroy et al., 2008). Precipitated nucleic acids were resuspended in water and extracted via a sequence of multiple separations with low-pH (5.1) phenol, phenol-

chloroform, and chloroform, and subsequently precipitated overnight at –20°C in 0.7 by volume isopropanol and 0.5 by volume ammonium acetate (Lin et al., 1995; MacGregor et al., 1997). Nucleic acid pellets were resuspended in nuclease free water, purified using the RNeasy RNA cleanup kit (Qiagen, Germantown, MD) and one or more DNase treatments, using Turbo DNase I (Thermo Fisher Scientific, Waltham, MA) either on the column during RNeasy cleanup or in solution or both, were necessary to eliminate PCR-detectable DNA. Because post-extraction RNA concentrations in most samples were extremely low (< 1 ng μl^{-1}), PCR amplification of reverse-transcribed extracted RNA was necessary to achieve adequate concentrations for downstream 454 pyrosequencing. Resuspended rRNA was reverse transcribed to cDNA and amplified at the 787 – 1391 nucleotide position (corresponding to the 16S rRNA gene from *E. coli*) with the SuperScript® III One-Step RT-PCR system with Platinum® Taq DNA Polymerase (Thermo Fisher Scientific, Waltham, MA) according to the recommended reaction conditions. For targeted amplification of the V5 – V8 region of 16S rRNA for archaea and bacteria, universal forward primer 787 (5′-ATTAGATACCCNGGTAG-3′) (Roesch et al., 2007) and universal reverse primer 1391 (5′-ACGGGCGGTGWGTRC-3′) (Lane et al., 1985; Jorgensen et al., 2012) were used in the reaction. To confirm the absence of DNA in RNA samples, duplicated PCR reactions were performed on all samples without the addition of the reverse transcriptase enzyme. Successful RT-PCR amplifications were analyzed for product length by gel electrophoresis and subsequently extracted from the gel using the Wizard SV Gel Cleanup kit from Promega (Madison, WI).

454-pyrosequencing and analysis

Reverse-transcribed and PCR-amplified V5-V8 fragments of 16S rRNA, now in the form of DNA, were submitted to the Microbiome Core Facility at UNC-Chapel Hill for barcoding and

454 pyrosequencing (Roche, Branford, CT). Sequences were filtered for quality with the split libraries and de novo operational taxonomic unit (OTU) picking commands in Qiime, which requires a built-in PyNAST generated alignment (Caporaso et al., 2010). OTU limits were designated at 97% sequence similarity, and the resulting OTUs were used for initial assessments of alpha diversity from rarefaction analysis and principle component analysis-based beta diversity across samples. OTU networks were created with Qiime and analyzed with Cytoscape v2.8.0 software (Cline et al., 2007), which was also used to make OTU network figures. ARB software was used to generate neighbor-joining 16S rRNA phylogenetic trees using the Jukes-Cantor correction, bootstrapped at 500 iterations. Trees were based on modified Silva alignments of Qiime-picked OTUs and were built for total archaea, total bacteria, methane processing archaea, *Deltaproteobacteria*, and *Epsilonproteobacteria*. An additional tree was generated from co-occurring OTUs across the four hottest samples as indicated by the OTU network.

Results and Discussion

Thermal and geochemical structure of sediment cores

Profiles of temperature, methane and DIC concentrations, stable isotopic values of methane and DIC, and sulfate and sulfide porewater concentrations describe, in part, the physicochemical environments of each of the four high temperature sedimentary environments sampled by Alvin push coring (Figure 13). All sample sites have temperatures that reach above 100°C at depth, with a maximum subsurface temperature of 185°C in core 4573-16 at 40 cmbsf. While these four sites reach the highest sediment temperatures measured in shallow Guaymas sediments (McKay et al., 2012) and are presumably highly influenced by the hydrothermal system, the porewater concentrations and isotopic signatures of carbon and sulfur species are

quite distinct across these cores.

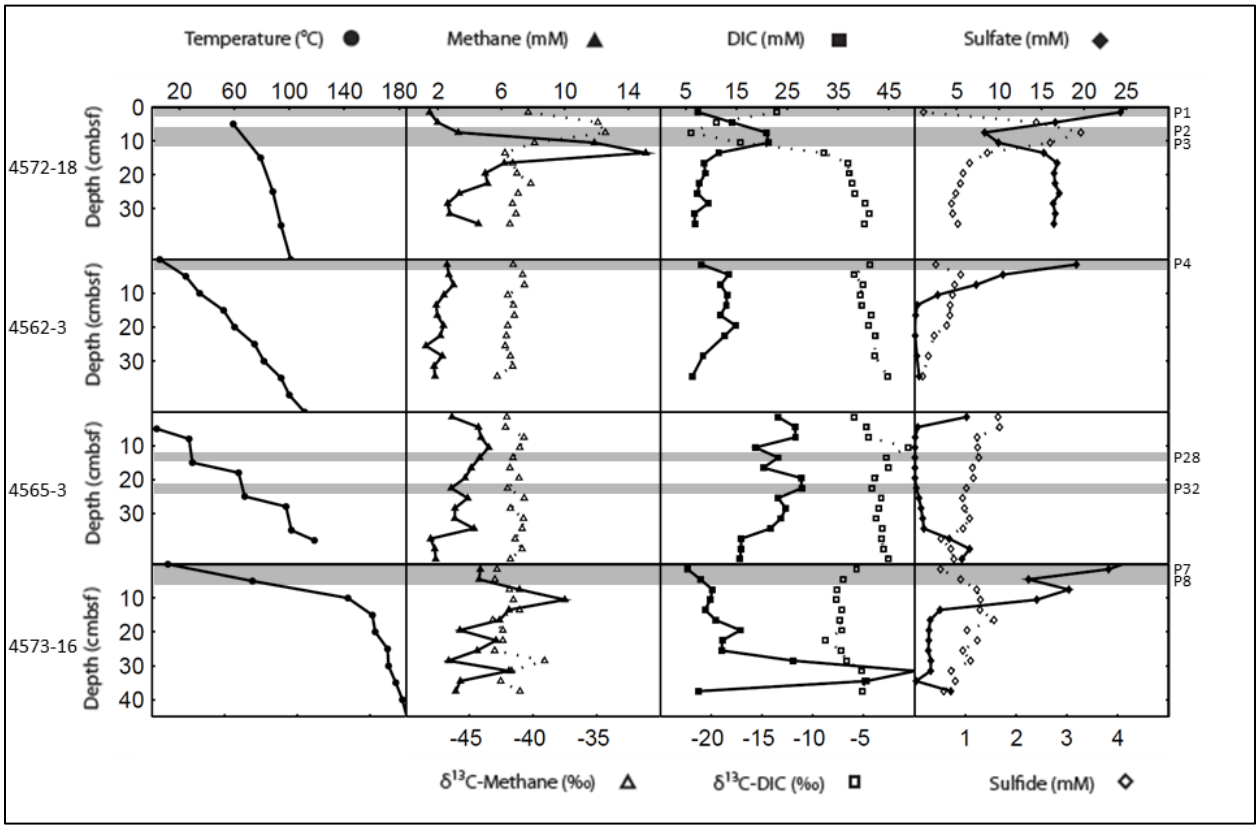

Figure 13. Shallow sediment profiles of temperature, methane concentrations and isotopes, DIC concentrations and isotopes, and sulfate and sulfide concentrations from four high temperature push cores sampled in Guaymas Basin.

Methane concentrations are supersaturated and generally range from around 2 mM to 6 mM with sharp peaks up to ca. 10 mM and 15 mM in cores 4573-16 and 4572-18, respectively. Although methane is abundant, microbial processing by anaerobic oxidation of methane (AOM)—as indicated by a deviation in stable isotopic values of methane towards more ^{13}C-enriched values—is only evident near the surface of core 4572-18. This probable occurrence of AOM coincides with a sharp decrease in methane concentrations towards the sediment surface. Measured ex situ high methane concentrations above 1 to 1.5 mM should be interpreted cautiously due to probable outgassing during core retrieval, and most likely underestimate the in

situ methane concentration. Apart from the δ^{13}C-methane deviation in 4572-18, values in all cores are consistent with the signature of thermocatalytically altered methane at Guaymas Basin at -43‰ (Pearson et al., 2005; Welhan and Lupton, 1987; chapter two of this dissertation). And, while the subsurface temperature maximum reaches 100°C in core 4572-18, the near-surface layer in this core suggestive of AOM has an in situ temperature of approximately 60-70°C and does not exceed the predicted upper thermal limit of AOM at 80°C (chapter two of this dissertation).

DIC concentration profiles are rather distinct across the four coring sites, ranging between 5 mM and 50 mM with notable peaks near the surface of core 4572-18 and at depth in core 4573-16. Stable isotopic values of DIC range between -22 ‰ and 0 ‰. Like δ^{13}C-methane values, microbial processing is implicated at the same shallow layer in core 4572-1. Here, a local minimum in δ^{13}C-DIC values indicates microbial remineralization of organic matter or a methane-derived contribution to the DIC pool, and co-occurs with a peak in DIC concentrations that reaches approximately 25 mM. By contrast, the conspicuous peak in DIC concentrations up to 50 mM between 30 and 33 cmbsf in 4573-16 coincides with a slight ^{13}C-enrichment of DIC towards -5 ‰, suggesting that this source of DIC may be abiogenic. Consistently among all four cores, δ^{13}C-DIC tends to become more ^{13}C-enriched towards values > -5 ‰ downcore, a source signature of most likely abiogenic δ^{13}C-DIC as downcore temperatures become incompatible with life. This abiogenic DIC source falls within the range of previous δ^{13}C-DIC measurements of Guaymas Basin bottom water at -0.6 ‰ (Pearson et al., 2005) and Guaymas hydrothermal venting fluids at -9.4 ‰ (Seewald et al., 1998). It should also be noted that in some cases downcore DIC accumulation is insufficient to account for the amount of sulfate reduction implicated by the decreasing sulfate profiles. Under acidic sedimentary conditions, which may

be likely (see discussion of Figure 11 in Chapter 2 of this dissertation), most DIC would be in the form of CO_2 and thus ebullition from the sediments during retrieval provides a possible explanation for missing downcore DIC. These data show that the Guaymas sediments are a highly dynamic, DIC and methane-rich sedimentary habitat where numerous physical and chemical processes that cannot be systematically disentangled impact DIC and methane gradients at any given sampling site.

Sharply decreasing sulfate concentration profiles characterize the surface layers of all four cores, suggesting that sulfate reduction may be a dominant microbial process in very hot sediments. Three out of four cores present sulfate concentration profiles that decrease from a bottom water concentration of presumably 27-28 mM to nearly 0 mM while core 4572-18 is again the outlier, decreasing to a local minimum of 8 mM around 10 cm depth. Interestingly, at depths below the troughs of sulfate depletion in every core sulfate concentrations increase either slightly (cores 4562-3 and 4573-16) or considerably (cores 4572-18 and 4565-3) with increasing depth. This observation is consistent with previous studies of sulfur cycling in Guaymas Basin, where sulfate concentration profiles appear to be impacted by subsurface hydrothermal circulation and mixing and are not controlled by diffusion (Weber and Jorgensen, 2002; Elsgaard et al., 1994). Due to the prevalence of downcore increases in sulfate concentrations—which, including this study, have been observed in at least nine cores at Guaymas Basin (Biddle et al., 2012; McKay et al., 2012)—we hypothesize that dynamic circulation processes in shallow Guaymas sediments may replenish deeper sediments with seawater sulfate, and overprint microbial sulfate consumption. Microbially generated sulfate depletion re-emerges in cooler sediments with attenuated hydrothermal circulation and mixing. Support for this hypothesis is evident when core 4572-18 is considered together with two other cores making a three-core

transect across a *Beggiatoa* mat; as sediments become cooler away from the center of the mat, sulfate concentration minima move deeper (McKay et al., 2012). Slight increases in sulfate concentrations towards the bottom layers of cores 4562-3 and 4573-16 may result from seawater intrusion during the sampling process.

Sulfide concentrations are less than 4 mM in all cores, with a maximum concentration 3.3 mM in core 4572-18 at 7.5 cmbsf. In all cores except 4565-3 sulfide increases from low concentrations at the sediment-water interface to higher concentrations as sulfate concentrations decrease. In core 4565-3, which has the most immediate depletion of sulfate at the surface, sulfide concentrations are highest at the surface and decrease steadily downcore. This suggests an extremely active sulfate reducing community in the first few cm of sediment of all cores, but especially in 4565-3. None of the cores exhibit sulfate and sulfide concentration profiles in stoichiometric agreement with one another, which may indicate the presence of elemental or intermediate, partially oxidized sulfur species. The absence of a sulfate-sulfide balance may also result from sequestration of reduced sulfur species by iron, which effectively removes them from the pool of microbially processed sulfur. Lastly, the possibility of hydrothermal sulfide sources means that a stoichiometric balance of sulfate and hydrogen sulfide in the surface sediments is not always a reasonable expectation.

Examination of alpha and beta diversity

RNA extractions, conversions of the V5-V8 region of 16S rRNA to cDNA (crDNA), and subsequent amplifications were attempted at 12 depth horizons of the four cores presented in Figure 13. For every depth where RNA extraction, conversion to cDNA, amplification, and sequencing was successful (grey bars, Figure 13), the directly adjacent deeper layer in each core failed after multiple attempts at a step in the full protocol, or was contaminated with DNA. For

three samples, P1, P7, and P8, RT-PCR product replicates were sequenced to assess uncertainty in coverage of microbial diversity by the chosen extraction, amplification, and sequencing methods. Because universal primers that target both archaea and bacteria were utilized, rarefaction alpha diversity (observed OTU method) analysis and PCA beta diversity analysis were performed together on bacteria and archaea for all samples including replicates according to observed OTUs (3% threshold) (Figure 14).

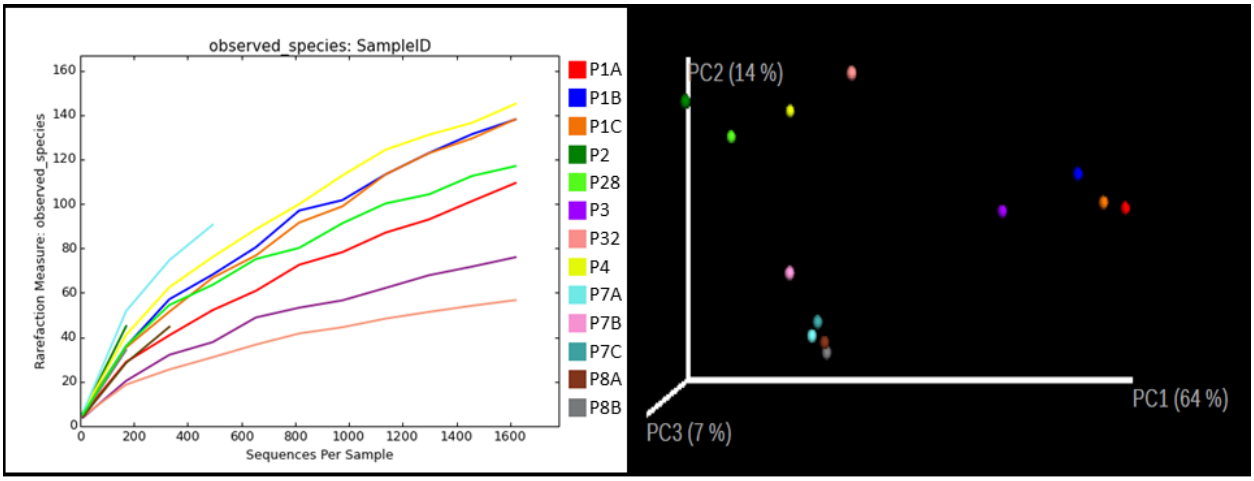

Figure 14. Observed OTU rarefaction (A) and PCA of beta diversity (B) for all samples including replicates.

Rarefaction curves do not reach saturation for any samples indicating that total diversity was not fully sampled. Chao1 estimates of species richness for each sample are listed separately for archaea and bacteria (Table 3). According to the Chao1 estimates of species richness archaeal diversity increases in the following sample order, starting with the least diverse sample and ending with the most diverse: P3, P8, P32, P2, P4, P7, P1, P28. Bacterial diversity increases in the following order: P28, P32, P2, P3, P8, P7, P1, P4. The percentage of OTU richness sequenced was estimated by dividing the observed OTUs by the Chao1-predicted OTU number in each sample, and demonstrates that archaeal diversity was relatively well-sequenced in each sample (>50%) while samples P2 and P3 were poorly sequenced in terms of bacterial diversity

(<50%) (Table 3). Coverage of bacterial diversity was particularly poor in sample P2 (27%) as only 13 sequences were recovered. This sample was dominated by archaeal sequences which covered 58% of estimated archaeal diversity.

	ARC+BAC Sequence #	ARC+BAC Observed OTUs (3%)	ARC+BAC Chao1	ARC+BAC Obs/Chao1	ARC Sequence #	ARC Observed OTUS (3%)	ARC Chao1	ARC Obs/Chao1	BAC Sequence #	BAC Observed OTUS (3%)	BAC Chao1	BAC Obs/Chao1
P1-combined	**8594**	**n/a**	**n/a**	**n/a**	**1464**	**49.0**	**96.3**	**0.5**	**7130**	**63.2**	**136.5**	**0.5**
P1A	3144	109.4	235.2	0.5	n/a	n/a	n/a	n/a	n/a	n/a	n/a	n/a
P1B	3336	138.0	286.7	0.5	n/a	n/a	n/a	n/a	n/a	n/a	n/a	n/a
P1C	2735	138.1	282.0	0.5	n/a	n/a	n/a	n/a	n/a	n/a	n/a	n/a
P2	**277**	**45.0**	**89.6**	**0.5**	**264**	**37.3**	**64.4**	**0.6**	**13**	**9.2**	**33.8**	**0.3**
P3	**1446**	**76.0**	**183.6**	**0.4**	**219**	**20.5**	**26.8**	**0.8**	**1227**	**23.6**	**57.2**	**0.4**
P4	**3437**	**145.0**	**286.4**	**0.5**	**2608**	**51.1**	**86.1**	**0.6**	**829**	**93.0**	**148.8**	**0.6**
P28	**2095**	**117.0**	**208.5**	**0.6**	**2041**	**69.0**	**120.4**	**0.6**	**54**	**3.6**	**6.1**	**0.6**
P32	**3319**	**56.7**	**96.7**	**0.6**	**2075**	**25.4**	**48.7**	**0.5**	**1244**	**13.2**	**18.8**	**0.7**
P7-combined	**598**	**n/a**	**n/a**	**n/a**	**460**	**55.3**	**86.5**	**0.6**	**138**	**43.1**	**72.3**	**0.6**
P7A	539	90.6	155.8	0.6	n/a	n/a	n/a	n/a	n/a	n/a	n/a	n/a
P7B	54	6.9	14.9	0.5	n/a	n/a	n/a	n/a	n/a	n/a	n/a	n/a
P7C	72	6.3	12.3	0.5	n/a	n/a	n/a	n/a	n/a	n/a	n/a	n/a
P8-combined	**628**	**n/a**	**n/a**	**n/a**	**488**	**22.4**	**39.1**	**0.6**	**140**	**39.7**	**63.8**	**0.6**
P8A	456	44.7	80.1	0.6	n/a	n/a	n/a	n/a	n/a	n/a	n/a	n/a
P8B	226	34.2	122.7	0.3	n/a	n/a	n/a	n/a	n/a	n/a	n/a	n/a

Table 3. Recovery of total, archaeal, and bacterial sequences, Chao1 OTU richness estimates, and coverage of diversity for all samples. To achieve the highest possible sequence numbers, replicate samples were combined following initial analyses of alpha and beta diversity (Figure 14). Separated archaeal and bacterial Chao1 and diversity coverage are therefore presented for samples after replicates were combined and not presented separately for replicate samples.

A PCA plot of beta diversity between all samples including replicates demonstrates the likeness of samples according to initial taxonomic assignments of OTUs by UCLUST (Edgar, 2010) within each sample (Figure 14B). Even though sample P1 has the greatest estimated species richness, replicate samples P1A, P1B, and P1C still cluster more closely with each other

than with any other sample. Replicate samples from P7 and P8 all cluster tightly together except for P7B, which only had a total sequence recovery of 54. Elevated beta diversity between replicates of sample P7 is probably an artifact of relatively low sequence numbers in a highly diverse sediment horizon. The tight clustering of P7A,C and P8A,B replicate samples is not surprising given that these come from two adjacent sediment layers. Interestingly, this is not always the case; sample P3 and replicates of sample P1 are more similar in diversity to each other than to sample P2, located in the intervening sediment layer with distinct carbon and sulfur chemistry (Figure 13). The beta diversity of replicate and non-replicate samples expressed by PCA in Figure 14 thus confirms the suitability of the full protocol—from extraction to sequencing—to draw conclusions from sampled diversity. As a caveat, though, the extreme dissimilarity between sample P2 and adjacent sample P3 indicates that in some cases three-cm sediment intervals may be too coarsely resolved to identify small-scale changes in diversity. Additionally, attempts to assess methodological effects on beta diversity were unsuccessful due to low nucleic acid concentrations and failed sequencing efforts. Future work is needed to evaluate to the extent to which the observed variability reflects a biological response to small-scale variations in the geochemical or thermal environment or is related to methodological variability. Following this initial assessment of alpha and beta diversity, replicate samples were combined to yield the highest possible sequence number for each sediment layer. In other words, samples P1A, B, and C are now referred to as sample P1, samples P7A, B, and C are now P7, and samples P8A and B are now P8. With replicate samples collapsed, jackknifed beta diversity of weighted, normalized sequence information is presented for all samples (Supplementary Figure S8), and indicates variance in diversity between samples with confidence clouds.

Archaeal and bacterial richness versus temperature and electron acceptor availability

Chao1 estimates of sample richness reveal relationships between decreasing predicted OTU numbers, temperature, and porewater sulfate concentration (Figure 15). There is a notable similarity between Chao1 richness of archaea across samples and the corresponding in situ temperatures: as temperatures increase archaeal richness decreases. This suggests the specialization of archaea into relatively few high temperature-associated groups. As hot samples tend to also be deeper samples, it is possible that electron acceptor availability also acts as a control on microbial richness. For archaea, the very high OTU richness estimate of the sample P28, at 9-12 cmbsf where porewater sulfate concentrations are extremely low, indicates that concentration of oxidant has less influence on archaeal species richness than temperature. By contrast, bacterial richness appears to have a stronger relationship with sulfate concentration than in situ temperature. As a caveat, if samples with low bacterial sequence recovery (P2 and P28, indicated by asterisks) are removed from this analysis, it becomes difficult to distinguish whether in situ temperature or porewater sulfate concentration is the more influential factor controlling bacterial richness. Because of the limited number of samples in this study it is also possible that sample P28 is an uncommon outlier in terms of species richness; if so, it remains apparent that sulfate availability and temperature, whether working together or independently from one another, are important controls on microbial richness.

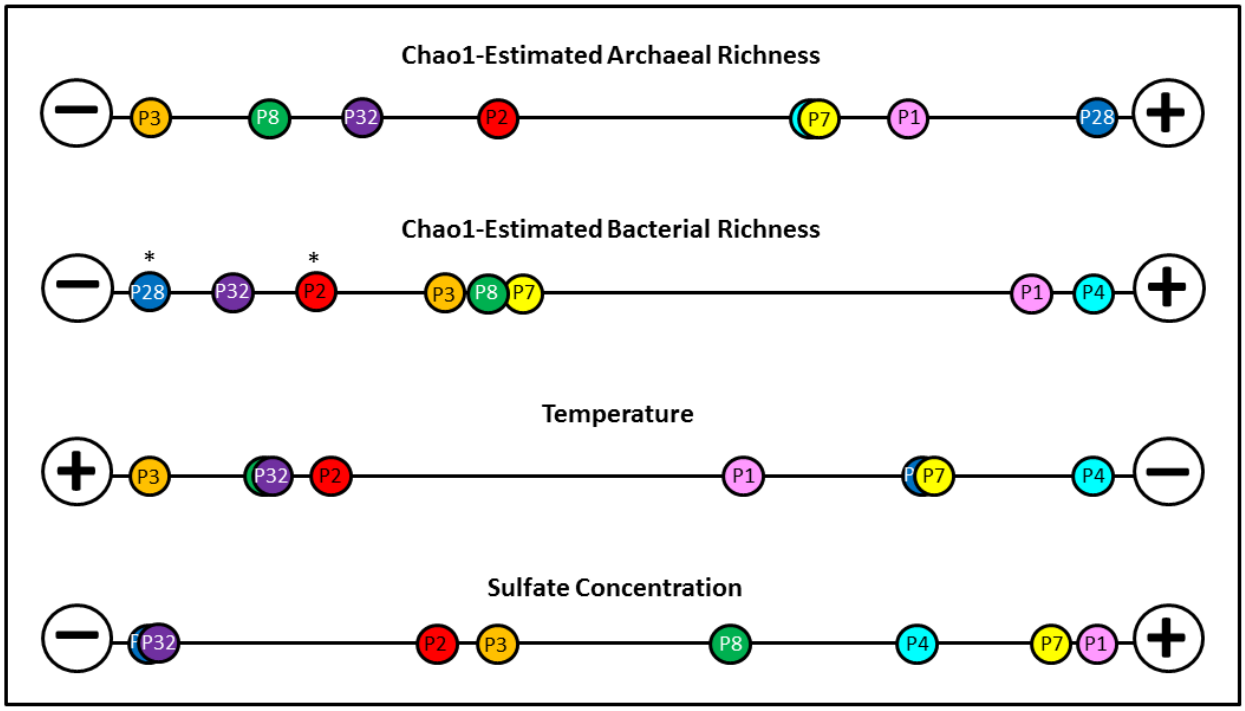

Figure 15. Normalized archaeal and bacterial diversity, temperature, and porewater sulfate concentrations for each sample. Chao1 estimates from table 3 were used for archaeal and bacterial diversity. Two samples with low bacterial sequence numbers (< 100), P28 and P3, are indicated by asterisks. Values were normalized by the highest value within each category, which is represented by the closest sample to the + side of the spectrum while the lowest value is represented by the closest sample to the – end of the spectrum.

Temperature ranges and thermal fluctuations

Because sediment cores were extracted in three-cm intervals, it is more accurate to consider in situ temperatures as a range between the upper and lower depths of a given sediment section. Further, because these are high temperature cores that increase rapidly from ca. 3°C of bottom water to greater than 100°C, the temperature profiles are represented by very steep gradients. Any slight error in assigning depths either to a temperature profile or a corresponding core section may have major consequences in associating a sample with its correct in situ temperature. Further, the temperature profiles presented in Figure 13 must be interpreted as one-time snapshots of a dynamic hydrothermal regime. To explore fluctuations of in situ thermal ranges, 36-cm probes that measured temperatures every five minutes across five depths were

deposited in sediments at sampling sites where cores 4572-18 and 4573-16 would be taken eight days later. Logged temperature data indicate extensive fluctuations in temperatures near the sediment surface of both sampling sites (Figure 16A, B) and relatively stable temperatures in deeper sediments below approximately 15 cm in sediments sampled by core 4572-18 (Figure 16A). Temperatures in the 4-cm surface layer of sediments associated with core 4572-18 fluctuate between 20°C and 40°C, while the temperature logger associated with the hottest core, 4573-16, reached temperatures above the maximum detection limit for all depths beyond the 4-cm surface layer; here, in situ temperatures fluctuated between 40°C and 60°C over eight days (Figure 16B).

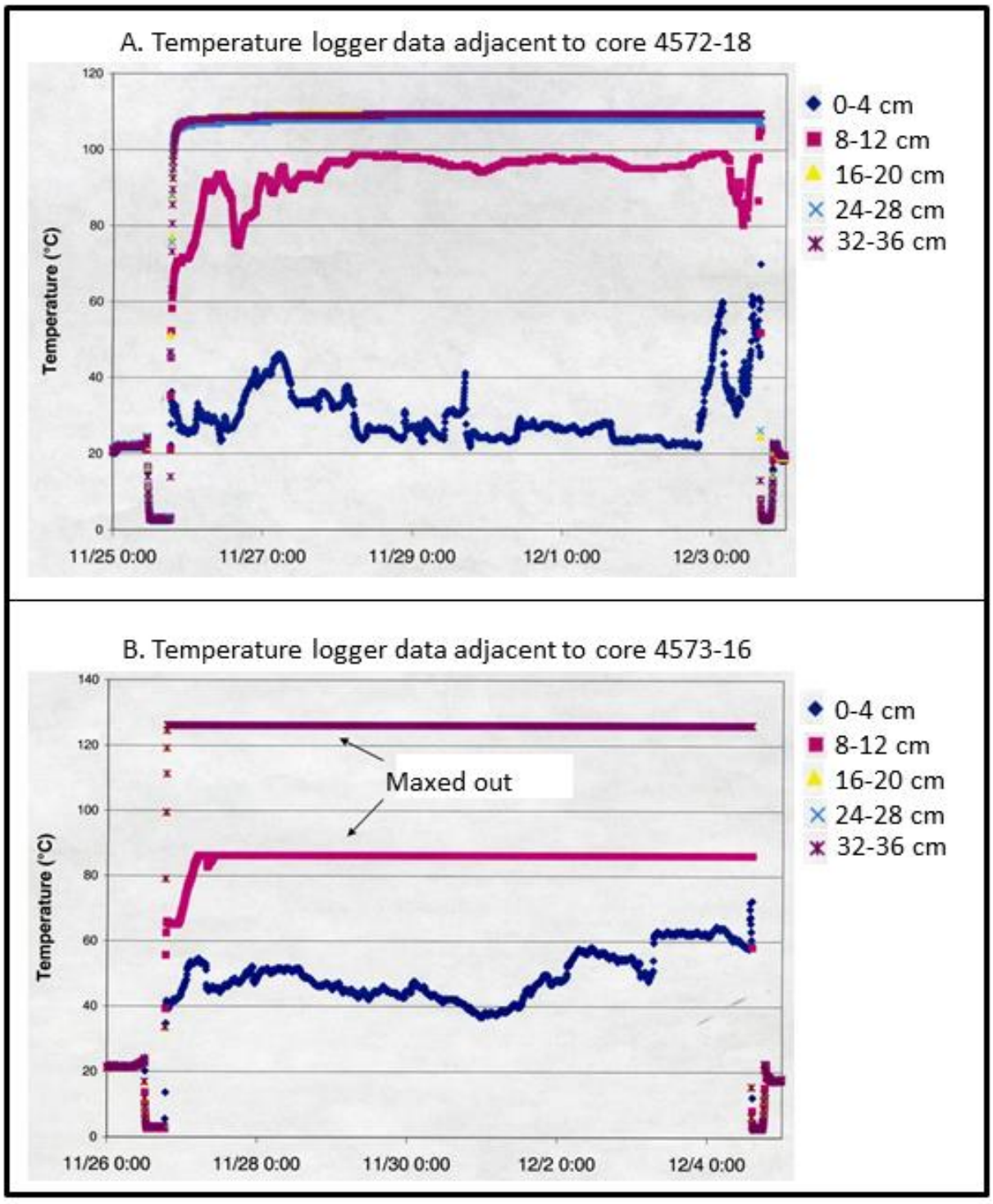

Figure 16A, B. Time-series temperatures profiles that recorded temperatures every five minutes over the course of 8 days. Temperature logging probes were deployed at sites corresponding to two of the four cores sampled: 4572-18 and 4573-16. For the latter, only the upper most thermistor was able to record because all deeper thermistors were associated with in situ temperatures beyond the upper detection limit at 125°C. Although the 8-12cm-depth thermistor

from the 4573-16 logger reads a temperature of approximately 90°C, this should not be assumed as the in situ temperature but rather the last recorded temperature before the thermistor failed. Examination of the one-time temperature profile for 4573-16 in Figure 13 demonstrates that the temperature at a depth of 8-12cm is well above 125°C. After eight days of temperature logging, sediment cores were retrieved from sites directly adjacent to the probes, which caused the temperature disturbances seen at the end of the time-series in both probes.

Sample P3, from a depth of 9-12 cmbsf in core 4572-18, represents the highest temperature sample with successful RNA recovery for which a thermal range can be relatively well-identified. Temperatures recorded by thermistors at 0-4 cm, 8-12 cm, 16-20cm depth within the temperature logging probe were assumed to represent the midpoint depth of each range (i.e., 2cm, 10cm, 18cm), as the interior thermistor most likely recorded the average temperature between the top and bottom of the metal thermistor housing.

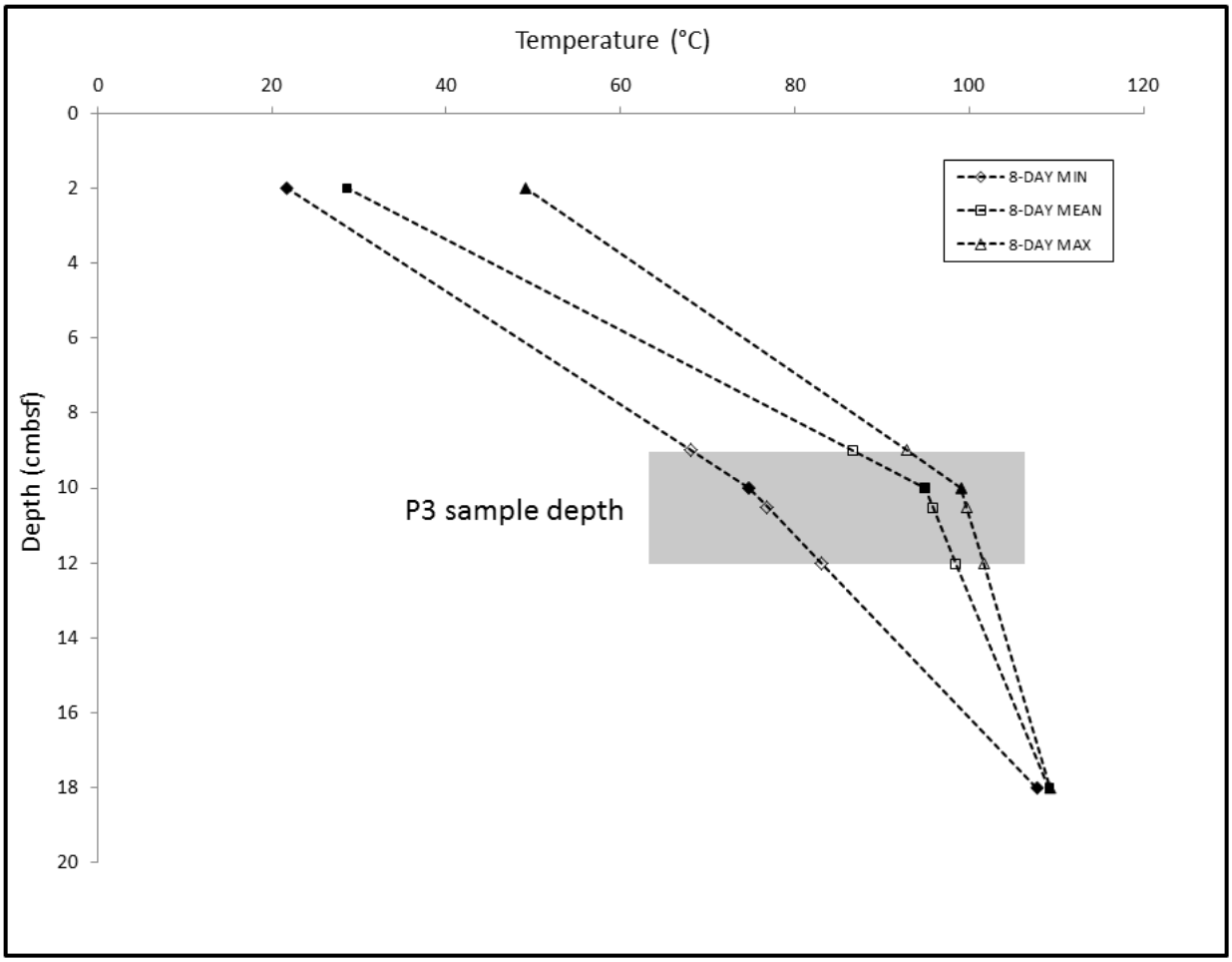

Figure 16C. Minimum in situ temperatures (filled diamonds), mean in situ temperatures (filled squares), and maximum in situ temperatures (filled triangles) are shown for the midpoint depths—2, 10 and 18 cm—of the upper three temperature sensors, over the 8-day temperature logging period. Interpolated minimum (open diamonds), mean (open squares), and maximum (open triangles) temperatures for sediments associated with the 9-12 cm section of core 4572-18 (at 9cm, 10.5cm, and 12cm) indicate a wide range of in situ temperatures.

Minimum, maximum, and mean temperatures over the eight-day logging period are plotted for 2cm, 10cm, and 18cm sediment depth (Figure 16C). Conservatively assuming that all RNA recovered from the 9 to 12-cm sediment section of 4572-18 was from the shallowest (and coolest) end of that range (i.e., 9cmbsf), interpolated temperatures indicate a minimum temperature of 68.1°C, a mean temperature of 86.6°C, and a maximum temperature of 92.9°C would have been experienced by the RNA-implicated microorganisms at this depth over the eight day logging period. However, if recovered RNA is assumed to have been from the 10.5-cmbsf midpoint of sample P3, minimum, mean, and maximum temperatures would be 76.8°C, 95.8°C, and 99.7°C, respectively. And, if the deepest extent of sample P3 (12cmbsf) yielded any RNA after the extraction, the eight-day temperature minimum, mean, and maximum experienced by microorganisms at that depth would be 83.0°C, 98.4°C, and 101.7°C, respectively, although this is unlikely since no RNA was recovered from the next deepest sediment section (12-15cmbsf). All three in situ temperature ranges for sample P3 from 9-12cmbsf in core 4572-18, from which rRNA was successfully reverse-transcribed and sequenced, increase the upper thermal extent of RNA based detection of life at high temperatures.

16S rRNA sequence recovery and taxonomic classifications

After extensive filtering of the sequence dataset 454-pyrosequencing of 16S rcDNA yielded 20,394 total sequences with assignable taxonomies within either the archaeal (9,619 sequences) or bacterial (10,775 sequences) domains. For six out of the eight samples the

majority of recovered sequences were archaeal with a bacterial majority only in samples P1 and P3 (Figure 17). Total (archaeal + bacterial) sequence numbers were greatest for samples P1 (8594), P3 (1446), P4 (3437), P28 (2095), and P32 (3319) and relatively low for samples P2 (277), P7 (598), and P8 (628) (Table 3). With 1464 archaeal sequences and 7130 bacterial sequences sample P1 yielded the highest sequence numbers accounting for 42% of total sequence recovery. With the lowest sequence recovery, sample P2 yielded 264 archaeal sequences and only 13 bacterial sequences, indicated by its estimated poor coverage of bacterial diversity at 27%.

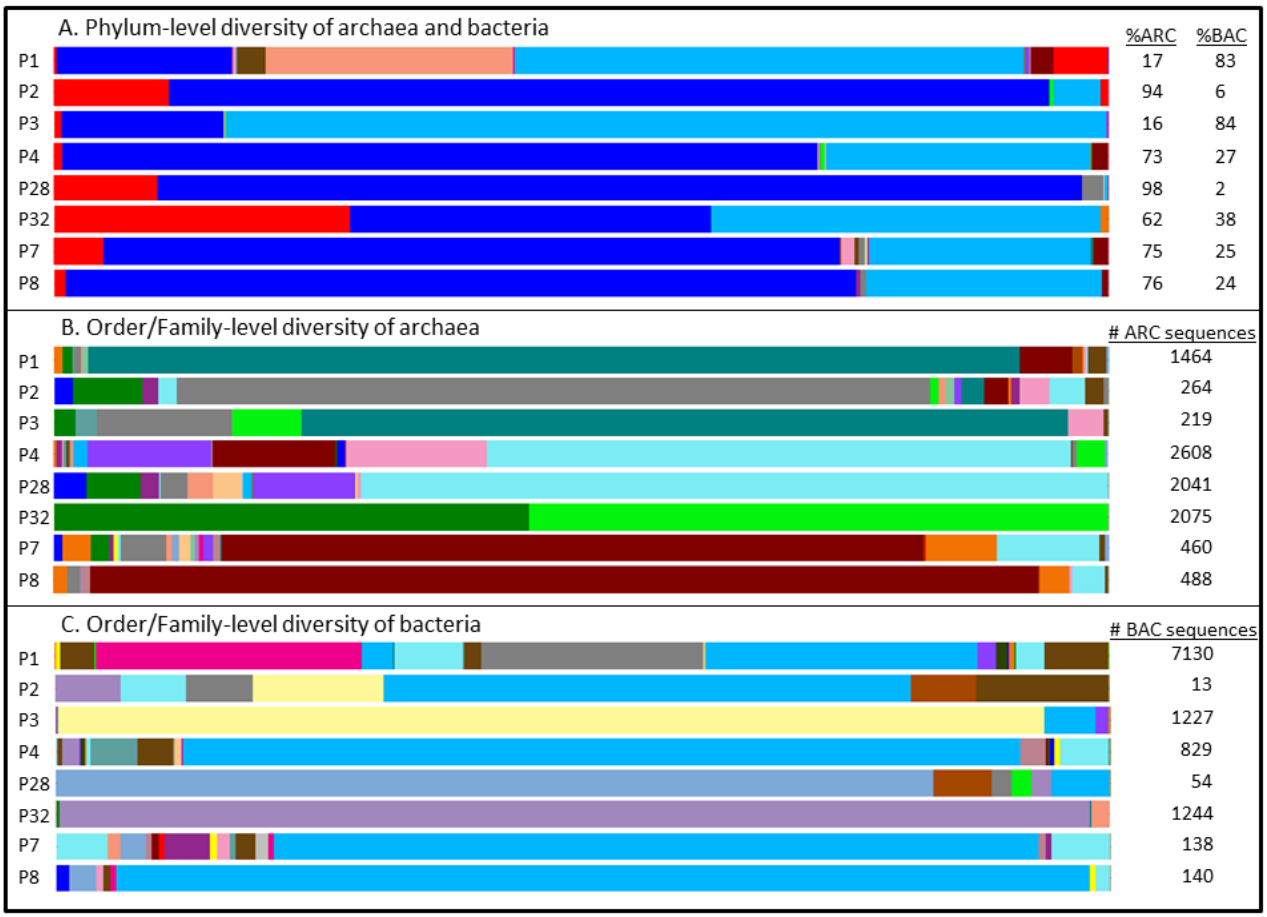

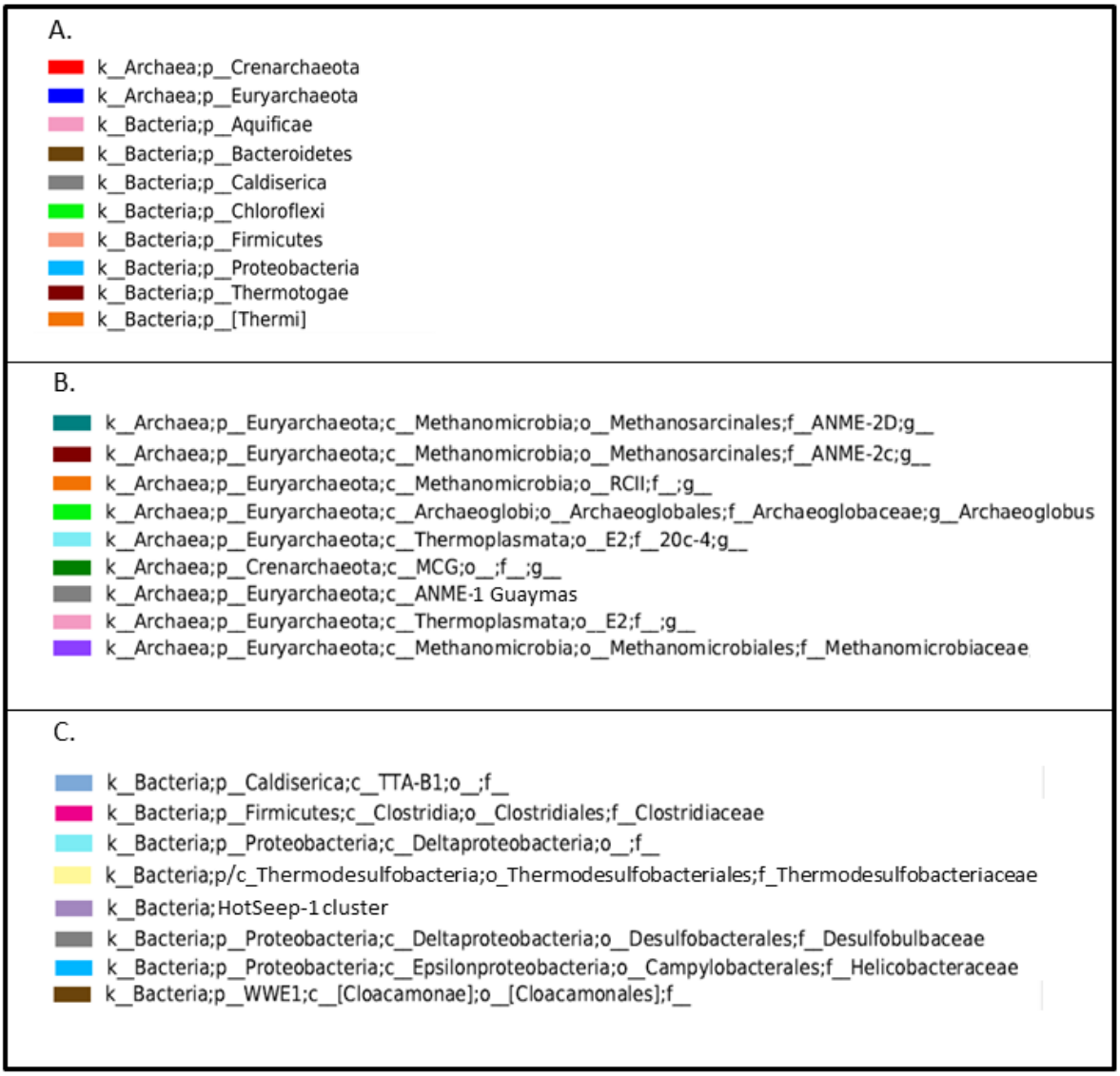

Figure 17. Relative distribution of OTU assignment according to sequence number for archaea and bacteria (A), just archaea (B), and just bacteria (C). In the interest of space, legends of taxonomic groups and associated colors only indicate dominant or significantly occurring (> 5% relative distribution) archaeal and bacterial groups. Full legends can be found as supplementary figures.

Archaeal diversity was dominated by members of the phylum Euryarchaeota, and particularly by anaerobic methane processing microorganisms such as ANME-1 Guaymas (Biddle et al., 2012; chapter two of this dissertation), ANME-2c (Orphan et al., 2001), *Methanomicrobiaceae* (Whitman et al., 2006), and *Methanoperedenaceae* (Haroon et al., 2013),

which is closely related to ANME-2d (Mills et al., 2004) and GoM Arc-1 archaea (Lloyd et al., 2010) (Supplementary Figure S7A). Closer examination of methane processing archaea shows that ANME-1 Guaymas archaea dominate sample P2 (Figure 18A), which corresponds to geochemical evidence for anaerobic methane oxidation (decreasing methane concentration and increasing δ^{13}C-methane values towards the sediment surface), organic matter remineralization (local DIC maximum and δ^{13}C-DIC minimum at 10 cm depth), and sulfate reduction (local sulfate minimum and sulfide maximum at 10 cm depth). The ANME-1 Guaymas archaea represent a separate phylogenetic lineage distinct from the widely distributed ANME-1a and -b Guaymas groups (Biddle et al., 2012; Merkel et al., 2013); consistent with their occurrence here, previous ANME-1 Guaymas recovery has been associated with high temperatures (Biddle et al., 2012; chapter two of this dissertation) and low sulfate concentrations (Yanagawa et al., 2014). On either side of this sediment layer, in samples P1 and P3, the archaeal community is dominated by the ANME-2D/GoM Arc-1/*Methanoperedenaceae* group. Family-level *Candidatus Methanoperedenaceae* contains a recently enriched ANME-2D lineage capable of anaerobic methane oxidation coupled to denitrification by a syntrophic partnership (Haroon et al., 2014) as well as other nitrate reducing methane oxidizers (Raghoebarsing et al., 2006; Hu et al., 2009). The archaeal shift from ANME-1 Guaymas in sample P2 to *Methanoperedenaceae* in samples P1 and P3 is striking. This differentiation of methane-processing archaea into closely-spaced but distinct niches with different populations could be driven by electron acceptor availability. Using sulfate as a proxy for total electron acceptor availability it is apparent that sediments corresponding to sample P2 are relatively depleted in oxidant. The *Methanoperedenaceae*-related archaea may be restricted to sediments with sufficient electron acceptor availability, above and below the localized sulfate minimum.


UnlA1509, AF419635, uncultured archaeon, Teske A.;
UnlA1687, AJ890142, uncultured archaeon, fos0626f11, Meyerdierk
Unl0x1o5, HQ588676, uncultured archaeon, AMSMV−25−A2, Pachiadaki
Unl02ckl, FJ404024, uncultured archaeon, 40H−260S−3, Zhang L.;
UnlA1980, AJ578115, uncultured archaeon, HydBeg125, Knittel K.
UnlA1889, AF354131, uncultured archaeon, 1438, Orphan V.J
NzgP4364, ARB_A527DDC0, denovo375 P4_3643 1..540
NzgP4440, ARB_75FA8A49, denovo361 P4_440 1..506
UnlA1688, AF354129, uncultured archaeon, 1447, Orphan V.J
NzgP4158, ARB_2452E489, denovo76 P4_15826 1..336
NzgP2713, ARB_1227A4D6, denovo91 P28_5412 1..528
NzgP4454, ARB_A9A2A49B, denovo873 P4_4548 1..410
NzgP8115, ARB_3299461C, denovo388 P8_11550 1..411
NzgP8215, ARB_261AB42E, denovo773 P8_21582 1..418
NzgP8160, ARB_9B8A5FAF, denovo373 P8_16056 1..409
NzgP8165, ARB_85760CC7, denovo295 P8_16538 1..510
NzgP7369, ARB_423CD574, denovo345 P7_369 1..417
UnlA1961, AF419650, uncultured archaeon, Teske A.;
NzgP7247, ARB_9CCB1693, denovo32 P7_2471 1..416
UnlA1798, AF419644, uncultured archaeon, Teske A.;
NzgP8569, ARB_18C8D19E, denovo813 P8_5691 1..334 (P1 = 65, P7 = 304, P8 = 440)
NzgP1290, ARB_3BCDF871, denovo450 P1_29005 1..440
ANME−2a,b
ANME-2c
BXXMahi4, M59133, Methanohalophilus mahii, Rouviere P
NzgP1147, ARB_3BA1685D, denovo747 P1_1474 1..392
MhdBurt4, X65537, Methanococcoides burtonii, Franzmann
MhrAcet5, M59137, Methanosarcina acetivorans, Rouviere P
Mt2Blatt, AJ238002, Methanimicrococcus blatticola, Sprenger W
Methanosarcinales
D49Sheng, DQ787474, Methermicoccus shengliensis, Cheng L.;
UnlA3197, AY835420, uncultured archaeon, 7A08, Dhillon A.
NzgP4263, ARB_A322617D, denovo312 P4_26384 1..335
NzgP4261, ARB_BB11C39B, denovo1004 P4_26178 1..475
NzgP4912, ARB_E4D3611E, denovo228 P4_9123 1..440
MhsHaru2, AY817738, Methanosaeta harundinacea, Ma K.; Liu
Methanosaeta
NzgP1112, ARB_957ED5F1, denovo907 P1_11518 1..345
NzgP1279, ARB_B19C2EF9, denovo763 P1_27949 1..444
NzgP1443, ARB_2BB9D1D8, denovo27 P1_443 1..44 (P3 = 88, P1 = 1287)
NzgP3373, ARB_F4CE84EE, denovo156 P2_1, P3_87
Unl02y72, FJ712371, uncultured archaeon, KZNMV−5−A21, Pachiadaki
NzgP1146, ARB_E9CE0DA1, denovo553 P1_14675 1..331
NzgP1283, ARB_1BEE4EA8, denovo269 P1_28313 1..381
NzgP1690, ARB_A422A02D, denovo751 P1_6903 1..414
NzgP1166, ARB_E4E075D1, denovo860 P1_16603 1..414
Unl0e2gt, FR682483, uncultured archaeon, GUAY_37enr_Arch23, Holler T.;
UnlA4271, DQ521782, uncultured archaeon, SMI1−GC205−Arc66, Lloyd K.G.
NzgP3142, ARB_9026CED1, denovo282 P3_3885 1..451 (P3 = 88)
UnlA1893, AF356643, uncultured archaeon, G72_C12, Longnecker
0016s000, ARB_89A0DB55, 2515322110 16S rRNA Archaeal SSU [Methanoperedens
Methanoperedenaceae
UnlGre18, AF293017, uncultured Green Bay ferromanganous micronodule ar, ARC3, Stein L.Y.
MeaPalud, AB196288, Methanocella paludicola SANAE, Sakai S.;
UnlA1950, AJ578125, uncultured archaeon, BS−K−E9, Knittel K.
NzgP1297, ARB_71D47DF3, denovo890 P1_29746 1..404
Methanocellales
NzgP2668, ARB_6E523FA6, denovo37 P28_21532 1..388
NzgP4160, ARB_1634DEFC, denovo689 P4_16045 1..405
MspHung2, AY196683, Methanospirillum hungatei, Wright A.D
NzgP2891, ARB_26221AE7, denovo208 P28_26408 1..474
NzgP4242, ARB_8CCF0333, denovo628 P4_24025 1..471
MhnMari5, M59134, Methanoculleus marisnigri, Rouviere P
NzgP4264, ARB_4A2A2140, denovo448 P4_269 1..370
NzgP2674, ARB_825673F8, denovo507 P28_22145 1..413
NzgP2899, ARB_EA157AB4, denovo29 P28_30357 1..519
NzgP4292, ARB_22D710E1, denovo353 P4_29250 1..452
NzgP2719, ARB_BCC3FB2, denovo99 P28_10865 1..450 (P28 = 41, P4 = 338)
NzgP2669, ARB_A22D5D33, denovo418 P28_22704 1..341
NzgP2709, ARB_20E5B175, denovo852 P28_27747 1..447
CZROrgan, M59131, Methanogenium organophilum, Rouviere P
NzgP4362, ARB_AC60B381, denovo521 P4_363 1..368
MpnLimi2, M59143, Methanoplanus limicola, Rouviere P
MtcHalot, AF033672, Methanocalculus halotolerans, Ollivier B
NzgP7132, ARB_CE76C14B, denovo274 P7_13240 1..505
Methanomicrobiales
NzgP2673, ARB_BF682889, denovo493 P28_9588 1..478
NzgP2703, ARB_667A1F18, denovo801 P28_27712 1..463
UnlA1689, AF354137, uncultured archaeon, 1447, Orphan V.J
UnlA2124, AJ578120, uncultured archaeon, HydCal52, Knittel K.
NzgP2890, ARB_1C6AA4F8, denovo167 P28_12008 1..417
NzgP2671, ARB_2E11BBB, denovo433 P28_14335 1..477
NzgP2898, ARB_3D7427A7, denovo287 P28_6941 1..471
NzgP1296, ARB_F8FC119D, denovo386 P1_29608 1..445
UnlA1930, AF419624, uncultured archaeon, Teske A.;
NzgP1120, ARB_B464A7B2, denovo908 P1_12044 1..471
UniArc14, AB019758, unidentified archaeon, pISA16, Takai K.;
NzgP1178, ARB_B0B88286, denovo911 P1_17837 1..403
NzgP4215, ARB_4F3B2173, denovo158 P4_21570 1..399
NzgP2708, ARB_4D3DFA29, denovo835 P2_28578 1..430
UnlA1958, AF419626, uncultured archaeon, Teske A.;
NzgP2657, ARB_107078F3, denovo224 P2_14421 1..430
Unl0e2h1, FR682491, uncultured archaeon, GUAY_50enr_Arch79, Holler T.;
UnlA1501, AF419654, uncultured archaeon, Teske A.;
Unl0e2gz, FR682490, uncultured archaeon, GUAY_50enr_Arch41, Holler T.;
UnlA1486, AF356640, uncultured archaeon, G72_C2, Longnecker
NzgP7545, ARB_7E409D97, denovo918 P7_545 1..426
NzgP7654, ARB_DD6EED0C, denovo342 P7_6545 1..440
NzgP7128, ARB_B1E94447, denovo1016 P7_12823 1..348
NzgP7232, ARB_61C25BF2, denovo308 P7_23206 1..353
NzgP1288, ARB_94C046E4, denovo255 P1_28810 1..385
ANME-1
Methanobacteriales
NzgDP322, ARB_398A84BE, denovo6 P3_62 1..335
NzgP2884, ARB_BF9C6937, denovo643 P2_2467 1..45 (P2 = 169)
UnlA1743, AF419655, uncultured archaeon, Teske A.;
UnlA1931, AF419632, uncultured archaeon, Teske A.;
NzgP2688, ARB_4488B1C9, denovo614 P2_2282 1..416
NzgP3147, ARB_4D511252, denovo550 P3_147 1..363
ANME-1 Guaymas
AcgVene2, Y10011, Archaeoglobus veneficus, Huber H.;
NzgP3178, ARB_1CCC078F, denovo175 P3_17857 1..551
AcgLitho, AJ299218, Archaeoglobus lithotrophicus, Boucher Y.
AcgFulg3, X05567, Archaeoglobus fulgidus, Achenbach−
AcgProf4, CP001857, Archaeoglobus profundus DSM 5631, von Jan M.
FgbPlac3, CP001899, Ferroglobus placidus DSM 10642, Lucas S.;
NzgP3259, ARB_9919EEB4, denovo649 P32_11752 1..429
NzgP3298, ARB_2256F69A, denovo159 P32_980 1..457 (P32 = 1129)
NzgP3260, ARB_40C0A96A, denovo659 P32_24672 1..352
Archaeoglobales
Methanococcales
0.10

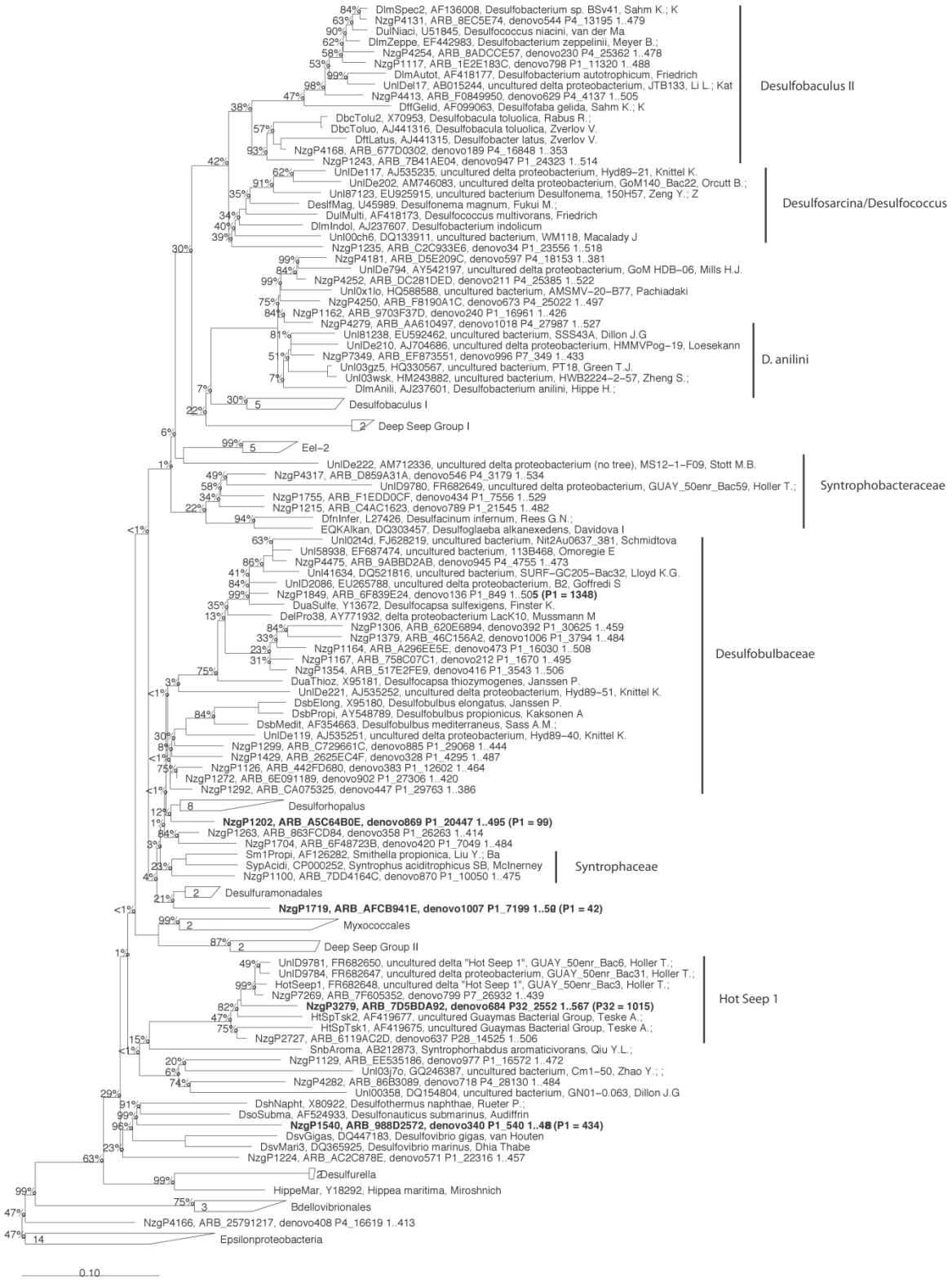
DlmSpec2, AF136008, Desulfobacterium sp. BSv41, Sahm K.; K
NzgP4131, ARB_8EC5E74, denovo544 P4_13195 1..479
DulNiaci, U51845, Desulfococcus niacini, van der Ma
DlmZeppe, EF442983, Desulfobacterium zeppelinii, Meyer B.;
NzgP4254, ARB_8ADCCE57, denovo230 P4_25362 1..478
NzgP1117, ARB_1E2E183C, denovo798 P1_11320 1..488
DlmAutot, AF418177, Desulfobacterium autotrophicum, Friedrich
UnlDel17, AB015244, uncultured delta proteobacterium, JTB133, Li L.; Kat
NzgP4413, ARB_F0849950, denovo629 P4_4137 1..505
DffGelid, AF099063, Desulfofaba gelida, Sahm K.; K
DbcTolu2, X70953, Desulfobacula toluolica, Rabus R.;
DbcToluo, AJ441316, Desulfobacula toluolica, Zverlov V.
DftLatus, AJ441315, Desulfobacter latus, Zverlov V.
NzgP4168, ARB_677D0302, denovo189 P4_16848 1..353
NzgP1243, ARB_7B41AE04, denovo947 P1_24323 1..514
Desulfobaculus II
UnlDe117, AJ535235, uncultured delta proteobacterium, Hyd89–21, Knittel K.
UnlDe202, AM746083, uncultured delta proteobacterium, GoM140_Bac22, Orcutt B.;
Unl87123, EU925915, uncultured bacterium Desulfonema, 150H57, Zeng Y.; Z
DeslfMag, U45989, Desulfonema magnum, Fukui M.;
DulMulti, AF418173, Desulfococcus multivorans, Friedrich
DlmIndol, AJ237607, Desulfobacterium indolicum
Unl00ch6, DQ133911, uncultured bacterium, WM118, Macalady J
NzgP1235, ARB_C2C933E6, denovo34 P1_23556 1..518
Desulfosarcina/Desulfococcus
NzgP4181, ARB_D5E209C, denovo597 P4_18153 1..381
UnlDe794, AY542197, uncultured delta proteobacterium, GoM HDB–06, Mills H.J.
NzgP4252, ARB_DC281DED, denovo211 P4_25385 1..522
Unl0x1lo, HQ588588, uncultured bacterium, AMSMV–20–B77, Pachiadaki
NzgP4250, ARB_F8190A1C, denovo673 P4_25022 1..497
NzgP1162, ARB_9703F37D, denovo240 P1_16961 1..426
NzgP4279, ARB_AA610497, denovo1018 P4_27987 1..527
Unl81238, EU592462, uncultured bacterium, SSS43A, Dillon J.G
UnlDe210, AJ704686, uncultured delta proteobacterium, HMMVPog–19, Loesekann
NzgP7349, ARB_EF873551, denovo996 P7_349 1..433
Unl03gz5, HQ330567, uncultured bacterium, PT18, Green T.J.
Unl03wsk, HM243882, uncultured bacterium, HWB2224–2–57, Zheng S.;
DlmAnili, AJ237601, Desulfobacterium anilini, Hippe H.;
D. anilini
Desulfobaculus I
Deep Seep Group I
Eel–2
UnlDe222, AM712336, uncultured delta proteobacterium (no tree), MS12–1–F09, Stott M.B.
NzgP4317, ARB_D859A31A, denovo546 P4_3179 1..534
UnlD9780, FR682649, uncultured delta proteobacterium, GUAY_50enr_Bac59, Holler T.;
NzgP1755, ARB_F1EDD0CF, denovo434 P1_7556 1..529
NzgP1215, ARB_C4AC1623, denovo789 P1_21545 1..482
DfnInfer, L27426, Desulfacinum infernum, Rees G.N.;
EQKAlkan, DQ303457, Desulfoglaeba alkanexedens, Davidova I
Syntrophobacteraceae
Unl02t4d, FJ628219, uncultured bacterium, Nit2Au0637_381, Schmidtova
Unl58938, EF687474, uncultured bacterium, 113B468, Omoregie E
NzgP4475, ARB_9ABBD2AB, denovo945 P4_4755 1..473
Unl41634, DQ521816, uncultured bacterium, SURF–GC205–Bac32, Lloyd K.G.
UnlD2086, EU265788, uncultured delta proteobacterium, B2, Goffredi S
NzgP1849, ARB_6F839E24, denovo136 P1_849 1..505 (P1 = 1348)
DuaSulfe, Y13672, Desulfocapsa sulfexigens, Finster K.
DelPro38, AY771932, delta proteobacterium LacK10, Mussmann M
NzgP1306, ARB_620E6894, denovo392 P1_30625 1..459
NzgP1379, ARB_46C156A2, denovo1006 P1_3794 1..484
NzgP1164, ARB_A296EE5E, denovo473 P1_16030 1..508
NzgP1167, ARB_758C07C1, denovo212 P1_1670 1..495
NzgP1354, ARB_517E2FE9, denovo416 P1_3543 1..506
DuaThioz, X95181, Desulfocapsa thiozymogenes, Janssen P.
UnlDe221, AJ535252, uncultured delta proteobacterium, Hyd89–51, Knittel K.
DsbElong, X95180, Desulfobulbus elongatus, Janssen P.
DsbPropi, AY548789, Desulfobulbus propionicus, Kaksonen A
DsbMedit, AF354663, Desulfobulbus mediterraneus, Sass A.M.;
UnlDe119, AJ535251, uncultured delta proteobacterium, Hyd89–40, Knittel K.
NzgP1299, ARB_C729661C, denovo885 P1_29068 1..444
NzgP1429, ARB_2625EC4F, denovo328 P1_4295 1..487
NzgP1126, ARB_442FD680, denovo383 P1_12602 1..464
NzgP1272, ARB_6E091189, denovo902 P1_27306 1..420
NzgP1292, ARB_CA075325, denovo447 P1_29763 1..386
Desulfobulbaceae
Desulforhopalus
NzgP1202, ARB_A5C64B0E, denovo869 P1_20447 1..495 (P1 = 99)
NzgP1263, ARB_863FCD84, denovo358 P1_26263 1..414
NzgP1704, ARB_6F48723B, denovo420 P1_7049 1..484
Sm1Propi, AF126282, Smithella propionica, Liu Y.; Ba
SypAcidi, CP000252, Syntrophus aciditrophicus SB, McInerney
NzgP1100, ARB_7DD4164C, denovo870 P1_10050 1..475
Syntrophaceae
Desulfuramonadales
NzgP1719, ARB_AFCB941E, denovo1007 P1_7199 1..508 (P1 = 42)
Myxococcales
Deep Seep Group II
UnlD9781, FR682650, uncultured delta "Hot Seep 1", GUAY_50enr_Bac6, Holler T.;
UnlD9784, FR682647, uncultured delta proteobacterium, GUAY_50enr_Bac31, Holler T.;
HotSeep1, FR682648, uncultured delta "Hot Seep 1", GUAY_50enr_Bac3, Holler T.;
NzgP7269, ARB_7F605352, denovo799 P7_26932 1..439
NzgP3279, ARB_7D5BDA92, denovo684 P32_2552 1..567 (P32 = 1015)
HtSpTsk2, AF419677, uncultured Guaymas Bacterial Group, Teske A.;
HtSpTsk1, AF419675, uncultured Guaymas Bacterial Group, Teske A.;
NzgP2727, ARB_6119AC2D, denovo637 P28_14525 1..506
Hot Seep 1
SnbAroma, AB212873, Syntrophorhabdus aromaticivorans, Qiu Y.L.;
NzgP1129, ARB_EE535186, denovo977 P1_16572 1..472
Unl03j7o, GQ246387, uncultured bacterium, Cm1–50, Zhao Y.; ;
NzgP4282, ARB_86B3089, denovo718 P4_28130 1..484
Unl00358, DQ154804, uncultured bacterium, GN01–0.063, Dillon J.G
DshNapht, X80922, Desulfothermus naphthae, Rueter P.;
DsoSubma, AF524933, Desulfonauticus submarinus, Audiffrin
NzgP1540, ARB_988D2572, denovo340 P1_540 1..488 (P1 = 434)
DsvGigas, DQ447183, Desulfovibrio gigas, van Houten
DsvMari3, DQ365925, Desulfovibrio marinus, Dhia Thabe
NzgP1224, ARB_AC2C878E, denovo571 P1_22316 1..457
Desulfurella
HippeMar, Y18292, Hippea maritima, Miroshnich
Bdellovibrionales
NzgP4166, ARB_25791217, denovo408 P4_16619 1..413
Epsilonproteobacteria
0.10


NzgP1157, ARB_F316C8A2, denovo905 P1_15011 1..477
NzgP8398, ARB_B87652D9, denovo1 P8_40, P3_52
NzgP4118, ARB_3DD33886, denovo456 P4_11779 1..412 (P4 = 41)
NzgP8232, ARB_79EF6888, denovo305 P8_2, P3_2
Unl73717, EU570858, uncultured bacterium, Nit2Au0650_128, Schmidtova
NzgP1269, ARB_3C32DA0C, denovo368 P1_26958 1..44 (P1 = 114)
NzgP4179, ARB_E94E4525, denovo1009 P4_17950 1..406
NzgP4243, ARB_EA36AD2, denovo202 P4_24266 1..445
Unl040u1, HQ203810, uncultured bacterium, SW–Oct–105, Bae H.; Le
Unl63589, EU265985, uncultured bacterium Sulfurimonas, Nit2A0626_59, Schmidtova
NzgP8192, ARB_302081C5, denovo169 P8_4, P2_2, P3_2
UnlG2652, FJ497632, uncultured gamma proteobacterium, VS_CL–380, Sudek L.A.
NzgP1256, ARB_B5BDE900, denovo990 P1_2564 1..477
Unl03l49, GQ356998, uncultured bacterium, FeLiveControl_B_16, Beal E.J.;
NzgP1305, ARB_C973AC4A, denovo66 P1_30543 1..481
NzgP1286, ARB_1EEE0924, denovo223 P1_28678 1..354
NzgP4375, ARB_B5D497C4, denovo196 P4_3759 1..338
NzgP4106, ARB_FCB129F8, denovo725 P4_10619 1..477
NzgP4258, ARB_F241757D, denovo779 P4_25245 1..361
NzgP4249, ARB_B82C5A, denovo225 P4_24949 1..425
NzgP1880, ARB_22BA295, denovo564 P1_880 1..580 (P1 = 1467, P3 = 52)
NzgP3984, ARB_3796594C, denovo543 P3_984 1..487
NzgP1858, ARB_97B318C1, denovo35 P1_8582 1..483
NzgP7282, ARB_FFCC32AE, denovo140 P7_2874 1..469
NzgP8285, ARB_C965CFEB, denovo650 P8_28565 1..366
NzgP8450, ARB_179D3671, denovo112 P8_4501 1..469
NzgP1284, ARB_8820313F, denovo394 P1_28842 1..451
NzgP4142, ARB_55E8C820, denovo402 P4_14337 1..465
NzgP8238, ARB_EF9A1665, denovo295 P8_17, P2_1
UnlEp102, AJ575997, uncultured epsilon proteobacterium, T6–Ph07–957, Alain K.;
NzgP4366, ARB_9F73A5B3, denovo941 P4_3666 1..489 (P4 = 105)
NzgP8302, ARB_8B3F15D6, denovo580 P8_30217 1..485
NzgP4116, ARB_4820C90A, denovo150 P4_11494 1..369
NzgP1244, ARB_FD6431A5, denovo95 P1_24610 1..403
NzgP4245, ARB_D96C939F, denovo498 P4_24550 1..451
NzgP4108, ARB_C9B4276, denovo796 P4_10862 1..423
NzgP4995, ARB_7B900C61, denovo84 P4_9958 1..433
NzgP1247, ARB_F25C57A, denovo690 P1_24798 1..424
NzgP8104, ARB_BB3413A8, denovo820 P8_1030 1..487
NzgP8282, ARB_4C49D3C6, denovo729 P8_28232 1..355
NzgP1227, ARB_FE7EB54, denovo928 P1_22297 1..351
NzgP8299, ARB_A0A33C3D, denovo124 P8_29964 1..342
NzgP8116, ARB_4800CABB, denovo822 P8_11691 1..442
NzgP1163, ARB_4B2AEC0A, denovo31 P1_16645 1..458
SlpSpec3, AF357198, Sulfurospirillum sp. Am–N, Campbell B
SlpArcac, Y11561, Sulfurospirillum arcachonense, Finster K.
SlpBarn2, U41564, Sulfurospirillum barnesii, Lonergan D
CamFet32, L04314, Campylobacter fetus, Wesley I.V
NzgP4139, ARB_4317914D, denovo17 P4_13937 1..484
AB189374, uncultured epsilon proteobacterium, JT75–305, Arakawa S.
NzgP7111, ARB_2664FB91, denovo396 P7_11142 1..488
ArcobNit, L14627, Arcobacter nitrofigilis, Wesley I.V
NzgP1128, ARB_114AC65, denovo953 P1_11936 1..474
NzgP1303, ARB_33391CDD, denovo653 P1_30395 1..418
NzgP8181, ARB_7897F553, denovo807 P8_18116 1..506
SlfParal, AB252048, Sulfurimonas paralvinellae, Takai K.;
NzgP8153, ARB_12CD21FB, denovo657 P8_1533 1..500
UnlEp288, AY225615, uncultured epsilon proteobacterium, AT–cs10, Lopez–Garc
NzgP4609, ARB_CE050579, denovo334 P4_6094 1..350
NzgP4234, ARB_90446218, denovo560 P4_23165 1..488
NzgP8103, ARB_E8404CC9, denovo108 P8_25, P2_1, P3_1
NzgP1757, ARB_2501F124, denovo531 P1_7579 1..417
NzgP7266, ARB_95FD7445, denovo645 P7_26634 1..361
NzgP8177, ARB_84EED4B1, denovo36 P8_17764 1..505
SlfDeni5, L40808, Sulfurimonas denitrificans, Muyzer G.;
TcrSpe15, U46506, Thiomicrospira sp. CVO, ARCO29, Voordouw G
NzgP1131, ARB_930DCAB2, denovo488 P1_13197 1..414
NzgP4257, ARB_E519C302, denovo463 P4_25216 1..365 (P4 = 50)
Unl030vj, FJ712606, uncultured bacterium, KZNMV–30–B30, Pachiadaki
NzgP4273, ARB_696901A5, denovo711 P4_27224 1..445
Unl02ye3, FJ712554, uncultured bacterium Epsilonproteo, KZNMV–10–B95, Pachiadaki
SlfAuto2, AB088432, Sulfurimonas autotrophica, Inagaki F.
NzgP4223, ARB_6298256F, denovo18 P4_22373 1..409
NzgP8214, ARB_190949B9, denovo538 P8_21464 1..385
NzgP4931, ARB_E4FC93D1, denovo914 P4_931 1..506 (P1 = 60, P4 = 154)
NzgP7700, ARB_373D2D1, denovo490 P7_7005 1..426
NzgP4164, ARB_67D64299, denovo602 P4_16401 1..420
NzgP1557, ARB_A140EF72, denovo618 P1_5572 1..451
Unl02qkx, FJ497591, uncultured bacterium, VS_CL–339, Sudek L.A.
NzgP4172, ARB_AB40C605, denovo2 P4_17653 1..411
NzgP1144, ARB_AB878DDA, denovo352 P1_1442 1..404
UnlHelic, AB188787, uncultured Helicobacter sp., SB5–24, Fang J.; A
NzgP4143, ARB_13A83680, denovo302 P4_1435 1..495
NzgP4272, ARB_1ADFE1EE, denovo310 P4_2727 1..496
SlcKuji2, AB080645, Sulfuricurvum kujiense, Kodama Y.;
NzgP4305, ARB_5A491AC5, denovo965 P4_3078 1..361
NzgP4395, ARB_B0629320, denovo582 P4_3951 1..497
NzgP4103, ARB_17AEB813, denovo49 P4_10330 1..389
NzgP4217, ARB_9BF7805E, denovo305 P4_21753 1..493
NzgP4259, ARB_F38831FB, denovo920 P4_2553 1..490
NzgP4295, ARB_81B1C311, denovo403 P4_29551 1..407
NzgP4371, ARB_337C3D79, denovo102 P4_3710 1..345
NzgP4480, ARB_7F21203B, denovo410 P4_4807 1..511
NzgP4540, ARB_263B65AC, denovo925 P4_5405 1..475
NzgP4283, ARB_6AF36892, denovo768 P4_28627 1..505
NzgP4325, ARB_74D5F1B4, denovo895 P4_3251 1..502
NzgP1132, ARB_7DE8838C, denovo332 P1_13548 1..499
UnlPro51, AF420345, uncultured proteobacterium, 1–2 cm layer of core A, Teske A.;
SlrLitho, AB091292, Sulfurovum lithotrophicum, Inagaki F.
UnlPro30, AF420358, uncultured proteobacterium, 0–1 cm layer of core C, Teske A.;
NzgP4203, ARB_90BE83D3, denovo812 P4_20315 1..475
NzgP7352, ARB_FAE0D5E8, denovo469 P7_3521 1..494
NzgP4754, ARB_65D89593, denovo184 P4_754 1..474
RcrExoc2, U29081, Rimicaris exoculata ectosymbiont, Polz M.F.;
AvnPomp5, L35523, Alvinella pompejana epibiont, Haddad A.;
NttSalsu, AB175500, Nitratifractor salsuginis, Nakagawa S
NzgP4237, ARB_9B75A698, denovo686 P4_23728 1..331
CmaProfu, AJ535664, Caminibacter profundus, Miroshnich
LebAcidi, AB167820, Lebetimonas acidiphila, Takai K.;
NaiAbyss, AM937002, Nautilia abyssi, Alain K.;
NzgP7196, ARB_A0E5771E, denovo185 P7_19616 1..493
TdcMican, AB175498, Thioreductor micantisoli, Nakagawa S
HdrTherm, AB105048, Hydrogenimonas thermophila, Takai K.;
NrtTerga, AB175499, Nitratiruptor tergarcus, Nakagawa S
HelPyl93, U01330, Helicobacter pylori, Eckloff B.
NzgP1798, ARB_1439C3A, denovo198 P1_7988 1..446
NzgP4502, ARB_3A9FF5C0, denovo594 P4_5024 1..476
NzgP1123, ARB_334AFFCB, denovo791 P1_12326 1..502
NzgP1245, ARB_87DA0B1F, denovo415 P1_24538 1..499
NzgP1218, ARB_9E0BEB27, denovo878 P1_21769 1..510
NzgP1956, ARB_125735E9, denovo77 P1_9569 1..497
NzgP1160, ARB_F322EBF7, denovo335 P1_16061 1..512
NzgP1134, ARB_ADC7BCFE, denovo759 P1_13526 1..478
NzgP1114, ARB_B116FB18, denovo520 P1_11994 1..495
NzgP1174, ARB_81023010, denovo611 P1_17756 1..519
NzgP1521, ARB_868EBEBE, denovo707 P1_5210 1..496
Deltaproteobacteria
0.10

Figure 18. 16S rRNA neighboring-joining phylogeny for ANME-related archaea (A), deltaproteobacteria (B), and epsilonproteobacteria (C) based on partial sequences between nucleotide positions 787 and 1391. Trees were constructed with Arb software using a Jukes-Cantor correction. Bootstrap values represent the confidence in branch placement based on 500 iterations of each tree.

Another group of putative anaerobic methanotrophs, the ANME-2c archaea, was observed as the dominant group in samples P7 and P8 at the surface of the hottest core, 4573-16. In the past ANME-2c archaeal sequences have often been associated with cold sediments replete in electron acceptor (Knittel et al., 2005; Lloyd et al., 2011; Rossel et al., 2011; Yanagawa et al., 2014; chapter two of this dissertation), which in part explains the occurrence of this group in surficial sediments where sulfate concentrations are still high. On the other hand their prevalence at a high in situ thermal range suggests they may be able to survive heat exposure as long as it remains temporary and temperatures fluctuate to cooler values. Interestingly, while methane concentrations decrease at the surface of this core, there is no corresponding shift towards heavier δ^{13}C-methane values that would indicate microbial methane oxidation. Since ANME-2c archaea are typically associated with cooler temperatures, recovery of ANME-2c rRNA in this case may signify a group of non-thermophiles that is dealing with the unfortunate situation of maintaining themselves in sediments that are increasing in temperature over time. Given the logged temperatures for eight days prior to sediment sampling it is apparent that the thermal conditions associated with 4573-16 are intensifying (Figure 16A). ANME-2c archaea at this layer may be in survival mode to cope with less favorable conditions, which might explain recovery of their rRNA from these samples. It could also be that, unlike the surface layer of core 4572-18 where isotopic evidence of AOM is strong, there is not enough methane being oxidized in core 4573-16 to noticeably fractionate and result in a deviation in the δ^{13}C-methane profile. It takes a 13 mM decrease in methane in 4572-18 to result in a 5-6 ‰ shift in δ^{13}C-methane while

there is only a 4-5 mM decrease in methane in 4573-16. Other possibilities are that elevated hydrothermal flux in these high temperature sediments might flush out available methane prior to microbial utilization, or isotopic fractionation of methane during oxidation by ANME-2c archaea could be smaller than expected. This has been shown to occur in hyperthermophilic methanogens grown at high pressure (Takai et al., 2008). Lastly, it could be that recovery of rcDNA sequences is in this case not representative of relative activity of microbial groups.

Members of class Thermoplasmata dominate two separate samples, P4 and P28, and are related to Deep-Sea Hydrothermal Vent Euryarchaeotal Group 1 (DHVE-1). Consistent with their occurrence in sulfidic Guaymas sediments, DHVE-1 archaea have been recovered in the past from hydrothermal sediments characterized by disseminated sulfides in Iheya Basin (Takai and Horikoshi, 1999). Since sample P4 is at the surface layer with abundant sulfate and P28 is a subsurface sample completed depleted of sulfate, DHVE archaea do not seem to be controlled by electron acceptor availability.

Sample P32 is an anomaly among the archaea, almost entirely made up of members of the family *Archaeoglobaceae* and Miscellaneous Crenarchaeota Group (MCG) archaea. Unfortunately, the recovered sequence information for the *Archaeoglobaceae* OTU is insufficient to distinguish it between *Archaeoglobus* and *Ferroglobus* archaea. While both are hyperthermophiles and closely related in the 16S rRNA gene, these two archaea are physiologically distinct. *Ferroglobus placidus* can oxidize iron, H_2, or sulfide in the presence of nitrate or thiosulfate as potential electron acceptors (Hafenbradl et al., 1996). *Archaeoglobus* spp., by contrast, are strict sulfate reducing hyperthermophiles which can utilize an array of organic compounds (Stetter, 1988; Huber et al., 1997). In this case, over half of archaeal sequences recovered from sample P32 (1129/2075) belonged to the family *Archaeoglobaceae*

which suggests a relatively high activity level for this group. Although low in concentration, porewater sulfate decreases to near zero at this sample depth, which may result from *Archaeoglobus* spp., or sulfate may be too low for growth of sulfate reducers in which case *Ferroglobus* spp. may account for the recovered *Archaeoglobaceae* sequences. MCG archaeal sequences found in sample P32 shared close identity with a 16S rRNA gene clone from the Bor Khlueng hot spring in Thailand (acc: AY555817, Kanokratana et al., 2004), which is a deeply branching member of the previously identified MCG-15 cluster (Kubo et al., 2012).

For bacteria, four of eight samples P2, P4, P7, and P8, present a highly specific epsilonproteobacterial-dominated community consisting of members of *Helicobacteraceae* family (Figure 18C). It should be noted, though, that sample P2 had a very low bacterial sequence number of 13 and low estimated coverage of diversity at 27%. *Epsilonproteobacteria* are often prevalent in sulfidic microbial mat habitats and, as a class, have the ability to utilize diverse electron acceptors including nitrate, sulfite, oxygen, and elemental sulfur (Campbell et al., 2006). Here they appear at least in part restricted to sediments nearer to the sediment surface, which may be regulated by thermal limitations, electron acceptor availability, or both.

Accounting for 1117 out of 1227 bacterial sequences in sample P3 was an OTU representative of family *Thermodesulfobacteriaceae* within the phylum *Thermodesulfobacteria*, which represents thermophilic sulfate reducing bacteria. This OTU was closely related to a 16S rRNA gene clone from a hot spring microbial mat system in Tibet (Lau et al., 2009) and here the recovery of *Thermodesulfobacteriaceae* sequences is consistent with decreasing sulfate and increasing sulfide concentrations at high temperatures. During the eight-day temperature logging interval, this sediment horizon reached average temperatures between 70°C and 95°C and experienced 25-30°C temperature variations in as little as one day (Figure 16). Given the good

sequence recovery at this depth, members of the *Thermodesulfobacteriaceae* thrive as specialized hyperthermophiles that withstand high temperatures when sulfate is not limiting.

Covering 1015 out of 1244 bacterial sequences, sample P32 was dominated by bacteria within the HotSeep-1 cluster (Holler et al., 2011). HotSeep-1 bacteria have been shown in laboratory incubations to be involved in putative sulfate reducing/methane oxidizing assemblages as partners with ANME-1 archaea at optimum temperatures between 45°C and 60°C (Holler et al., 2011). The association between HotSeep-1 bacteria and elevated temperatures is consistent with their occurrence in sample P32 which had an estimated in situ temperature of 68°C. Interestingly, though, archaeal sequence recovery from this depth did not yield any ANME archaea, but rather MCG and *Archaeoglobales*. This suggests that HotSeep-1 bacteria are not obligated to form partnerships with ANME archaea and may perform sulfate reduction independent from methane oxidation. Together with sulfate-reducing *Archaeoglobales*, the Hot Seep bacteria could draw down sulfate to the low concentrations observed for approximately 12 cm above and below this sediment horizon. Alternatively, HotSeep-1 bacteria may not be obligate sulfate reducers but rather have facultative capacity for other physiologies, such as the ability to utilize more reduced sulfur compounds.

Accounting for 19% (1348/7130) of the relatively large bacterial sequence recovery in sample P1 was an OTU within the family *Desulfobulbaceae*. Closer examination reveals this OTU is closely related to type sp. *Desulfocapsa sulfexigens*, a deltaproteobacterium that cannot grow by sulfate reduction but has the ability to disproportionate elemental sulfur (Finster et al., 2013). This is consistent with RNA sequence recovery of *D. sulfexigens* in sample P1, in the surficial sediments of core 4572-18 where microbial sulfur cycling is evident. Inmixing of seawater oxygen into surficial sediments could result in the oxidation of sulfide to elemental

sulfur, the electron donor for *Desulfocapsa*. Approximately a quarter of bacterial sequences in the surface of same core, sample P1, consisted of *Firmicutes* closely related to the thermophilic and anaerobic chemo-organotroph *Caloranaerobacter azorensis* isolated from a Mid-Atlantic Ridge hydrothermal vent (Wery et al., 2001). The immediate decrease in sulfate in the surface layer indicates a rapid transition to anoxic conditions within the 0-3cm sediment section, suitable for anaerobic microorganisms.

Although sample P28, at 9-12 cm depth in core 4565-3, had poor total bacterial sequence recovery, most sequences from this sample branch within the bacterial phylum *Caldiserica*, previously known as candidate division OP5 (Hugenholtz et al., 1998). Type species *Caldisericum exile* is a thermophilic, filamentous chemoheterotroph that oxidizes organic substrates using sulfur and sulfite as electron acceptors (Mori et al. 2009), and resourceful usage of electron acceptors may sustain *Caldiserica* in sample P28 where sulfate concentrations are near zero.

RNA recovery at increasing temperatures and identification of probable thermophiles

While thermal structure is certainly not the only factor controlling microbial diversity across samples, it represents an important metric for the understanding of the limits of life in extreme environments. In consideration of the uncertainty of giving thermal assignments to sampled sediment layers in this study, a cautious approach was taken to assess high temperature-associated archaea and bacteria. Rather than assuming thermophily for single occurrences of OTUs at high temperatures, an OTU network was created to identify shared OTUs among two or more of the four highest temperature samples, P2, P3, P8, and P32 (Figure 19A). This is based on the assumption that co-occurrence of OTUs among multiple hot samples is a more probable indication of preferred thermophily or strong thermotolerance. 16S rRNA phylogeny for shared

OTUs among the hottest four samples revealed ANME-1, ANME-1 Guaymas, ANME-2c, DHVE, and some MCG archaea as commonly associated with high temperatures, and members of the *Thermodesulfobacteriaceae* as well as *Epsilonproteobacteria* within the *Helicobacteriaceae* as the most probable thermo- or hyperthermophiles for bacteria (Figure 19B). Since ANME-2c archaea are typically associated with cold sediments this analysis may be too inclusive to identify microorganisms that prefer higher temperatures. To make a more conservative prediction of which of these microorganisms prefer higher temperatures, all OTUs shared among hot samples exclusively, with no co-occurrence in cooler samples, revealed that a certain ANME-1 Guaymas OTU and an uncultured relative of the MCG-15 archaea are the most probable thermophilic archaea, and bacterial OTUs related to the *Thermodesulfobacteriaceae* represent the most likely thermophilic bacteria.

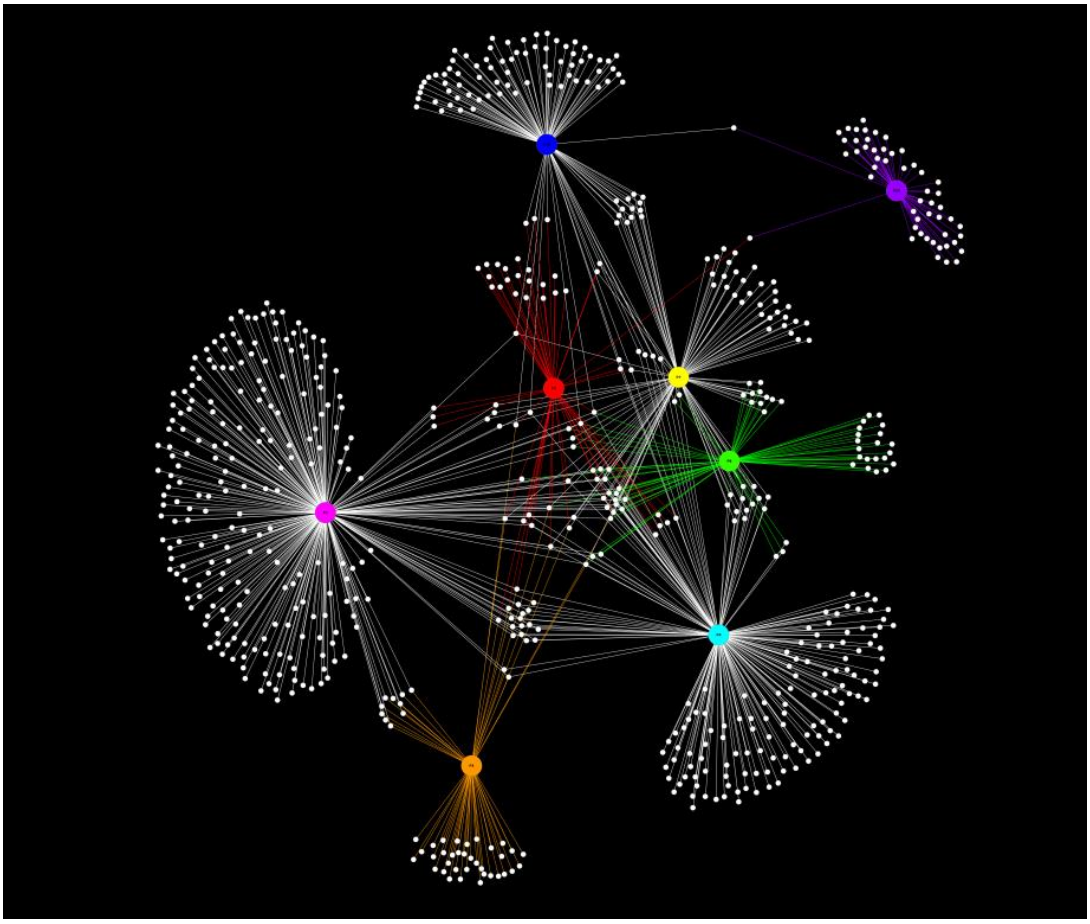

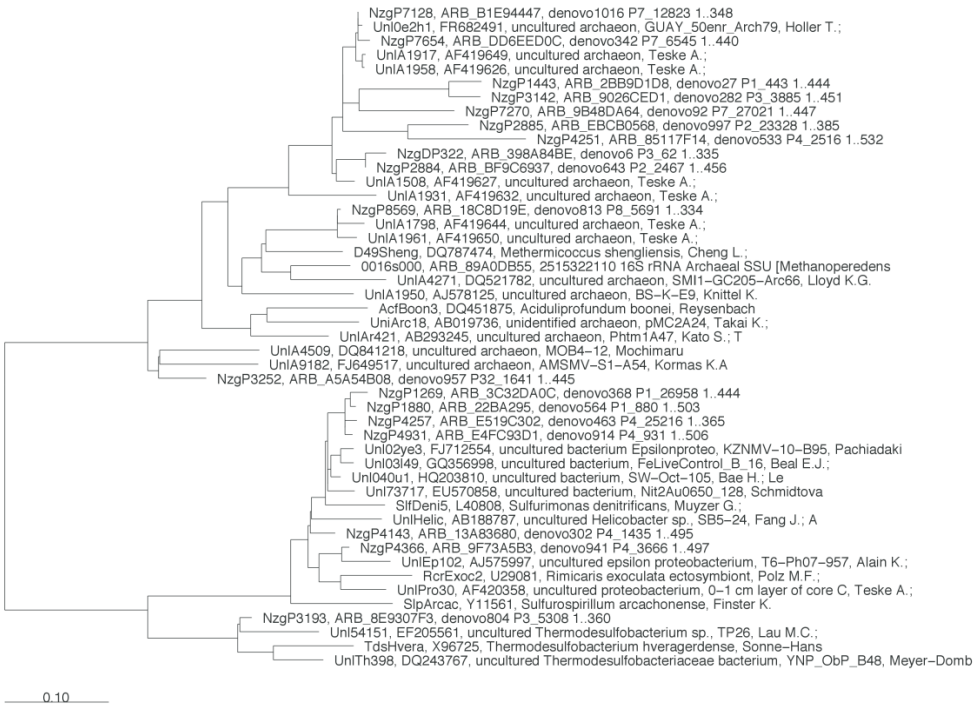
NzgP7128, ARB_B1E94447, denovo1016 P7_12823 1..348
Unl0e2h1, FR682491, uncultured archaeon, GUAY_50enr_Arch79, Holler T.;
NzgP7654, ARB_DD6EED0C, denovo342 P7_6545 1..440
UnlA1917, AF419649, uncultured archaeon, Teske A.;
UnlA1958, AF419626, uncultured archaeon, Teske A.;
NzgP1443, ARB_2BB9D1D8, denovo27 P1_443 1..444
NzgP3142, ARB_9026CED1, denovo282 P3_3885 1..451
NzgP7270, ARB_9B48DA64, denovo92 P7_27021 1..447
NzgP2885, ARB_EBCB0568, denovo997 P2_23328 1..385
NzgP4251, ARB_85117F14, denovo533 P4_2516 1..532
NzgDP322, ARB_398A84BE, denovo6 P3_62 1..335
NzgP2884, ARB_BF9C6937, denovo643 P2_2467 1..456
UnlA1508, AF419627, uncultured archaeon, Teske A.;
UnlA1931, AF419632, uncultured archaeon, Teske A.;
NzgP8569, ARB_18C8D19E, denovo813 P8_5691 1..334
UnlA1798, AF419644, uncultured archaeon, Teske A.;
UnlA1961, AF419650, uncultured archaeon, Teske A.;
D49Sheng, DQ787474, Methermicoccus shengliensis, Cheng L.;
0016s000, ARB_89A0DB55, 2515322110 16S rRNA Archaeal SSU [Methanoperedens
UnlA4271, DQ521782, uncultured archaeon, SMI1-GC205-Arc66, Lloyd K.G.
UnlA1950, AJ578125, uncultured archaeon, BS-K-E9, Knittel K.
AcfBoon3, DQ451875, Aciduliprofundum boonei, Reysenbach
UniArc18, AB019736, unidentified archaeon, pMC2A24, Takai K.;
UnlAr421, AB293245, uncultured archaeon, Phtm1A47, Kato S.; T
UnlA4509, DQ841218, uncultured archaeon, MOB4-12, Mochimaru
UnlA9182, FJ649517, uncultured archaeon, AMSMV-S1-A54, Kormas K.A
NzgP3252, ARB_A5A54B08, denovo957 P32_1641 1..445
NzgP1269, ARB_3C32DA0C, denovo368 P1_26958 1..444
NzgP1880, ARB_22BA295, denovo564 P1_880 1..503
NzgP4257, ARB_E519C302, denovo463 P4_25216 1..365
NzgP4931, ARB_E4FC93D1, denovo914 P4_931 1..506
Unl02ye3, FJ712554, uncultured bacterium Epsilonproteo, KZNMV-10-B95, Pachiadaki
Unl03l49, GQ356998, uncultured bacterium, FeLiveControl_B_16, Beal E.J.;
Unl040u1, HQ203810, uncultured bacterium, SW-Oct-105, Bae H.; Le
Unl73717, EU570858, uncultured bacterium, Nit2Au0650_128, Schmidtova
SlfDeni5, L40808, Sulfurimonas denitrificans, Muyzer G.;
UnlHelic, AB188787, uncultured Helicobacter sp., SB5-24, Fang J.; A
NzgP4143, ARB_13A83680, denovo302 P4_1435 1..495
NzgP4366, ARB_9F73A5B3, denovo941 P4_3666 1..497
UnlEp102, AJ575997, uncultured epsilon proteobacterium, T6-Ph07-957, Alain K.;
RcrExoc2, U29081, Rimicaris exoculata ectosymbiont, Polz M.F.;
UnlPro30, AF420358, uncultured proteobacterium, 0-1 cm layer of core C, Teske A.;
SlpArcac, Y11561, Sulfurospirillum arcachonense, Finster K.
NzgP3193, ARB_8E9307F3, denovo804 P3_5308 1..360
Unl54151, EF205561, uncultured Thermodesulfobacterium sp., TP26, Lau M.C.;
TdsHvera, X96725, Thermodesulfobacterium hveragerdense, Sonne-Hans
UnlTh398, DQ243767, uncultured Thermodesulfobacteriaceae bacterium, YNP_ObP_B48, Meyer-Domb
0.10

Figure 19. (A) Qiime-generated OTU network visualized with Cytoscape software indicates connectivity between samples (large colored circles) and OTUs (small white circles). Co-occurring OTUs among hot samples are connected to each sample by the color associated with that sample node. (B) Small subunit 16S rRNA phylogeny of most probable thermophiles as indicated by 19A.

Conclusion

While the average upper thermal temperature for microbial life in Guaymas Basin sediments appears to be around 80°C, extensive temperature fluctuations of up to 25°C in as little as a day make it difficult to infer optimal temperature conditions for microorganisms. Temperature and/or electron acceptor availability appear to impart strong controls on microbial richness, with archaeal and bacterial OTU numbers decreasing with increasing temperature and decreasing sulfate. Sulfate reduction appears to be a key microbial process occurring in hot sediments, as indicated by sharp decreases in porewater sulfate concentrations. Isotopic evidence for microbially mediated methane oxidation is only slight, yet putative methanotrophic archaea are commonly recovered in nearly all samples suggesting they may perform other physiological modes. Alternatively, high flux of thermogenic methane with isotopic signatures near Guaymas background (ca. – 43 ‰) might drown out the isotopic imprint of methane oxidation or methanogenesis. High temperature associated archaea appear to be OTUs related to uncultured MCG and ANME-1 Guaymas groups. For bacteria the dominant high temperature associated OTU was phylogenetically associated with the *Thermodesulfobacteriaceae*.

APPENDIX: SUPPLEMENTARY FIGURES AND TEXT

Figure S1

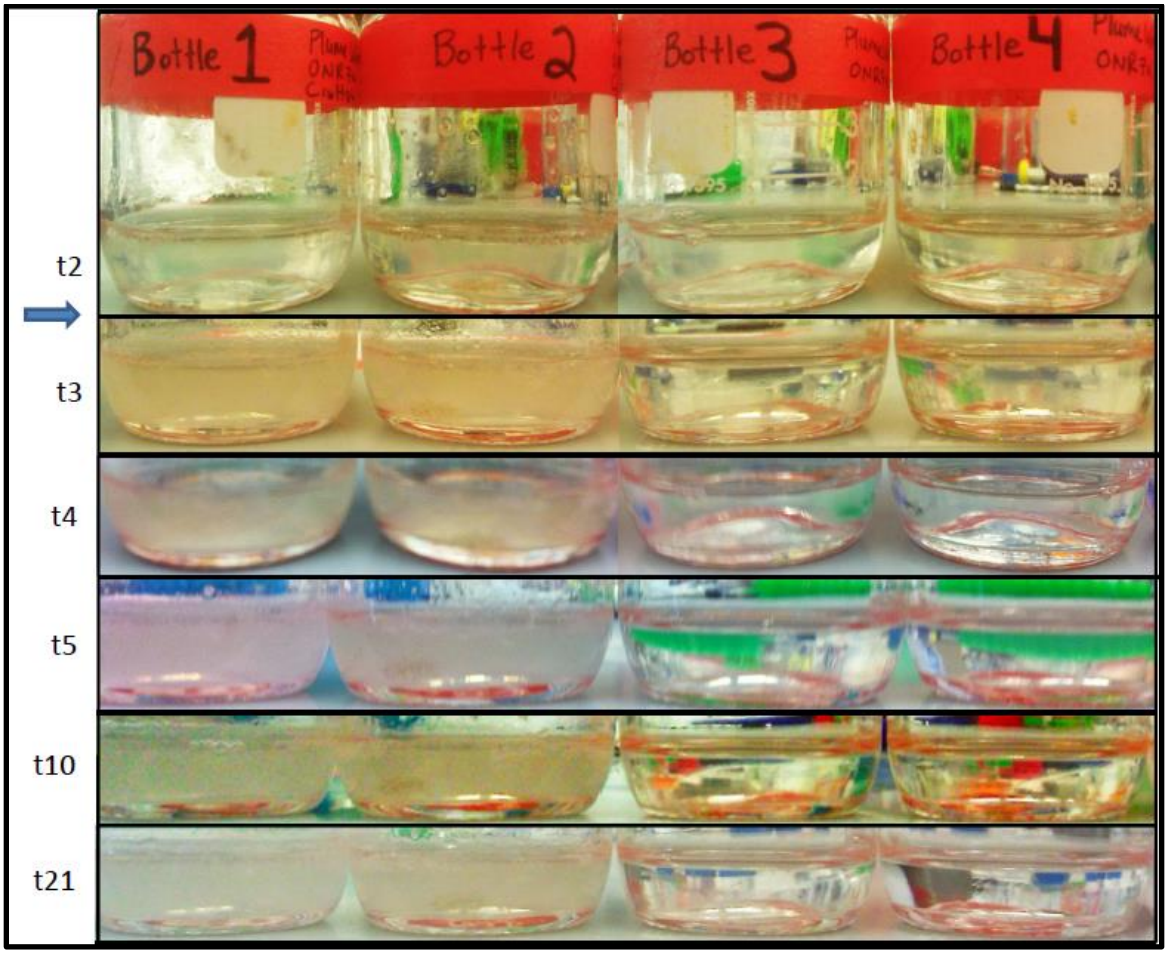

Supplementary Figure S1. Photographs of each vial at each timepoint demonstrate the sharp change in sample water turbidity between timepoints (days) 2 and 3 for hexadecane-amended vials 1 and 2 (indicated by blue arrow). Vials 3 and 4, which were not amended with hexadecane, do not become turbid throughout the 21 day incubation.

Figure S2

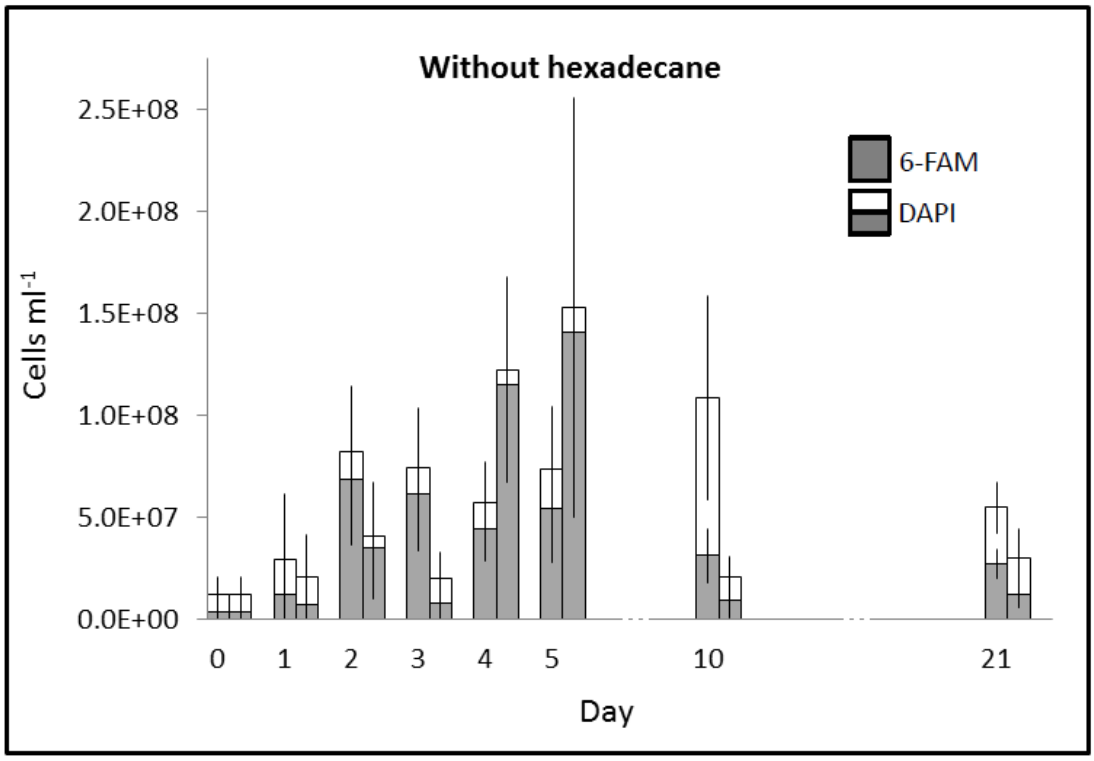

Supplementary Figure S2. Average cell numbers of DAPI-stained (white and grey) and Mrb-0625-a-targeted (grey only) cells for non-hexadecane-amended vial 3 (left-hand column) and vial 4 (right-hand column) from days 0, 1, 2, 3, 4, 5, 10, and 21 of the enrichment. This is the same data showed in Figure 5B but the y-axis maximum has been decreased from 4.0E9 to 2.75E8. DAPI and FISH counts for these duplicated assays are plotted separately in two neighboring columns for all time points, to show the consistency of the microbial growth and enrichment response. Error bars represent standard deviation from mean cell counts. The x-axis is abbreviated between days 5 and 10 and between days 10 and 21.

Supplementary Text.

As can be seen from Figure 7A, microbial methanogenesis may also be happening but isotopic evidence of this process is only observed at temperatures below 25°C. Above 25°C, if methanogenesis is happening, the isotopic signature for it is not observable because the influence of AOM on δ^{13}C-CH_4 is too strong. This is not to say that methanogenesis takes over at temperatures lower than 25°C—in many cases AOM is evidenced at low temperatures by ^{13}C-

enriched methane—but rather that biological methanogenesis is only isotopically detectable at low temperatures. High temperature microbial mediated methanogenesis thus appears to be less significant than AOM in terms of bulk methane processing by microorganisms.

Using in situ profiler measurements made by Dirk deBeer, a strong correlation between decreasing pH and increasing temperature was noted. Using this relationship pH estimates were made for the five cores according to their temperature profiles and these estimates were used in calculations of Gibb's free energy of the reaction. However, previously measured pH values from hot, hydrothermal fluids were consistently 5.9 across 8 distinct sites in Guaymas Basin (Von Damm et al., 1985). Therefore a separate set of Gibb's free energy calculations was made for the reaction using a pH of 5.9, and although the thermodynamic potentials reduced in all cores, the relationship between higher potential and higher temperature persists. It should be noted that the pH measurements by Von Damm et al. were performed shipboard after samples had been somewhat compromised during ROV ascension.

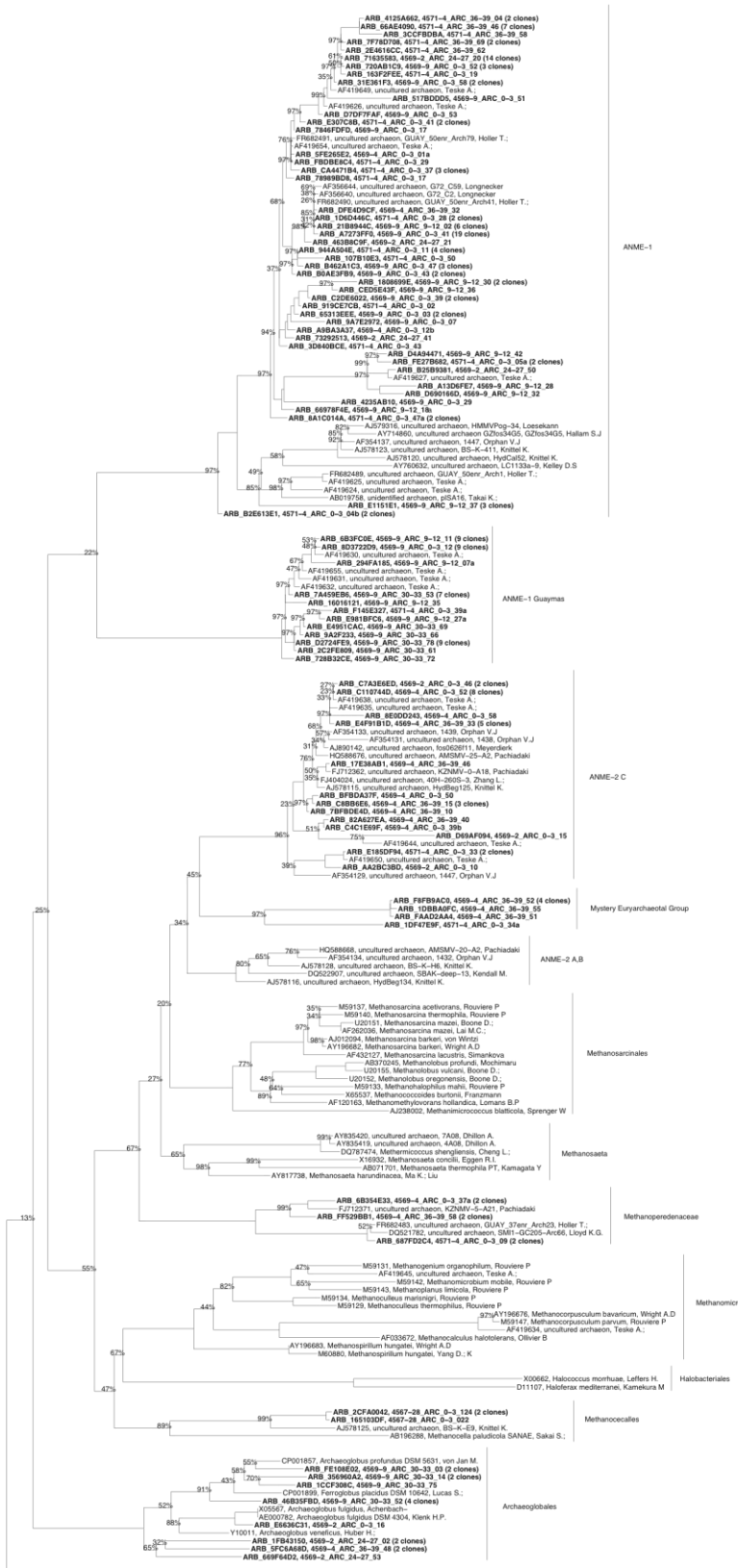
ANME−1
ANME−1 Guaymas
ANME−2 C
Mystery Euryarchaeotal Group
ANME−2 A,B
Methanosarcinales
Methanosaeta
Methanoperedenaceae
Methanomicrobiales
Halobacteriales
Methanocellales
Archaeoglobales


MBGD & friends
DHVE–6
Thermococcales
Methanopyrales
Methanococcales
SAGMEG
Methanobacteriales
Guaymas Euryarchaeotal Group
MBGE
DSEG–2
DSEG–3
DSEG–1
MCG
Cultured Crenarchaeota
MG–1
0.10

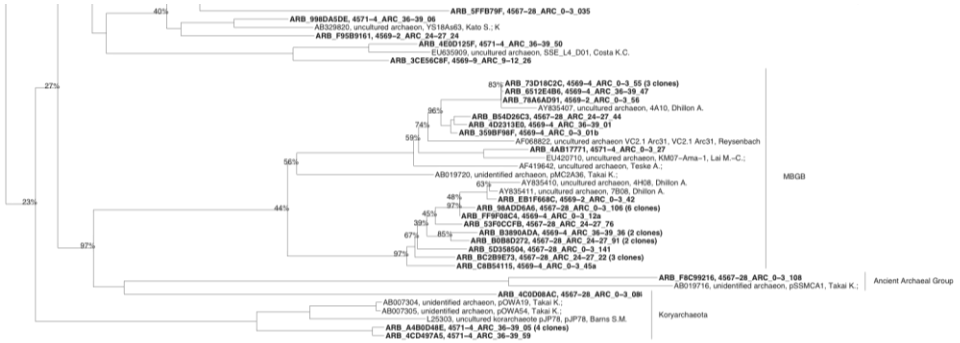
ARB_5FFB79F, 4567-28_ARC_0-3_035
ARB_998DA5DE, 4571-4_ARC_36-39_06
AB329820, uncultured archaeon, YS18Au63, Kato S.; K
ARB_F95B9161, 4569-2_ARC_24-27_24
ARB_4E0D125F, 4571-4_ARC_36-39_50
EU635909, uncultured archaeon, SSE_L4_D01, Costa K.C.
ARB_3CE56C8F, 4569-9_ARC_9-12_26
ARB_73D18C2C, 4569-4_ARC_0-3_55 (3 clones)
ARB_6512E4B6, 4569-4_ARC_36-39_47
ARB_78A6AD91, 4569-2_ARC_0-3_56
AY835407, uncultured archaeon, 4A10, Dhillon A.
ARB_B54D26C3, 4567-28_ARC_24-27_44
ARB_4D2313E0, 4569-4_ARC_36-39_01
ARB_359BF98F, 4569-4_ARC_0-3_01b
AF068822, uncultured archaeon VC2.1 Arc31, VC2.1 Arc31, Reysenbach
ARB_4AB17771, 4571-4_ARC_0-3_27
EU420710, uncultured archaeon, KM07-Ama-1, Lai M.-C.;
AF419642, uncultured archaeon, Teske A.;
AB019720, unidentified archaeon, pMC2A36, Takai K.;
AY835410, uncultured archaeon, 4H08, Dhillon A.
AY835411, uncultured archaeon, 7B08, Dhillon A.
ARB_EB1F668C, 4569-2_ARC_0-3_42
ARB_98ADD6A6, 4567-28_ARC_0-3_106 (6 clones)
ARB_FF9F08C4, 4569-4_ARC_0-3_12a
ARB_53F0CCFB, 4567-28_ARC_24-27_76
ARB_B3B90ADA, 4569-4_ARC_36-39_36 (2 clones)
ARB_B0B8D272, 4567-28_ARC_24-27_91 (2 clones)
ARB_5D35B504, 4567-28_ARC_0-3_141
ARB_BC2B9E73, 4567-28_ARC_24-27_22 (3 clones)
ARB_C8B54115, 4569-4_ARC_0-3_45a
MBGB
ARB_F6C99216, 4567-28_ARC_0-3_108
AB019716, unidentified archaeon, pSSMCA1, Takai K.;
Ancient Archaeal Group
ARB_4C0D08AC, 4567-28_ARC_0-3_08
AB007304, unidentified archaeon, pOWA19, Takai K.;
AB007305, unidentified archaeon, pOWA54, Takai K.;
L25303, uncultured korarchaeote pJP78, pJP78, Barns S.M.
Korvarchaeota
ARB_A4B0D48E, 4571-4_ARC_36-39_05 (4 clones)
ARB_4CD497A5, 4571-4_ARC_36-39_59
40%
27%
23%
97%
83%
96%
74%
59%
56%
63%
48%
97%
44%
45%
39%
67%
85%
97%

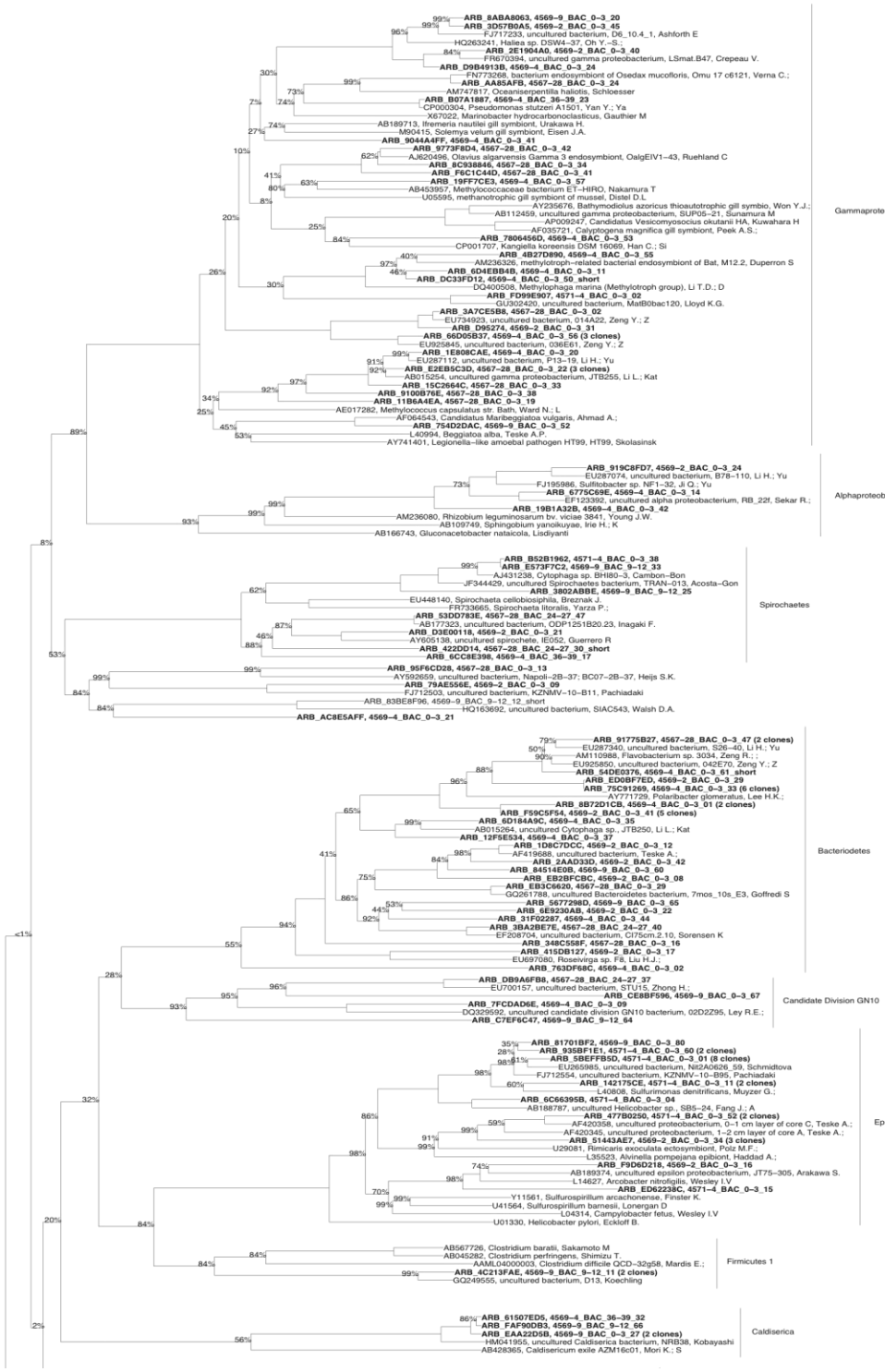
Gammaproteobacteria
Alphaproteobacteria
Spirochaetes
Bacteriodetes
Candidate Division GN10
Epsilonproteobacteria
Firmicutes 1
Caldiserica

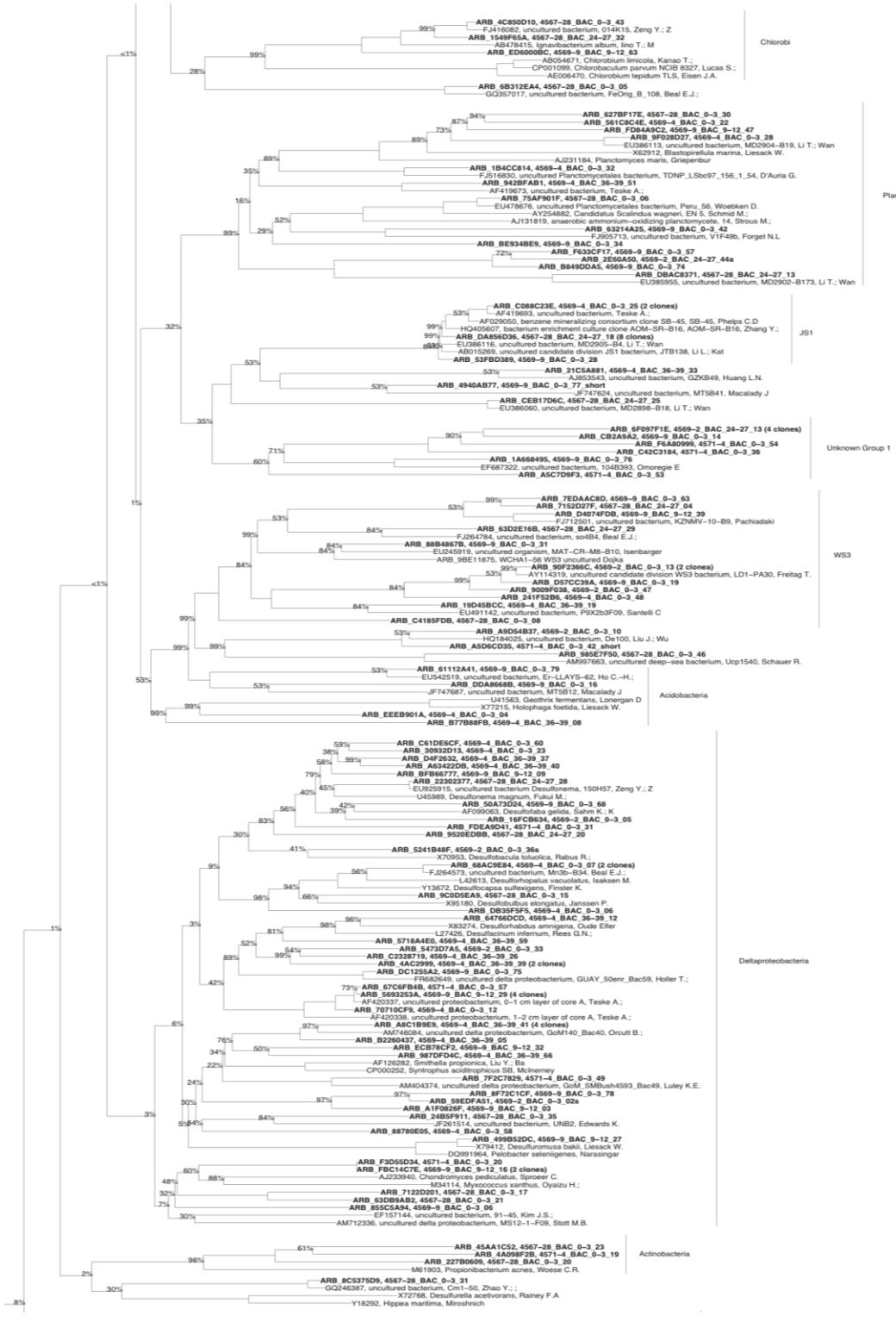
Chlorobi
Planktomycetales
JS1
Unknown Group 1
WS3
Acidobacteria
Deltaproteobacteria
Actinobacteria


0.10
Chloroflexi
Hot Seep 1
Thermodesulfobacteria
OP1
Unknown Group 2
Thermotogae

Supplementary Figure S3A, B. Complete Archaeal (A) and Bacterial (B) neighbor-joining 16S phylogeny for chapter 2. Trees were generated using Arb software and the neighbor-joining method with a Jukes-Cantor correction. Bootstrap values indicate the confidence in branch placement after 500 iterations of the tree. Representative sequences from this study are presented in bold and the number of replicate clones can be seen in parentheses after the sequence name. Branch designations without indicated bootstrap values have 100% bootstrap support.

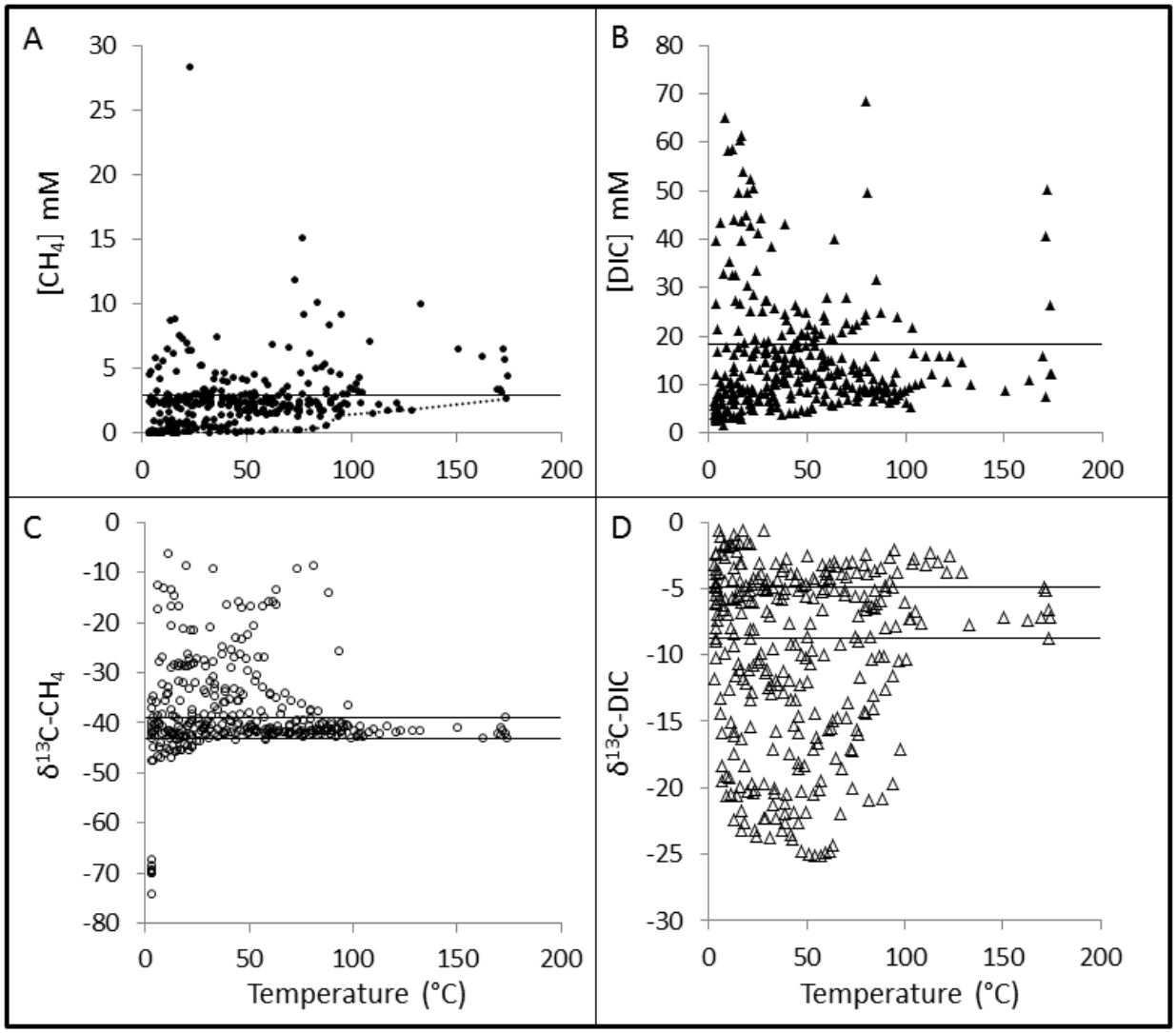

Supplementary Figure S4. Carbon geochemical data versus in situ temperature for methane (A), DIC (B), δ^{13}C-methane (C), and δ^{13}C-DIC (D). For methane and DIC average concentrations are repesented by black lines. For methane concentrations a dotted line indicates the minimum concentration value which increases with increasing temperature. Once the methanotrophic microorganisms are thermally limited, they are no longer present to keep methane concentrations near zero. For stable isotope plots of methane (C) and DIC (D), black lines indicate the maximum and minimum isotopic values at temperatures above 150°C.

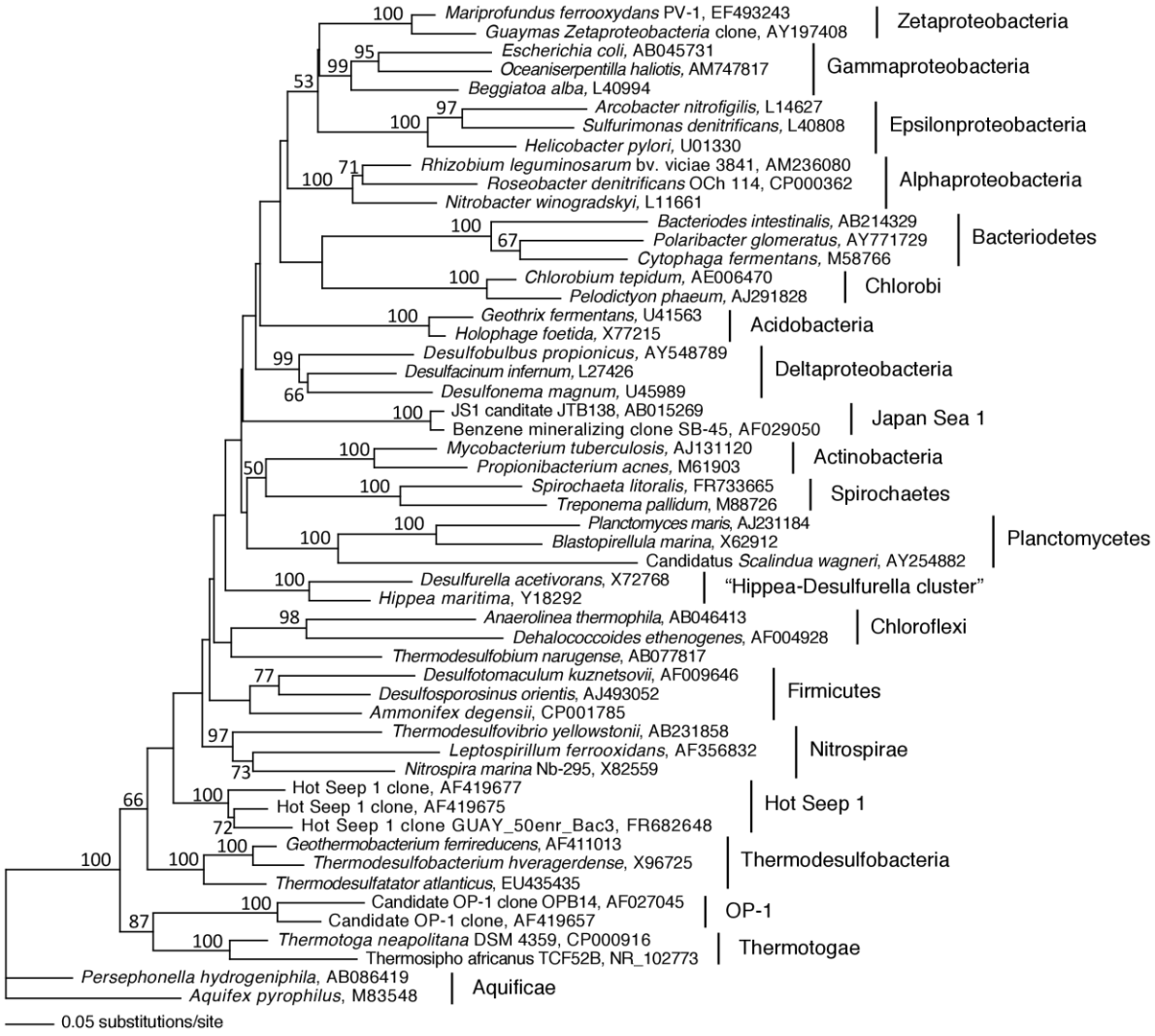

Supplementary Figure S5. 16S small rRNA subunit gene sequence phylogeny detailing paraphyly of *Deltaproteobacteria*, Hot Seep 1 group, and the *Hippea* cluster.

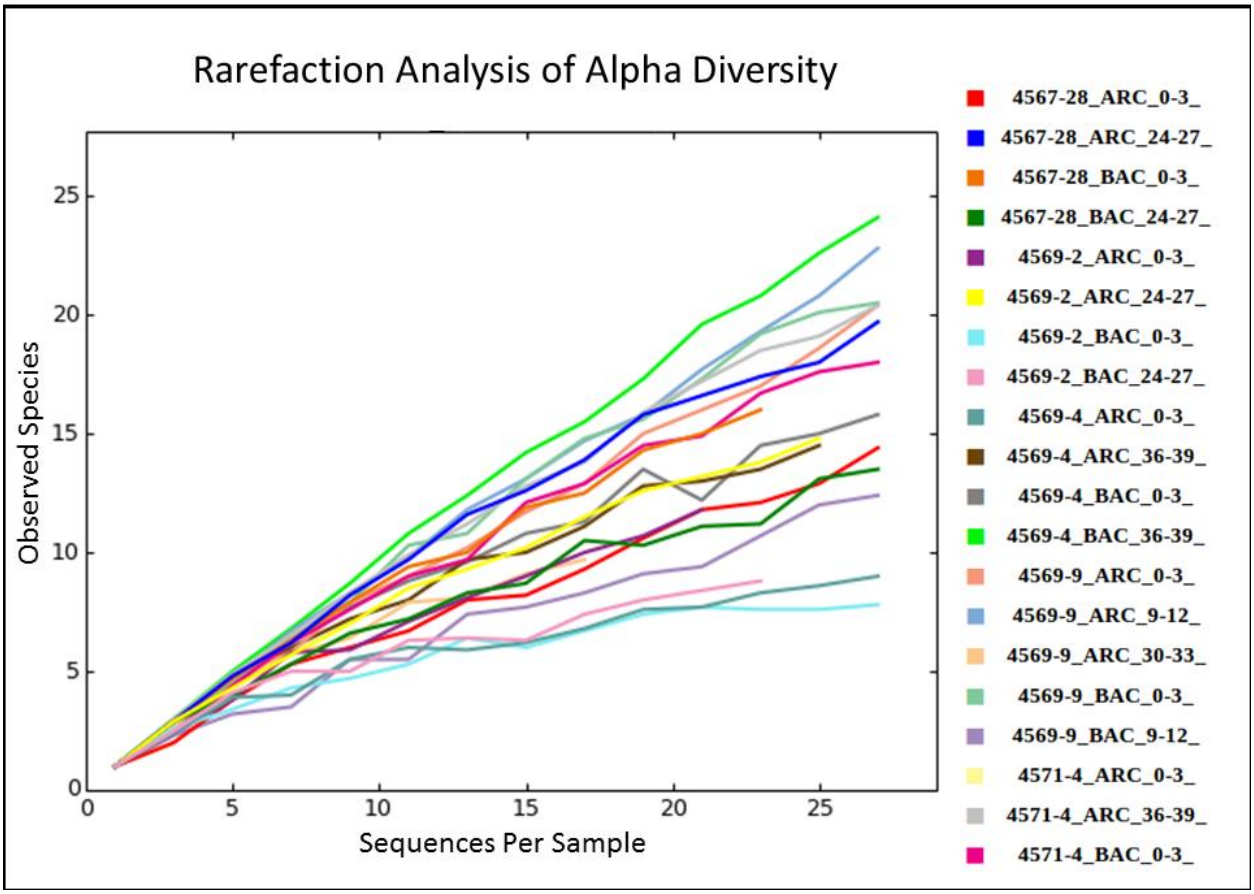

Supplementary Figure S6. Rarefaction analysis of observed species for each sample is plotted separately for archaea and bacteria.

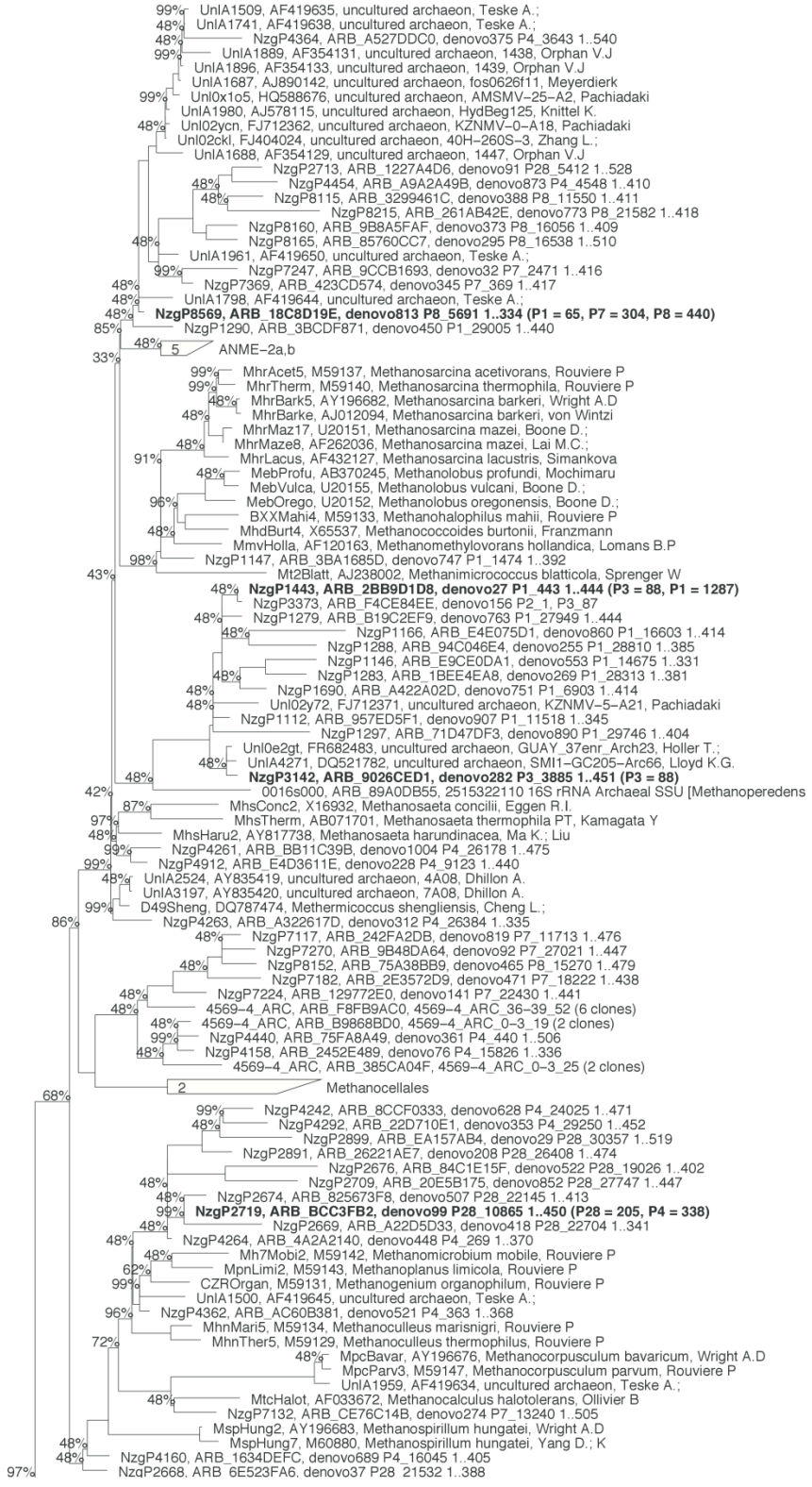
UnlA1509, AF419635, uncultured archaeon, Teske A.;
UnlA1741, AF419638, uncultured archaeon, Teske A.;
NzgP4364, ARB_A527DDC0, denovo375 P4_3643 1..540
UnlA1889, AF354131, uncultured archaeon, 1438, Orphan V.J
UnlA1896, AF354133, uncultured archaeon, 1439, Orphan V.J
UnlA1687, AJ890142, uncultured archaeon, fos0626f11, Meyerdierk
Unl0x1o5, HQ588676, uncultured archaeon, AMSMV–25–A2, Pachiadaki
UnlA1980, AJ578115, uncultured archaeon, HydBeg125, Knittel K.
Unl02ycn, FJ712362, uncultured archaeon, KZNMV–0–A18, Pachiadaki
Unl02ckl, FJ404024, uncultured archaeon, 40H–260S–3, Zhang L.;
UnlA1688, AF354129, uncultured archaeon, 1447, Orphan V.J
NzgP2713, ARB_1227A4D6, denovo91 P28_5412 1..528
NzgP4454, ARB_A9A2A49B, denovo873 P4_4548 1..410
NzgP8115, ARB_3299461C, denovo388 P8_11550 1..411
NzgP8215, ARB_261AB42E, denovo773 P8_21582 1..418
NzgP8160, ARB_9B8A5FAF, denovo373 P8_16056 1..409
NzgP8165, ARB_85760CC7, denovo295 P8_16538 1..510
UnlA1961, AF419650, uncultured archaeon, Teske A.;
NzgP7247, ARB_9CCB1693, denovo32 P7_2471 1..416
NzgP7369, ARB_423CD574, denovo345 P7_369 1..417
UnlA1798, AF419644, uncultured archaeon, Teske A.;
NzgP8569, ARB_18C8D19E, denovo813 P8_5691 1..334 (P1 = 65, P7 = 304, P8 = 440)
NzgP1290, ARB_3BCDF871, denovo450 P1_29005 1..440
5
ANME–2a,b
MhrAcet5, M59137, Methanosarcina acetivorans, Rouviere P
MhrTherm, M59140, Methanosarcina thermophila, Rouviere P
MhrBark5, AY196682, Methanosarcina barkeri, Wright A.D
MhrBarke, AJ012094, Methanosarcina barkeri, von Wintzi
MhrMaz17, U20151, Methanosarcina mazei, Boone D.;
MhrMaze8, AF262036, Methanosarcina mazei, Lai M.C.;
MhrLacus, AF432127, Methanosarcina lacustris, Simankova
MebProfu, AB370245, Methanolobus profundi, Mochimaru
MebVulca, U20155, Methanolobus vulcani, Boone D.;
MebOrego, U20152, Methanolobus oregonensis, Boone D.;
BXXMahi4, M59133, Methanohalophilus mahii, Rouviere P
MhdBurt4, X65537, Methanococcoides burtonii, Franzmann
MmvHolla, AF120163, Methanomethylovorans hollandica, Lomans B.P
NzgP1147, ARB_3BA1685D, denovo747 P1_1474 1..392
Mt2Blatt, AJ238002, Methanimicrococcus blatticola, Sprenger W
NzgP1443, ARB_2BB9D1D8, denovo27 P1_443 1..444 (P3 = 88, P1 = 1287)
NzgP3373, ARB_F4CE84EE, denovo156 P2_1, P3_87
NzgP1279, ARB_B19C2EF9, denovo763 P1_27949 1..444
NzgP1166, ARB_E4E075D1, denovo860 P1_16603 1..414
NzgP1288, ARB_94C046E4, denovo255 P1_28810 1..385
NzgP1146, ARB_E9CE0DA1, denovo553 P1_14675 1..331
NzgP1283, ARB_1BEE4EA8, denovo269 P1_28313 1..381
NzgP1690, ARB_A422A02D, denovo751 P1_6903 1..414
Unl02y72, FJ712371, uncultured archaeon, KZNMV–5–A21, Pachiadaki
NzgP1112, ARB_957ED5F1, denovo907 P1_11518 1..345
NzgP1297, ARB_71D47DF3, denovo890 P1_29746 1..404
Unl0e2gt, FR682483, uncultured archaeon, GUAY_37enr_Arch23, Holler T.;
UnlA4271, DQ521782, uncultured archaeon, SMI1–GC205–Arc66, Lloyd K.G.
NzgP3142, ARB_9026CED1, denovo282 P3_3885 1..451 (P3 = 88)
0016s000, ARB_89A0DB55, 2515322110 16S rRNA Archaeal SSU [Methanoperedens
MhsConc2, X16932, Methanosaeta concilii, Eggen R.I.
MhsTherm, AB071701, Methanosaeta thermophila PT, Kamagata Y
MhsHaru2, AY817738, Methanosaeta harundinacea, Ma K.; Liu
NzgP4261, ARB_BB11C39B, denovo1004 P4_26178 1..475
NzgP4912, ARB_E4D3611E, denovo228 P4_9123 1..440
UnlA2524, AY835419, uncultured archaeon, 4A08, Dhillon A.
UnlA3197, AY835420, uncultured archaeon, 7A08, Dhillon A.
D49Sheng, DQ787474, Methermicoccus shengliensis, Cheng L.;
NzgP4263, ARB_A322617D, denovo312 P4_26384 1..335
NzgP7117, ARB_242FA2DB, denovo819 P7_11713 1..476
NzgP7270, ARB_9B48DA64, denovo92 P7_27021 1..447
NzgP8152, ARB_75A38BB9, denovo465 P8_15270 1..479
NzgP7182, ARB_2E3572D9, denovo471 P7_18222 1..438
NzgP7224, ARB_129772E0, denovo141 P7_22430 1..441
4569–4_ARC, ARB_F8FB9AC0, 4569–4_ARC_36–39_52 (6 clones)
4569–4_ARC, ARB_B9868BD0, 4569–4_ARC_0–3_19 (2 clones)
NzgP4440, ARB_75FA8A49, denovo361 P4_440 1..506
NzgP4158, ARB_2452E489, denovo76 P4_15826 1..336
4569–4_ARC, ARB_385CA04F, 4569–4_ARC_0–3_25 (2 clones)
2
Methanocellales
NzgP4242, ARB_8CCF0333, denovo628 P4_24025 1..471
NzgP4292, ARB_22D710E1, denovo353 P4_29250 1..452
NzgP2899, ARB_EA157AB4, denovo29 P28_30357 1..519
NzgP2891, ARB_26221AE7, denovo208 P28_26408 1..474
NzgP2676, ARB_84C1E15F, denovo522 P28_19026 1..402
NzgP2709, ARB_20E5B175, denovo852 P28_27747 1..447
NzgP2674, ARB_825673F8, denovo507 P28_22145 1..413
NzgP2719, ARB_BCC3FB2, denovo99 P28_10865 1..450 (P28 = 205, P4 = 338)
NzgP2669, ARB_A22D5D33, denovo418 P28_22704 1..341
NzgP4264, ARB_4A2A2140, denovo448 P4_269 1..370
Mh7Mobi2, M59142, Methanomicrobium mobile, Rouviere P
MpnLimi2, M59143, Methanoplanus limicola, Rouviere P
CZROrgan, M59131, Methanogenium organophilum, Rouviere P
UnlA1500, AF419645, uncultured archaeon, Teske A.;
NzgP4362, ARB_AC60B381, denovo521 P4_363 1..368
MhnMari5, M59134, Methanoculleus marisnigri, Rouviere P
MhnTher5, M59129, Methanoculleus thermophilus, Rouviere P
MpcBavar, AY196676, Methanocorpusculum bavaricum, Wright A.D
MpcParv3, M59147, Methanocorpusculum parvum, Rouviere P
UnlA1959, AF419634, uncultured archaeon, Teske A.;
MtcHalot, AF033672, Methanocalculus halotolerans, Ollivier B
NzgP7132, ARB_CE76C14B, denovo274 P7_13240 1..505
MspHung2, AY196683, Methanospirillum hungatei, Wright A.D
MspHung7, M60880, Methanospirillum hungatei, Yang D.; K
NzgP4160, ARB_1634DEFC, denovo689 P4_16045 1..405
NzgP2668, ARB_6E523FA6, denovo37 P28_21532 1..388

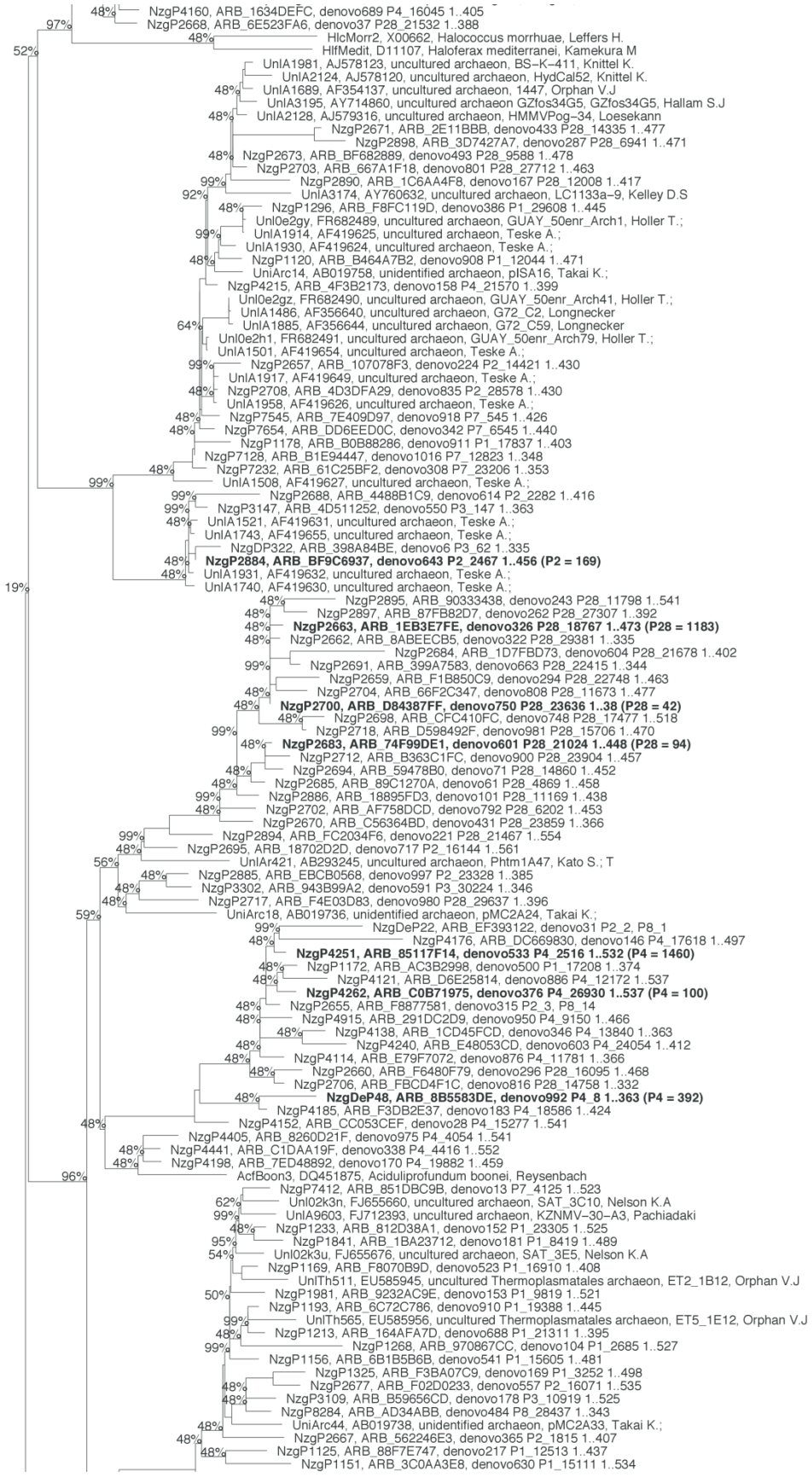
NzgP4160, ARB_1634DEFC, denovo689 P4_16045 1..405
NzgP2668, ARB_6E523FA6, denovo37 P28_21532 1..388
HlcMorr2, X00662, Halococcus morrhuae, Leffers H.
HlfMedit, D11107, Haloferax mediterranei, Kamekura M
UnlA1981, AJ578123, uncultured archaeon, BS–K–411, Knittel K.
UnlA2124, AJ578120, uncultured archaeon, HydCal52, Knittel K.
UnlA1689, AF354137, uncultured archaeon, 1447, Orphan V.J
UnlA3195, AY714860, uncultured archaeon GZfos34G5, GZfos34G5, Hallam S.J
UnlA2128, AJ579316, uncultured archaeon, HMMVPog–34, Loesekann
NzgP2671, ARB_2E11BBB, denovo433 P28_14335 1..477
NzgP2898, ARB_3D7427A7, denovo287 P28_6941 1..471
NzgP2673, ARB_BF682889, denovo493 P28_9588 1..478
NzgP2703, ARB_667A1F18, denovo801 P28_27712 1..463
NzgP2890, ARB_1C6AA4F8, denovo167 P28_12008 1..417
UnlA3174, AY760632, uncultured archaeon, LC1133a–9, Kelley D.S
NzgP1296, ARB_F8FC119D, denovo386 P1_29608 1..445
Unl0e2gy, FR682489, uncultured archaeon, GUAY_50enr_Arch1, Holler T.;
UnlA1914, AF419625, uncultured archaeon, Teske A.;
UnlA1930, AF419624, uncultured archaeon, Teske A.;
NzgP1120, ARB_B464A7B2, denovo908 P1_12044 1..471
UniArc14, AB019758, unidentified archaeon, pISA16, Takai K.;
NzgP4215, ARB_4F3B2173, denovo158 P4_21570 1..399
Unl0e2gz, FR682490, uncultured archaeon, GUAY_50enr_Arch41, Holler T.;
UnlA1486, AF356640, uncultured archaeon, G72_C2, Longnecker
UnlA1885, AF356644, uncultured archaeon, G72_C59, Longnecker
Unl0e2h1, FR682491, uncultured archaeon, GUAY_50enr_Arch79, Holler T.;
UnlA1501, AF419654, uncultured archaeon, Teske A.;
NzgP2657, ARB_107078F3, denovo224 P2_14421 1..430
UnlA1917, AF419649, uncultured archaeon, Teske A.;
NzgP2708, ARB_4D3DFA29, denovo835 P2_28578 1..430
UnlA1958, AF419626, uncultured archaeon, Teske A.;
NzgP7545, ARB_7E409D97, denovo918 P7_545 1..426
NzgP7654, ARB_DD6EED0C, denovo342 P7_6545 1..440
NzgP1178, ARB_B0B88286, denovo911 P1_17837 1..403
NzgP7128, ARB_B1E94447, denovo1016 P7_12823 1..348
NzgP7232, ARB_61C25BF2, denovo308 P7_23206 1..353
UnlA1508, AF419627, uncultured archaeon, Teske A.;
NzgP2688, ARB_4488B1C9, denovo614 P2_2282 1..416
NzgP3147, ARB_4D511252, denovo550 P3_147 1..363
UnlA1521, AF419631, uncultured archaeon, Teske A.;
UnlA1743, AF419655, uncultured archaeon, Teske A.;
NzgDP322, ARB_398A84BE, denovo6 P3_62 1..335
NzgP2884, ARB_BF9C6937, denovo643 P2_2467 1..456 (P2 = 169)
UnlA1931, AF419632, uncultured archaeon, Teske A.;
UnlA1740, AF419630, uncultured archaeon, Teske A.;
NzgP2895, ARB_90333438, denovo243 P28_11798 1..541
NzgP2897, ARB_87FB82D7, denovo262 P28_27307 1..392
NzgP2663, ARB_1EB3E7FE, denovo326 P28_18767 1..473 (P28 = 1183)
NzgP2662, ARB_8ABEECB5, denovo322 P28_29381 1..335
NzgP2684, ARB_1D7FBD73, denovo604 P28_21678 1..402
NzgP2691, ARB_399A7583, denovo663 P28_22415 1..344
NzgP2659, ARB_F1B850C9, denovo294 P28_22748 1..463
NzgP2704, ARB_66F2C347, denovo808 P28_11673 1..477
NzgP2700, ARB_D84387FF, denovo750 P28_23636 1..38 (P28 = 42)
NzgP2698, ARB_CFC410FC, denovo748 P28_17477 1..518
NzgP2718, ARB_D598492F, denovo981 P28_15706 1..470
NzgP2683, ARB_74F99DE1, denovo601 P28_21024 1..448 (P28 = 94)
NzgP2712, ARB_B363C1FC, denovo900 P28_23904 1..457
NzgP2694, ARB_59478B0, denovo71 P28_14860 1..452
NzgP2685, ARB_89C1270A, denovo61 P28_4869 1..458
NzgP2886, ARB_18895FD3, denovo101 P28_11169 1..438
NzgP2702, ARB_AF758DCD, denovo792 P28_6202 1..453
NzgP2670, ARB_C56364BD, denovo431 P28_23859 1..366
NzgP2894, ARB_FC2034F6, denovo221 P28_21467 1..554
NzgP2695, ARB_18702D2D, denovo717 P2_16144 1..561
UnlAr421, AB293245, uncultured archaeon, Phtm1A47, Kato S.; T
NzgP2885, ARB_EBCB0568, denovo997 P2_23328 1..385
NzgP3302, ARB_943B99A2, denovo591 P3_30224 1..346
NzgP2717, ARB_F4E03D83, denovo980 P28_29637 1..396
UniArc18, AB019736, unidentified archaeon, pMC2A24, Takai K.;
NzgDeP22, ARB_EF393122, denovo31 P2_2, P8_1
NzgP4176, ARB_DC669830, denovo146 P4_17618 1..497
NzgP4251, ARB_85117F14, denovo533 P4_2516 1..532 (P4 = 1460)
NzgP1172, ARB_AC3B2998, denovo500 P1_17208 1..374
NzgP4121, ARB_D6E25814, denovo886 P4_12172 1..537
NzgP4262, ARB_C0B71975, denovo376 P4_26930 1..537 (P4 = 100)
NzgP2655, ARB_F8877581, denovo315 P2_3, P8_14
NzgP4915, ARB_291DC2D9, denovo950 P4_9150 1..466
NzgP4138, ARB_1CD45FCD, denovo346 P4_13840 1..363
NzgP4240, ARB_E48053CD, denovo603 P4_24054 1..412
NzgP4114, ARB_E79F7072, denovo876 P4_11781 1..366
NzgP2660, ARB_F6480F79, denovo296 P28_16095 1..468
NzgP2706, ARB_FBCD4F1C, denovo816 P28_14758 1..332
NzgDeP48, ARB_8B5583DE, denovo992 P4_8 1..363 (P4 = 392)
NzgP4185, ARB_F3DB2E37, denovo183 P4_18586 1..424
NzgP4152, ARB_CC053CEF, denovo28 P4_15277 1..541
NzgP4405, ARB_8260D21F, denovo975 P4_4054 1..541
NzgP4441, ARB_C1DAA19F, denovo338 P4_4416 1..552
NzgP4198, ARB_7ED48892, denovo170 P4_19882 1..459
AcfBoon3, DQ451875, Aciduliprofundum boonei, Reysenbach
NzgP7412, ARB_851DBC9B, denovo13 P7_4125 1..523
Unl02k3n, FJ655660, uncultured archaeon, SAT_3C10, Nelson K.A
UnlA9603, FJ712393, uncultured archaeon, KZNMV–30–A3, Pachiadaki
NzgP1233, ARB_812D38A1, denovo152 P1_23305 1..525
NzgP1841, ARB_1BA23712, denovo181 P1_8419 1..489
Unl02k3u, FJ655676, uncultured archaeon, SAT_3E5, Nelson K.A
NzgP1169, ARB_F8070B9D, denovo523 P1_16910 1..408
UnlTh511, EU585945, uncultured Thermoplasmatales archaeon, ET2_1B12, Orphan V.J
NzgP1981, ARB_9232AC9E, denovo153 P1_9819 1..521
NzgP1193, ARB_6C72C786, denovo910 P1_19388 1..445
UnlTh565, EU585956, uncultured Thermoplasmatales archaeon, ET5_1E12, Orphan V.J
NzgP1213, ARB_164AFA7D, denovo688 P1_21311 1..395
NzgP1268, ARB_970867CC, denovo104 P1_2685 1..527
NzgP1156, ARB_6B1B5B6B, denovo541 P1_15605 1..481
NzgP1325, ARB_F3BA07C9, denovo169 P1_3252 1..498
NzgP2677, ARB_F02D0233, denovo557 P2_16071 1..535
NzgP3109, ARB_B59656CD, denovo178 P3_10919 1..525
NzgP8284, ARB_AD34ABB, denovo484 P8_28437 1..343
UniArc44, AB019738, unidentified archaeon, pMC2A33, Takai K.;
NzgP2667, ARB_562246E3, denovo365 P2_1815 1..407
NzgP1125, ARB_88F7E747, denovo217 P1_12513 1..437
NzgP1151, ARB_3C0AA3E8, denovo630 P1_15111 1..534

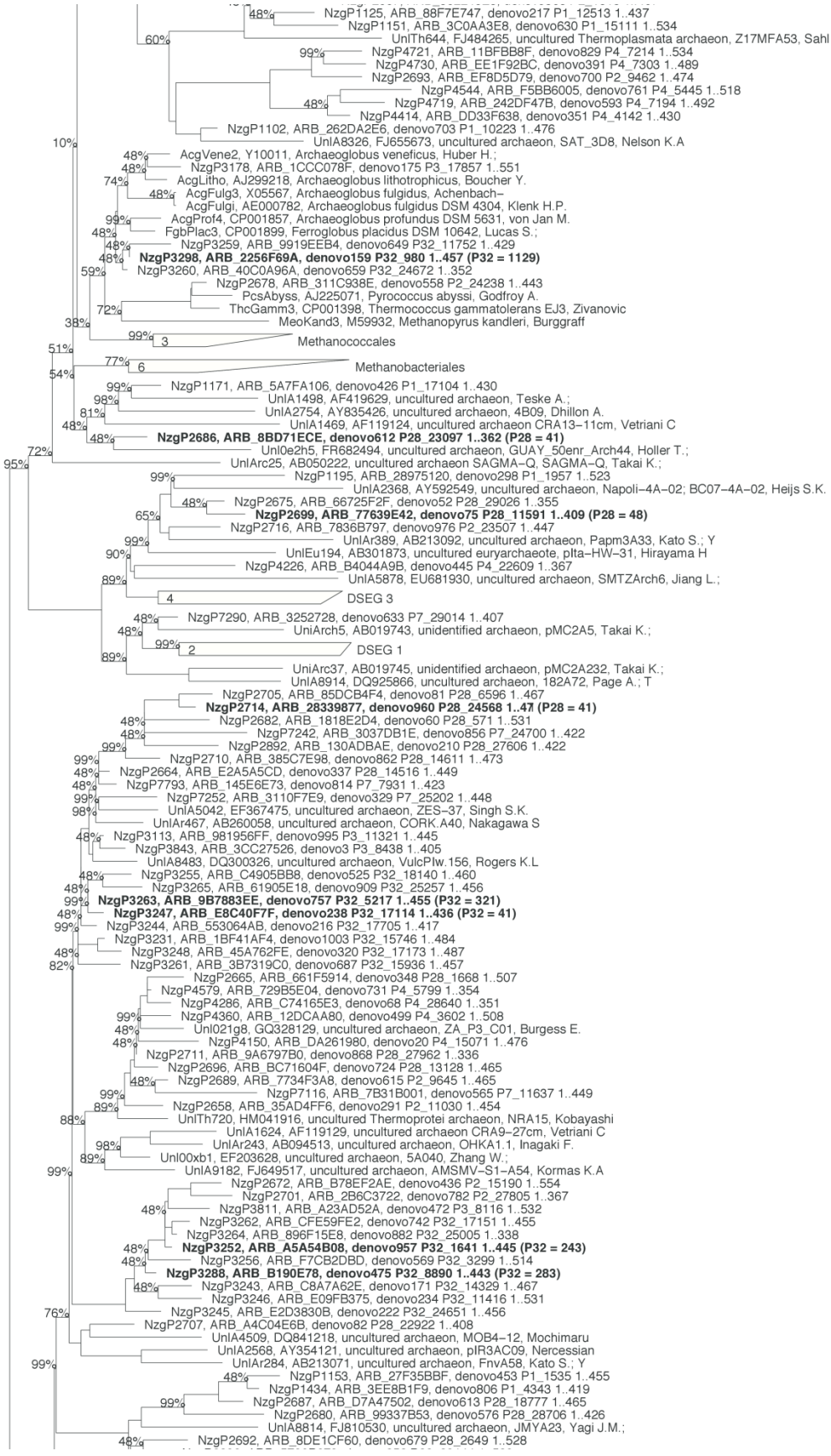
NzgP1125, ARB_88F7E747, denovo217 P1_12513 1..437
NzgP1151, ARB_3C0AA3E8, denovo630 P1_15111 1..534
UnlTh644, FJ484265, uncultured Thermoplasmata archaeon, Z17MFA53, Sahl J.W.;
NzgP4721, ARB_11BFBB8F, denovo829 P4_7214 1..534
NzgP4730, ARB_EE1F92BC, denovo391 P4_7303 1..489
NzgP2693, ARB_EF8D5D79, denovo700 P2_9462 1..474
NzgP4544, ARB_F5BB6005, denovo761 P4_5445 1..518
NzgP4719, ARB_242DF47B, denovo593 P4_7194 1..492
NzgP4414, ARB_DD33F638, denovo351 P4_4142 1..430
NzgP1102, ARB_262DA2E6, denovo703 P1_10223 1..476
UnlA8326, FJ655673, uncultured archaeon, SAT_3D8, Nelson K.A
AcgVene2, Y10011, Archaeoglobus veneficus, Huber H.;
NzgP3178, ARB_1CCC078F, denovo175 P3_17857 1..551
AcgLitho, AJ299218, Archaeoglobus lithotrophicus, Boucher Y.
AcgFulg3, X05567, Archaeoglobus fulgidus, Achenbach–
AcgFulgi, AE000782, Archaeoglobus fulgidus DSM 4304, Klenk H.P.
AcgProf4, CP001857, Archaeoglobus profundus DSM 5631, von Jan M.
FgbPlac3, CP001899, Ferroglobus placidus DSM 10642, Lucas S.;
NzgP3259, ARB_9919EEB4, denovo649 P32_11752 1..429
NzgP3298, ARB_2256F69A, denovo159 P32_980 1..457 (P32 = 1129)
NzgP3260, ARB_40C0A96A, denovo659 P32_24672 1..352
NzgP2678, ARB_311C938E, denovo558 P2_24238 1..443
PcsAbyss, AJ225071, Pyrococcus abyssi, Godfroy A.
ThcGamm3, CP001398, Thermococcus gammatolerans EJ3, Zivanovic
MeoKand3, M59932, Methanopyrus kandleri, Burggraff
Methanococcales
Methanobacteriales
NzgP1171, ARB_5A7FA106, denovo426 P1_17104 1..430
UnlA1498, AF419629, uncultured archaeon, Teske A.;
UnlA2754, AY835426, uncultured archaeon, 4B09, Dhillon A.
UnlA1469, AF119124, uncultured archaeon CRA13–11cm, Vetriani C
NzgP2686, ARB_8BD71ECE, denovo612 P28_23097 1..362 (P28 = 41)
Unl0e2h5, FR682494, uncultured archaeon, GUAY_50enr_Arch44, Holler T.;
UnlArc25, AB050222, uncultured archaeon SAGMA–Q, SAGMA–Q, Takai K.;
NzgP1195, ARB_28975120, denovo298 P1_1957 1..523
UnlA2368, AY592549, uncultured archaeon, Napoli–4A–02; BC07–4A–02, Heijs S.K.
NzgP2675, ARB_66725F2F, denovo52 P28_29026 1..355
NzgP2699, ARB_77639E42, denovo75 P28_11591 1..409 (P28 = 48)
NzgP2716, ARB_7836B797, denovo976 P2_23507 1..447
UnlAr389, AB213092, uncultured archaeon, Papm3A33, Kato S.; Y
UnlEu194, AB301873, uncultured euryarchaeote, pIta–HW–31, Hirayama H
NzgP4226, ARB_B4044A9B, denovo445 P4_22609 1..367
UnlA5878, EU681930, uncultured archaeon, SMTZArch6, Jiang L.;
DSEG 3
NzgP7290, ARB_3252728, denovo633 P7_29014 1..407
UniArch5, AB019743, unidentified archaeon, pMC2A5, Takai K.;
DSEG 1
UniArc37, AB019745, unidentified archaeon, pMC2A232, Takai K.;
UnlA8914, DQ925866, uncultured archaeon, 182A72, Page A.; T
NzgP2705, ARB_85DCB4F4, denovo81 P28_6596 1..467
NzgP2714, ARB_28339877, denovo960 P28_24568 1..47 (P28 = 41)
NzgP2682, ARB_1818E2D4, denovo60 P28_571 1..531
NzgP7242, ARB_3037DB1E, denovo856 P7_24700 1..422
NzgP2892, ARB_130ADBAE, denovo210 P28_27606 1..422
NzgP2710, ARB_385C7E98, denovo862 P28_14611 1..473
NzgP2664, ARB_E2A5A5CD, denovo337 P28_14516 1..449
NzgP7793, ARB_145E6E73, denovo814 P7_7931 1..423
NzgP7252, ARB_3110F7E9, denovo329 P7_25202 1..448
UnlA5042, EF367475, uncultured archaeon, ZES–37, Singh S.K.
UnlAr467, AB260058, uncultured archaeon, CORK.A40, Nakagawa S
NzgP3113, ARB_981956FF, denovo995 P3_11321 1..445
NzgP3843, ARB_3CC27526, denovo3 P3_8438 1..405
UnlA8483, DQ300326, uncultured archaeon, VulcPlw.156, Rogers K.L
NzgP3255, ARB_C4905BB8, denovo525 P32_18140 1..460
NzgP3265, ARB_61905E18, denovo909 P32_25257 1..456
NzgP3263, ARB_9B7883EE, denovo757 P32_5217 1..455 (P32 = 321)
NzgP3247, ARB_E8C40F7F, denovo238 P32_17114 1..436 (P32 = 41)
NzgP3244, ARB_553064AB, denovo216 P32_17705 1..417
NzgP3231, ARB_1BF41AF4, denovo1003 P32_15746 1..484
NzgP3248, ARB_45A762FE, denovo320 P32_17173 1..487
NzgP3261, ARB_3B7319C0, denovo687 P32_15936 1..457
NzgP2665, ARB_661F5914, denovo348 P28_1668 1..507
NzgP4579, ARB_729B5E04, denovo731 P4_5799 1..354
NzgP4286, ARB_C74165E3, denovo68 P4_28640 1..351
NzgP4360, ARB_12DCAA80, denovo499 P4_3602 1..508
Unl021g8, GQ328129, uncultured archaeon, ZA_P3_C01, Burgess E.
NzgP4150, ARB_DA261980, denovo20 P4_15071 1..476
NzgP2711, ARB_9A6797B0, denovo868 P28_27962 1..336
NzgP2696, ARB_BC71604F, denovo724 P28_13128 1..465
NzgP2689, ARB_7734F3A8, denovo615 P2_9645 1..465
NzgP7116, ARB_7B31B001, denovo565 P7_11637 1..449
NzgP2658, ARB_35AD4FF6, denovo291 P2_11030 1..454
UnlTh720, HM041916, uncultured Thermoprotei archaeon, NRA15, Kobayashi
UnlA1624, AF119129, uncultured archaeon CRA9–27cm, Vetriani C
UnlAr243, AB094513, uncultured archaeon, OHKA1.1, Inagaki F.
Unl00xb1, EF203628, uncultured archaeon, 5A040, Zhang W.;
UnlA9182, FJ649517, uncultured archaeon, AMSMV–S1–A54, Kormas K.A
NzgP2672, ARB_B78EF2AE, denovo436 P2_15190 1..554
NzgP2701, ARB_2B6C3722, denovo782 P2_27805 1..367
NzgP3811, ARB_A23AD52A, denovo472 P3_8116 1..532
NzgP3262, ARB_CFE59FE2, denovo742 P32_17151 1..455
NzgP3264, ARB_896F15E8, denovo882 P32_25005 1..338
NzgP3252, ARB_A5A54B08, denovo957 P32_1641 1..445 (P32 = 243)
NzgP3256, ARB_F7CB2DBD, denovo569 P32_3299 1..514
NzgP3288, ARB_B190E78, denovo475 P32_8890 1..443 (P32 = 283)
NzgP3243, ARB_C8A7A62E, denovo171 P32_14329 1..467
NzgP3246, ARB_E09FB375, denovo234 P32_11416 1..531
NzgP3245, ARB_E2D3830B, denovo222 P32_24651 1..456
NzgP2707, ARB_A4C04E6B, denovo82 P28_22922 1..408
UnlA4509, DQ841218, uncultured archaeon, MOB4–12, Mochimaru
UnlA2568, AY354121, uncultured archaeon, pIR3AC09, Nercessian
UnlAr284, AB213071, uncultured archaeon, FnvA58, Kato S.; Y
NzgP1153, ARB_27F35BBF, denovo453 P1_1535 1..455
NzgP1434, ARB_3EE8B1F9, denovo806 P1_4343 1..419
NzgP2687, ARB_D7A47502, denovo613 P28_18777 1..465
NzgP2680, ARB_99337B53, denovo576 P28_28706 1..426
UnlA8814, FJ810530, uncultured archaeon, JMYA23, Yagi J.M.;
NzgP2692, ARB_8DE1CF60, denovo679 P28_2649 1..528

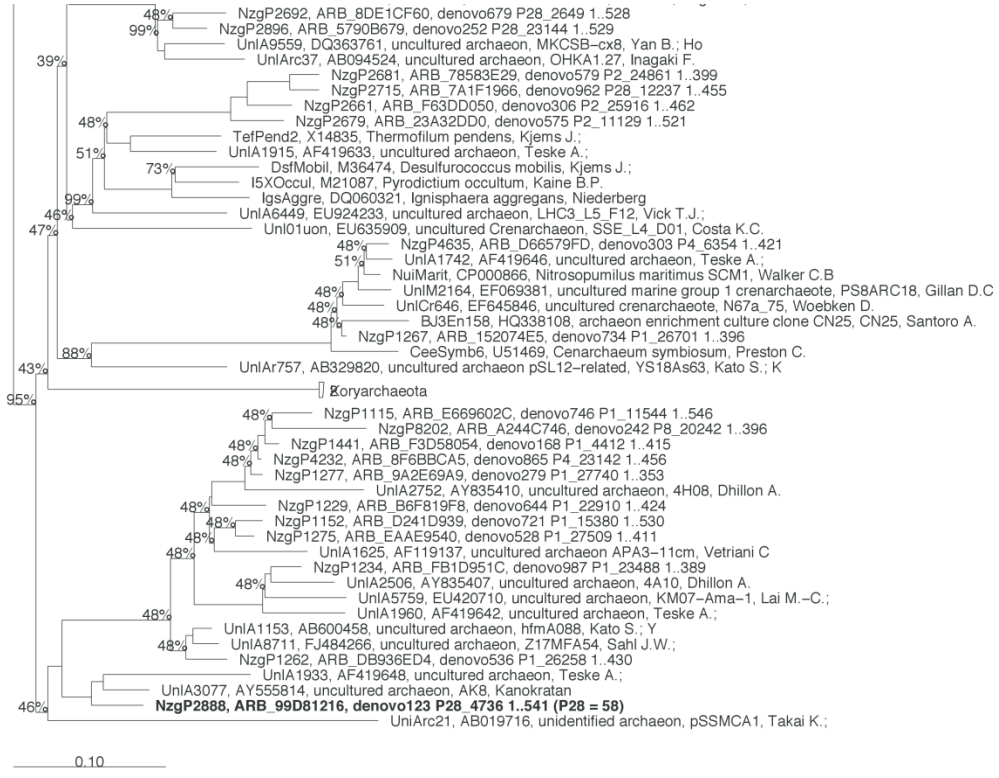
48%
NzgP2692, ARB_8DE1CF60, denovo679 P28_2649 1..528
99%
NzgP2896, ARB_5790B679, denovo252 P28_23144 1..529
UnlA9559, DQ363761, uncultured archaeon, MKCSB–cx8, Yan B.; Ho
39%
UnlArc37, AB094524, uncultured archaeon, OHKA1.27, Inagaki F.
NzgP2681, ARB_78583E29, denovo579 P2_24861 1..399
NzgP2715, ARB_7A1F1966, denovo962 P28_12237 1..455
NzgP2661, ARB_F63DD050, denovo306 P2_25916 1..462
48%
NzgP2679, ARB_23A32DD0, denovo575 P2_11129 1..521
TefPend2, X14835, Thermofilum pendens, Kjems J.;
51%
UnlA1915, AF419633, uncultured archaeon, Teske A.;
73%
DsfMobil, M36474, Desulfurococcus mobilis, Kjems J.;
I5XOccul, M21087, Pyrodictium occultum, Kaine B.P.
99%
IgsAggre, DQ060321, Ignisphaera aggregans, Niederberg
46%
UnlA6449, EU924233, uncultured archaeon, LHC3_L5_F12, Vick T.J.;
47%
Unl01uon, EU635909, uncultured Crenarchaeon, SSE_L4_D01, Costa K.C.
48%
NzgP4635, ARB_D66579FD, denovo303 P4_6354 1..421
51%
UnlA1742, AF419646, uncultured archaeon, Teske A.;
NuiMarit, CP000866, Nitrosopumilus maritimus SCM1, Walker C.B
48%
UnlM2164, EF069381, uncultured marine group 1 crenarchaeote, PS8ARC18, Gillan D.C
48%
UnlCr646, EF645846, uncultured crenarchaeote, N67a_75, Woebken D.
48%
BJ3En158, HQ338108, archaeon enrichment culture clone CN25, CN25, Santoro A.
NzgP1267, ARB_152074E5, denovo734 P1_26701 1..396
88%
CeeSymb6, U51469, Cenarchaeum symbiosum, Preston C.
43%
UnlAr757, AB329820, uncultured archaeon pSL12–related, YS18As63, Kato S.; K
Korarchaeota
95%
48%
NzgP1115, ARB_E669602C, denovo746 P1_11544 1..546
NzgP8202, ARB_A244C746, denovo242 P8_20242 1..396
48%
NzgP1441, ARB_F3D58054, denovo168 P1_4412 1..415
48%
NzgP4232, ARB_8F6BBCA5, denovo865 P4_23142 1..456
NzgP1277, ARB_9A2E69A9, denovo279 P1_27740 1..353
UnlA2752, AY835410, uncultured archaeon, 4H08, Dhillon A.
48%
NzgP1229, ARB_B6F819F8, denovo644 P1_22910 1..424
48%
NzgP1152, ARB_D241D939, denovo721 P1_15380 1..530
48%
NzgP1275, ARB_EAAE9540, denovo528 P1_27509 1..411
UnlA1625, AF119137, uncultured archaeon APA3–11cm, Vetriani C
48%
NzgP1234, ARB_FB1D951C, denovo987 P1_23488 1..389
48%
UnlA2506, AY835407, uncultured archaeon, 4A10, Dhillon A.
UnlA5759, EU420710, uncultured archaeon, KM07–Ama–1, Lai M.–C.;
UnlA1960, AF419642, uncultured archaeon, Teske A.;
48%
UnlA1153, AB600458, uncultured archaeon, hfmA088, Kato S.; Y
48%
UnlA8711, FJ484266, uncultured archaeon, Z17MFA54, Sahl J.W.;
NzgP1262, ARB_DB936ED4, denovo536 P1_26258 1..430
UnlA1933, AF419648, uncultured archaeon, Teske A.;
UnlA3077, AY555814, uncultured archaeon, AK8, Kanokratan
46%
NzgP2888, ARB_99D81216, denovo123 P28_4736 1..541 (P28 = 58)
UniArc21, AB019716, unidentified archaeon, pSSMCA1, Takai K.;
0.10

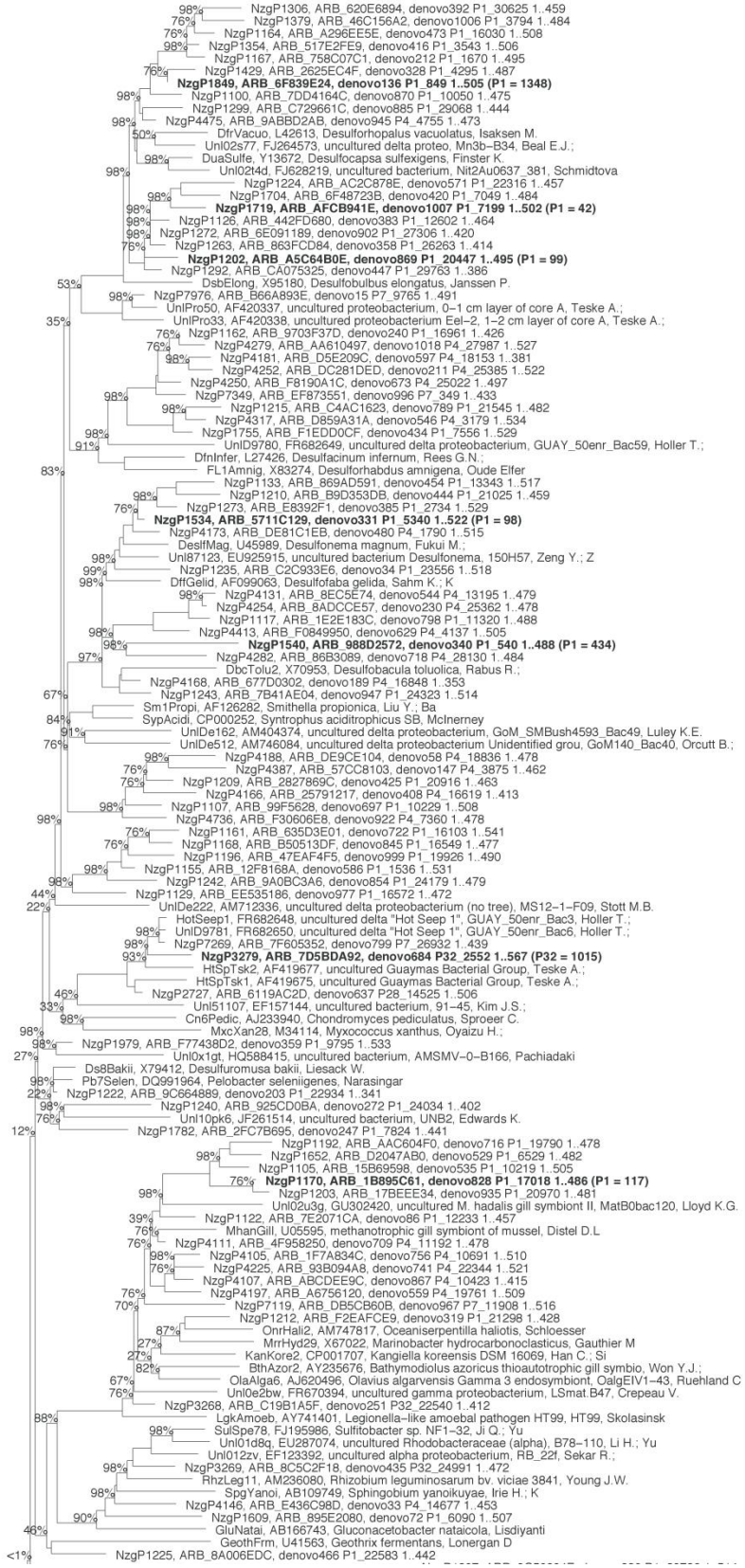
NzgP1306, ARB_620E6894, denovo392 P1_30625 1..459
NzgP1379, ARB_46C156A2, denovo1006 P1_3794 1..484
NzgP1164, ARB_A296EE5E, denovo473 P1_16030 1..508
NzgP1354, ARB_517E2FE9, denovo416 P1_3543 1..506
NzgP1167, ARB_758C07C1, denovo212 P1_1670 1..495
NzgP1429, ARB_2625EC4F, denovo328 P1_4295 1..487
NzgP1849, ARB_6F839E24, denovo136 P1_849 1..505 (P1 = 1348)
NzgP1100, ARB_7DD4164C, denovo870 P1_10050 1..475
NzgP1299, ARB_C729661C, denovo885 P1_29068 1..444
NzgP4475, ARB_9ABBD2AB, denovo945 P4_4755 1..473
DfrVacuo, L42613, Desulforhopalus vacuolatus, Isaksen M.
Unl02s77, FJ264573, uncultured delta proteo, Mn3b–B34, Beal E.J.;
DuaSulfe, Y13672, Desulfocapsa sulfexigens, Finster K.
Unl02t4d, FJ628219, uncultured bacterium, Nit2Au0637_381, Schmidtova
NzgP1224, ARB_AC2C878E, denovo571 P1_22316 1..457
NzgP1704, ARB_6F48723B, denovo420 P1_7049 1..484
NzgP1719, ARB_AFCB941E, denovo1007 P1_7199 1..502 (P1 = 42)
NzgP1126, ARB_442FD680, denovo383 P1_12602 1..464
NzgP1272, ARB_6E091189, denovo902 P1_27306 1..420
NzgP1263, ARB_863FCD84, denovo358 P1_26263 1..414
NzgP1202, ARB_A5C64B0E, denovo869 P1_20447 1..495 (P1 = 99)
NzgP1292, ARB_CA075325, denovo447 P1_29763 1..386
DsbElong, X95180, Desulfobulbus elongatus, Janssen P.
NzgP7976, ARB_B66A893E, denovo15 P7_9765 1..491
UnlPro50, AF420337, uncultured proteobacterium, 0–1 cm layer of core A, Teske A.;
UnlPro33, AF420338, uncultured proteobacterium Eel–2, 1–2 cm layer of core A, Teske A.;
NzgP1162, ARB_9703F37D, denovo240 P1_16961 1..426
NzgP4279, ARB_AA610497, denovo1018 P4_27987 1..527
NzgP4181, ARB_D5E209C, denovo597 P4_18153 1..381
NzgP4252, ARB_DC281DED, denovo211 P4_25385 1..522
NzgP4250, ARB_F8190A1C, denovo673 P4_25022 1..497
NzgP7349, ARB_EF873551, denovo996 P7_349 1..433
NzgP1215, ARB_C4AC1623, denovo789 P1_21545 1..482
NzgP4317, ARB_D859A31A, denovo546 P4_3179 1..534
NzgP1755, ARB_F1EDD0CF, denovo434 P1_7556 1..529
UnlD9780, FR682649, uncultured delta proteobacterium, GUAY_50enr_Bac59, Holler T.;
DfnInfer, L27426, Desulfacinum infernum, Rees G.N.;
FL1Amnig, X83274, Desulforhabdus amnigena, Oude Elfer
NzgP1133, ARB_869AD591, denovo454 P1_13343 1..517
NzgP1210, ARB_B9D353DB, denovo444 P1_21025 1..459
NzgP1273, ARB_E8392F1, denovo385 P1_2734 1..529
NzgP1534, ARB_5711C129, denovo331 P1_5340 1..522 (P1 = 98)
NzgP4173, ARB_DE81C1EB, denovo480 P4_1790 1..515
DeslfMag, U45989, Desulfonema magnum, Fukui M.;
Unl87123, EU925915, uncultured bacterium Desulfonema, 150H57, Zeng Y.; Z
NzgP1235, ARB_C2C933E6, denovo34 P1_23556 1..518
DffGelid, AF099063, Desulfofaba gelida, Sahm K.; K
NzgP4131, ARB_8EC5E74, denovo544 P4_13195 1..479
NzgP4254, ARB_8ADCCE57, denovo230 P4_25362 1..478
NzgP1117, ARB_1E2E183C, denovo798 P1_11320 1..488
NzgP4413, ARB_F0849950, denovo629 P4_4137 1..505
NzgP1540, ARB_988D2572, denovo340 P1_540 1..488 (P1 = 434)
NzgP4282, ARB_86B3089, denovo718 P4_28130 1..484
DbcTolu2, X70953, Desulfobacula toluolica, Rabus R.;
NzgP4168, ARB_677D0302, denovo189 P4_16848 1..353
NzgP1243, ARB_7B41AE04, denovo947 P1_24323 1..514
Sm1Propi, AF126282, Smithella propionica, Liu Y.; Ba
SypAcidi, CP000252, Syntrophus aciditrophicus SB, McInerney
UnlDe162, AM404374, uncultured delta proteobacterium, GoM_SMBush4593_Bac49, Luley K.E.
UnlDe512, AM746084, uncultured delta proteobacterium Unidentified grou, GoM140_Bac40, Orcutt B.;
NzgP4188, ARB_DE9CE104, denovo58 P4_18836 1..478
NzgP4387, ARB_57CC8103, denovo147 P4_3875 1..462
NzgP1209, ARB_2827869C, denovo425 P1_20916 1..463
NzgP4166, ARB_25791217, denovo408 P4_16619 1..413
NzgP1107, ARB_99F5628, denovo697 P1_10229 1..508
NzgP4736, ARB_F30606E8, denovo922 P4_7360 1..478
NzgP1161, ARB_635D3E01, denovo722 P1_16103 1..541
NzgP1168, ARB_B50513DF, denovo845 P1_16549 1..477
NzgP1196, ARB_47EAF4F5, denovo999 P1_19926 1..490
NzgP1155, ARB_12F8168A, denovo586 P1_1536 1..531
NzgP1242, ARB_9A0BC3A6, denovo854 P1_24179 1..479
NzgP1129, ARB_EE535186, denovo977 P1_16572 1..472
UnlDe222, AM712336, uncultured delta proteobacterium (no tree), MS12–1–F09, Stott M.B.
HotSeep1, FR682648, uncultured delta "Hot Seep 1", GUAY_50enr_Bac3, Holler T.;
UnlD9781, FR682650, uncultured delta "Hot Seep 1", GUAY_50enr_Bac6, Holler T.;
NzgP7269, ARB_7F605352, denovo799 P7_26932 1..439
NzgP3279, ARB_7D5BDA92, denovo684 P32_2552 1..567 (P32 = 1015)
HtSpTsk2, AF419677, uncultured Guaymas Bacterial Group, Teske A.;
HtSpTsk1, AF419675, uncultured Guaymas Bacterial Group, Teske A.;
NzgP2727, ARB_6119AC2D, denovo637 P28_14525 1..506
Unl51107, EF157144, uncultured bacterium, 91–45, Kim J.S.;
Cn6Pedic, AJ233940, Chondromyces pediculatus, Sproeer C.
MxcXan28, M34114, Myxococcus xanthus, Oyaizu H.;
NzgP1979, ARB_F77438D2, denovo359 P1_9795 1..533
Unl0x1gt, HQ588415, uncultured bacterium, AMSMV–0–B166, Pachiadaki
Ds8Bakii, X79412, Desulfuromusa bakii, Liesack W.
Pb7Selen, DQ991964, Pelobacter seleniigenes, Narasingar
NzgP1222, ARB_9C664889, denovo203 P1_22934 1..341
NzgP1240, ARB_925CD0BA, denovo272 P1_24034 1..402
Unl10pk6, JF261514, uncultured bacterium, UNB2, Edwards K.
NzgP1782, ARB_2FC7B695, denovo247 P1_7824 1..441
NzgP1192, ARB_AAC604F0, denovo716 P1_19790 1..478
NzgP1652, ARB_D2047AB0, denovo529 P1_6529 1..482
NzgP1105, ARB_15B69598, denovo535 P1_10219 1..505
NzgP1170, ARB_1B895C61, denovo828 P1_17018 1..486 (P1 = 117)
NzgP1203, ARB_17BEEE34, denovo935 P1_20970 1..481
Unl02u3g, GU302420, uncultured M. hadalis gill symbiont II, MatB0bac120, Lloyd K.G.
NzgP1122, ARB_7E2071CA, denovo86 P1_12233 1..457
MhanGill, U05595, methanotrophic gill symbiont of mussel, Distel D.L
NzgP4111, ARB_4F958250, denovo709 P4_11192 1..478
NzgP4105, ARB_1F7A834C, denovo756 P4_10691 1..510
NzgP4225, ARB_93B094A8, denovo741 P4_22344 1..521
NzgP4107, ARB_ABCDEE9C, denovo867 P4_10423 1..415
NzgP4197, ARB_A6756120, denovo559 P4_19761 1..509
NzgP7119, ARB_DB5CB60B, denovo967 P7_11908 1..516
NzgP1212, ARB_F2EAFCE9, denovo319 P1_21298 1..428
OnrHali2, AM747817, Oceaniserpentilla haliotis, Schloesser
MrrHyd29, X67022, Marinobacter hydrocarbonoclasticus, Gauthier M
KanKore2, CP001707, Kangiella koreensis DSM 16069, Han C.; Si
BthAzor2, AY235676, Bathymodiolus azoricus thioautotrophic gill symbio, Won Y.J.;
OlaAlga6, AJ620496, Olavius algarvensis Gamma 3 endosymbiont, OalgEIV1–43, Ruehland C
Unl0e2bw, FR670394, uncultured gamma proteobacterium, LSmat.B47, Crepeau V.
NzgP3268, ARB_C19B1A5F, denovo251 P32_22540 1..412
LgkAmoeb, AY741401, Legionella–like amoebal pathogen HT99, HT99, Skolasinsk
SulSpe78, FJ195986, Sulfitobacter sp. NF1–32, Ji Q.; Yu
Unl01d8q, EU287074, uncultured Rhodobacteraceae (alpha), B78–110, Li H.; Yu
Unl012zv, EF123392, uncultured alpha proteobacterium, RB_22f, Sekar R.;
NzgP3269, ARB_8C5C2F18, denovo435 P32_24991 1..472
RhzLeg11, AM236080, Rhizobium leguminosarum bv. viciae 3841, Young J.W.
SpgYanoi, AB109749, Sphingobium yanoikuyae, Irie H.; K
NzgP4146, ARB_E436C98D, denovo33 P4_14677 1..453
NzgP1609, ARB_895E2080, denovo72 P1_6090 1..507
GluNatai, AB166743, Gluconacetobacter nataicola, Lisdiyanti
GeothFrm, U41563, Geothrix fermentans, Lonergan D
NzgP1225, ARB_8A006EDC, denovo466 P1_22583 1..442


NzgP1207, ARB_3C50934F, denovo280 P1_20786 1..514
NzgP1952, ARB_7EFDE060, denovo85 P1_9563 1..484
NzgP1214, ARB_3E69C740, denovo660 P1_2127 1..521
98%
NzgP1143, ARB_A2DC7343, denovo949 P1_14254 1..510
NzgP1783, ARB_8796EA8D, denovo131 P1_7836 1..495
NzgP1173, ARB_89AC5258, denovo214 P1_1779 1..48 (P1 = 220)
NzgP1236, ARB_49B56303, denovo38 P1_23632 1..468
98%
NzgP1194, ARB_739A2AB8, denovo794 P1_19804 1..530
98%
Unl03o76, GQ261788, uncultured Bacteroidetes bacterium Cytophagacaea, 7mos_10s_E3, Goffredi S
NzgP1298, ARB_B52A6106, denovo639 P1_29276 1..422
62%
NzgP1850, ARB_FAC769E5, denovo774 P1_8504 1..446
NzgP1265, ARB_6F222EA, denovo693 P1_26963 1..366
78%
UnlB7567, AF419688, uncultured bacterium Cytophaga/Flavo/Bacteroidetes, Teske A.;
NzgP4130, ARB_110420FA, denovo23 P4_1300 1..432
97%
Unl54161, EF208704, uncultured bacterium Bacteroidetes, CI75cm.2.10, Sorensen K
98%
UnlCyto3, AB015264, uncultured Cytophaga sp., JTB250, Li L.; Kat
NzgP7334, ARB_39EC7532, denovo694 P7_3349 1..476
88%
Unl02dtx, EU925850, uncultured bacterium Bacteroidetes Bizionia, 042E70, Zeng Y.; Z
FlaSpe45, AM110988, Flavobacterium sp. 3034, Zeng R.; ;
Unl61773, EU287340, uncultured bacterium Cytoph/Flavo/Bacteroidetes, S26–40, Li H.; Yu
98%
PolGlome, AY771729, Polaribacter glomeratus, Lee H.K.;
NzgP7158, ARB_D80DC4E, denovo797 P7_1589 1..477
98%
RsgSpeci, EU697080, Roseivirga sp. F8, Liu H.J.;
2
Chlorobi
98%
31%
IgvAlbum, AB478415, Ignavibacterium album, Iino T.; M
13%
Unl024ml, GQ357017, uncultured bacterium, FeOrig_B_108, Beal E.J.;
6
Spirochaetes
76%
76%
MycHyop4, E02783, Mycoplasma hyopneumoniae, Nunofuji S
98%
MycMyco2, BX293980, Mycoplasma mycoides subsp. mycoides SC str. PG1, Westberg J
98%
NzgP7134, ARB_AB46216C, denovo236 P7_13451 1..370
UnlF1291, HM992539, uncultured Firmicutes bacterium, Ctrl2–5A, Siddique T
6%
Unl02c7f, GQ850577, uncultured bacterium, d128, Zeng Y.; ;
NzgP1175, ARB_9C5747DC, denovo843 P1_17394 1..459
98%
NzgP1216, ARB_494BC672, denovo818 P1_21437 1..451
98%
NzgP1103, ARB_E06FAC10, denovo339 P1_1035 1..522 (P1 = 46)
98%
NzgP1285, ARB_54EE9041, denovo984 P1_28269 1..353
NzgP1165, ARB_5B39BDF, denovo805 P1_16096 1..509
NzgP2722, ARB_5F9B0B48, denovo244 P2_29312 1..344
76%
NzgP1108, ARB_E60DECE0, denovo783 P1_10899 1..522
98%
NzgP1111, ARB_CEBA307E, denovo40 P1_11163 1..510
27%
Unl03lsp, HQ163692, uncultured bacterium, SIAC543, Walsh D.A.
NzgP1182, ARB_1A1B1E0F, denovo534 P1_18202 1..518
73%
Unl11v3z, JF747687, uncultured bacterium, MT5B12, Macalady J
Unl00als, FJ712503, uncultured bacterium, KZNMV–10–B11, Pachiadaki
10%
NzgP4189, ARB_31C4E9A9, denovo126 P4_18970 1..485
NzgP7104, ARB_85428AAE, denovo79 P7_10489 1..488
73%
Unl79364, EU542519, uncultured Unidentified group but with tree, Er–LLAYS–62, Ho C.–H.;
29%
Unl13626, AY592659, uncultured bacterium, Napoli–2B–37; BC07–2B–37, Heijs S.K.
2%
UnlDe346, AM997663, uncultured deep–sea bacterium, Ucp1540, Schauer R.
UnlO2233, EU245919, uncultured organism, MAT–CR–M8–B10, Isenbarger
34%
WCHA1–56, ARB_9BE11875, WCHA1–56 WS3 uncultured Dojka
98%
Unl00a1o, FJ712501, uncultured bacterium, KZNMV–10–B9, Pachiadaki
78%
NzgP7248, ARB_6C0BF15C, denovo971 P7_24837 1..372
58%
Unl001kd, FJ264784, uncultured bacterium, so4B4, Beal E.J.;
41%
Unl01qhb, EU491142, uncultured bacterium, P9X2b3F09, Santelli C
NzgP4255, ARB_BB79B2F5, denovo25 P4_25408 1..468
1%
UnlCa174, AY114319, uncultured candidate division WS3 bacterium, LD1–PA30, Freitag T.
ScaliWag, AY254882, Candidatus Scalindua wagneri, EN 5, Schmid M.;
UnlPl379, EU47867, uncultured Planctomycetales bacterium, Peru_56, Woebken D.
85%
AnbAmmo3, AJ131819, anaerobic ammonium–oxidizing planctomycete, 14, Strous M.;
NzgP7240, ARB_AB1D2A2C, denovo16 P7_24067 1..436
Unl02t9v, FJ905713, uncultured bacterium, V1F49b, Forget N.L
70%
NzgP1199, ARB_6E1184ED, denovo752 P1_19997 1..469
73%
UnlB9605, AF419673, uncultured bacterium Planktomycetales, Teske A.;
99%
BlaMari2, X62912, Blastopirellula marina, Liesack W.
Unl62902, EU386113, uncultured bacterium, MD2904–B19, Li T.; Wan
97%
PlancMar, AJ231184, Planctomyces maris, Griepenbur
99%
UnlPl910, FJ516830, uncultured Planctomycetales bacterium, TDNP_LSbc97_156_1_54, D'Auria G.
4%
Unl69882, EU385955, uncultured bacterium, MD2902–B173, Li T.; Wan
76%
B7USpec2, JF825448, Psychrilyobacter sp. STAB704, Finnegan L
76%
NzgP1686, ARB_A61EF558, denovo1017 P1_6866 1..465
Unl0x1fa, HQ588359, uncultured bacterium, AMSMV–0–B51, Pachiadaki
27%
Unl03gbh, HQ184025, uncultured bacterium, De100, Liu J.; Wu
1%
ProAc116, M61903, Propionibacterium acnes, Woese C.R.
95%
JS1candi, AB015269, uncultured candidate division JS1 bacterium, JTB138, Li L.; Kat
49%
Unl01ftn, EU386116, uncultured bacterium, MD2905–B4, Li T.; Wan
BcrEn443, HQ405607, bacterium enrichment culture clone AOM–SR–B16, AOM–SR–B16, Wang F.; C
83%
JS1benzn, AF029050, benzene mineralizing consortium clone SB–45, SB–45, Phelps C.D
UnlB7401, AF419693, uncultured bacterium, Teske A.;
NzgP4657, ARB_42941E7, denovo712 P4_6575 1..505
NzgP4821, ARB_72C2E793, denovo554 P4_8219 1..499
76%
NzgP4205, ARB_5E2983B5, denovo853 P4_20566 1..444
98%
Unl12290, AY197406, uncultured bacterium, B03R012, Dhillon A.
UnlCa841, HM041948, uncultured candidate division JS1 bacterium, NRB31, Kobayashi
47%
6%
Unl01ftb, EU386060, uncultured bacterium, MD2898–B18, Li T.; Wan
34%
Unl11v1z, JF747624, uncultured bacterium, MT5B41, Macalady J
98%
NzgP1256, ARB_B5BDE900, denovo990 P1_2564 1..477
98%
NzgP1286, ARB_1EEE0924, denovo223 P1_28678 1..354
98%
NzgP4375, ARB_85D497C4, denovo196 P4_3759 1..338
NzgP1157, ARB_F316C8A2, denovo905 P1_15011 1..477
NzgP8232, ARB_79EF6888, denovo305 P8_2, P3_2
98%
NzgP1269, ARB_3C32DA0C, denovo368 P1_26958 1..44 (P1 = 114)
85%
Unl040u1, HQ203810, uncultured bacterium, SW–Oct–105, Bae H.; Le
98%
Unl63589, EU265985, uncultured bacterium Sulfurimonas, Nit2A0626_59, Schmidtova
58%
UnlG2652, FJ497632, uncultured gamma proteobacterium, VS_CL–380, Sudek L.A.
98%
Unl03l49, GQ356998, uncultured bacterium, FeLiveControl_B_16, Beal E.J.;
NzgP1880, ARB_22BA295, denovo564 P1_880 1..503 (P1 = 1467, P3 = 52)
98%
NzgP3984, ARB_3796594C, denovo543 P3_984 1..487
98%
NzgP8192, ARB_302081C5, denovo169 P8_4, P2_2, P3_2
98%
NzgP4245, ARB_D96C939F, denovo498 P4_24550 1..451
98%
NzgP8398, ARB_B87652D9, denovo1 P8_40, P3_52
98%
NzgP4118, ARB_3DD33886, denovo456 P4_11779 1..412 (P4 = 41)
98%
NzgP8282, ARB_4C49D3C6, denovo729 P8_28232 1..355
98%
NzgP7700, ARB_373D2D1, denovo490 P7_7005 1..426
98%
NzgP8214, ARB_190949B9, denovo538 P8_21464 1..385
NzgP4931, ARB_E4FC93D1, denovo914 P4_931 1..506 (P1 = 60, P4 = 154)
62%
NzgP4223, ARB_6298256F, denovo18 P4_22373 1..409
75%
Unl02ye3, FJ712554, uncultured bacterium Epsilonproteo, KZNMV–10–B95, Pachiadaki
82%
Unl030vj, FJ712606, uncultured bacterium, KZNMV–30–B30, Pachiadaki
NzgP4106, ARB_FCB129F8, denovo725 P4_10619 1..477
98%
NzgP4258, ARB_F241757D, denovo779 P4_25245 1..361
98%
NzgP4249, ARB_B82C5A, denovo225 P4_24949 1..425
98%
NzgP1305, ARB_C973AC4A, denovo66 P1_30543 1..481
98%
Unl73717, EU570858, uncultured bacterium, Nit2Au0650_128, Schmidtova
61%
NzgP8116, ARB_4800CABB, denovo822 P8_11691 1..442
98%
NzgP8177, ARB_84EED4B1, denovo36 P8_17764 1..505
91%
SlfDeni5, L40808, Sulfurimonas denitrificans, Muyzer G.;
82%
Unl02qkx, FJ497591, uncultured bacterium, VS_CL–339, Sudek L.A.
99%
SlfParal, AB252048, Sulfurimonas paralvinellae, Takai K.;
98%
UnlEp288, AY225615, uncultured epsilon proteobacterium, AT–cs10, Lopez–Garc
94%
NzgP1131, ARB_930DCAB2, denovo488 P1_13197 1..414
NzgP4143, ARB_13A83680, denovo302 P4_1435 1..495
98%
NzgP4237, ARB_9B75A698, denovo686 P4_23728 1..331
NzgP4272, ARB_1ADFE1EE, denovo310 P4_2727 1..496
NzgP1144, ARB_AB878DDA, denovo352 P1_1442 1..404
98%
UnlHelic, AB188787, uncultured Helicobacter sp., SB5–24, Fang J.; A
98%
NzgP4395, ARB_B0629320, denovo582 P4_3951 1..497
NzgP4305, ARB_5A491AC5, denovo965 P4_3078 1..361

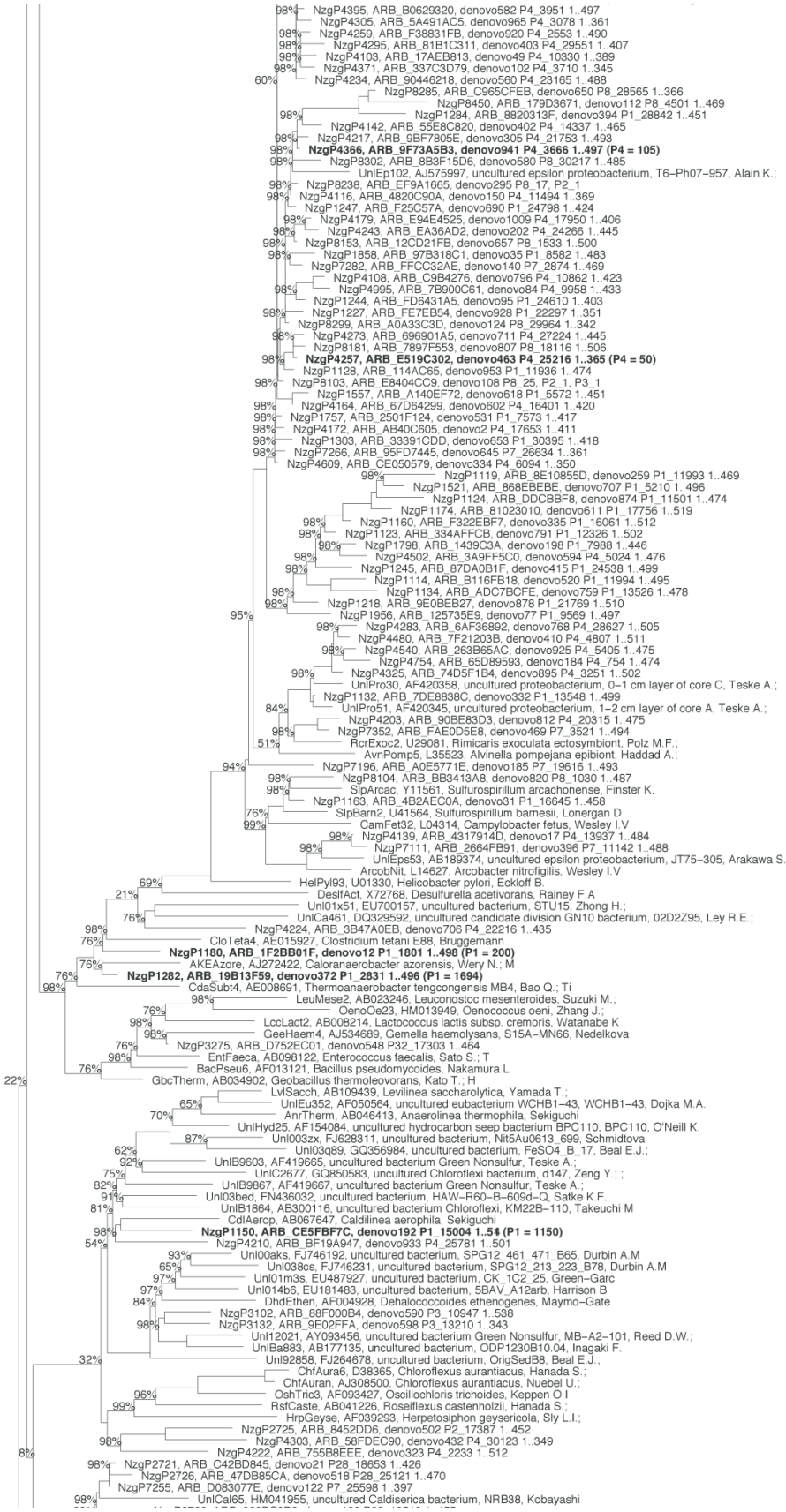
NzgP4395, ARB_B0629320, denovo582 P4_3951 1..497
NzgP4305, ARB_5A491AC5, denovo965 P4_3078 1..361
NzgP4259, ARB_F38831FB, denovo920 P4_2553 1..490
NzgP4295, ARB_81B1C311, denovo403 P4_29551 1..407
NzgP4103, ARB_17AEB813, denovo49 P4_10330 1..389
NzgP4371, ARB_337C3D79, denovo102 P4_3710 1..345
NzgP4234, ARB_90446218, denovo560 P4_23165 1..488
NzgP8285, ARB_C965CFEB, denovo650 P8_28565 1..366
NzgP8450, ARB_179D3671, denovo112 P8_4501 1..469
NzgP1284, ARB_8820313F, denovo394 P1_28842 1..451
NzgP4142, ARB_55E8C820, denovo402 P4_14337 1..465
NzgP4217, ARB_9BF7805E, denovo305 P4_21753 1..493
NzgP4366, ARB_9F73A5B3, denovo941 P4_3666 1..497 (P4 = 105)
NzgP8302, ARB_8B3F15D6, denovo580 P8_30217 1..485
UnlEp102, AJ575997, uncultured epsilon proteobacterium, T6–Ph07–957, Alain K.;
NzgP8238, ARB_EF9A1665, denovo295 P8_17, P2_1
NzgP4116, ARB_4820C90A, denovo150 P4_11494 1..369
NzgP1247, ARB_F25C57A, denovo690 P1_24798 1..424
NzgP4179, ARB_E94E4525, denovo1009 P4_17950 1..406
NzgP4243, ARB_EA36AD2, denovo202 P4_24266 1..445
NzgP8153, ARB_12CD21FB, denovo657 P8_1533 1..500
NzgP1858, ARB_97B318C1, denovo35 P1_8582 1..483
NzgP7282, ARB_FFCC32AE, denovo140 P7_2874 1..469
NzgP4108, ARB_C9B4276, denovo796 P4_10862 1..423
NzgP4995, ARB_7B900C61, denovo84 P4_9958 1..433
NzgP1244, ARB_FD6431A5, denovo95 P1_24610 1..403
NzgP1227, ARB_FE7EB54, denovo928 P1_22297 1..351
NzgP8299, ARB_A0A33C3D, denovo124 P8_29964 1..342
NzgP4273, ARB_696901A5, denovo711 P4_27224 1..445
NzgP8181, ARB_7897F553, denovo807 P8_18116 1..506
NzgP4257, ARB_E519C302, denovo463 P4_25216 1..365 (P4 = 50)
NzgP1128, ARB_114AC65, denovo953 P1_11936 1..474
NzgP8103, ARB_E8404CC9, denovo108 P8_25, P2_1, P3_1
NzgP1557, ARB_A140EF72, denovo618 P1_5572 1..451
NzgP4164, ARB_67D64299, denovo602 P4_16401 1..420
NzgP1757, ARB_2501F124, denovo531 P1_7573 1..417
NzgP4172, ARB_AB40C605, denovo2 P4_17653 1..411
NzgP1303, ARB_33391CDD, denovo653 P1_30395 1..418
NzgP7266, ARB_95FD7445, denovo645 P7_26634 1..361
NzgP4609, ARB_CE050579, denovo334 P4_6094 1..350
NzgP1119, ARB_8E10855D, denovo259 P1_11993 1..469
NzgP1521, ARB_868EBEBE, denovo707 P1_5210 1..496
NzgP1124, ARB_DDCBBF8, denovo874 P1_11501 1..474
NzgP1174, ARB_81023010, denovo611 P1_17756 1..519
NzgP1160, ARB_F322EBF7, denovo335 P1_16061 1..512
NzgP1123, ARB_334AFFCB, denovo791 P1_12326 1..502
NzgP1798, ARB_1439C3A, denovo198 P1_7988 1..446
NzgP4502, ARB_3A9FF5C0, denovo594 P4_5024 1..476
NzgP1245, ARB_87DA0B1F, denovo415 P1_24538 1..499
NzgP1114, ARB_B116FB18, denovo520 P1_11994 1..495
NzgP1134, ARB_ADC7BCFE, denovo759 P1_13526 1..478
NzgP1218, ARB_9E0BEB27, denovo878 P1_21769 1..510
NzgP1956, ARB_125735E9, denovo77 P1_9569 1..497
NzgP4283, ARB_6AF36892, denovo768 P4_28627 1..505
NzgP4480, ARB_7F21203B, denovo410 P4_4807 1..511
NzgP4540, ARB_263B65AC, denovo925 P4_5405 1..475
NzgP4754, ARB_65D89593, denovo184 P4_754 1..474
NzgP4325, ARB_74D5F1B4, denovo895 P4_3251 1..502
UnlPro30, AF420358, uncultured proteobacterium, 0–1 cm layer of core C, Teske A.;
NzgP1132, ARB_7DE8838C, denovo332 P1_13548 1..499
UnlPro51, AF420345, uncultured proteobacterium, 1–2 cm layer of core A, Teske A.;
NzgP4203, ARB_90BE83D3, denovo812 P4_20315 1..475
NzgP7352, ARB_FAE0D5E8, denovo469 P7_3521 1..494
RcrExoc2, U29081, Rimicaris exoculata ectosymbiont, Polz M.F.;
AvnPomp5, L35523, Alvinella pompejana epibiont, Haddad A.;
NzgP7196, ARB_A0E5771E, denovo185 P7_19616 1..493
NzgP8104, ARB_BB3413A8, denovo820 P8_1030 1..487
SlpArcac, Y11561, Sulfurospirillum arcachonense, Finster K.
NzgP1163, ARB_4B2AEC0A, denovo31 P1_16645 1..458
SlpBarn2, U41564, Sulfurospirillum barnesii, Lonergan D
CamFet32, L04314, Campylobacter fetus, Wesley I.V
NzgP4139, ARB_4317914D, denovo17 P4_13937 1..484
NzgP7111, ARB_2664FB91, denovo396 P7_11142 1..488
UnlEps53, AB189374, uncultured epsilon proteobacterium, JT75–305, Arakawa S.
ArcobNit, L14627, Arcobacter nitrofigilis, Wesley I.V
HelPyl93, U01330, Helicobacter pylori, Eckloff B.
DeslfAct, X72768, Desulfurella acetivorans, Rainey F.A
UnlO1x51, EU700157, uncultured bacterium, STU15, Zhong H.;
UnlCa461, DQ329592, uncultured candidate division GN10 bacterium, 02D2Z95, Ley R.E.;
NzgP4224, ARB_3B47A0EB, denovo706 P4_22216 1..435
CloTeta4, AE015927, Clostridium tetani E88, Bruggemann
NzgP1180, ARB_1F2BB01F, denovo12 P1_1801 1..498 (P1 = 200)
AKEAzore, AJ272422, Caloranaerobacter azorensis, Wery N.; M
NzgP1282, ARB_19B13F59, denovo372 P1_2831 1..496 (P1 = 1694)
CdaSubt4, AE008691, Thermoanaerobacter tengcongensis MB4, Bao Q.; Ti
LeuMese2, AB023246, Leuconostoc mesenteroides, Suzuki M.;
OenoOe23, HM013949, Oenococcus oeni, Zhang J.;
LccLact2, AB008214, Lactococcus lactis subsp. cremoris, Watanabe K
GeeHaem4, AJ534689, Gemella haemolysans, S15A–MN66, Nedelkova
NzgP3275, ARB_D752EC01, denovo548 P32_17303 1..464
EntFaeca, AB098122, Enterococcus faecalis, Sato S.; T
BacPseu6, AF013121, Bacillus pseudomycoides, Nakamura L
GbcTherm, AB034902, Geobacillus thermoleovorans, Kato T.; H
LvlSacch, AB109439, Levilinea saccharolytica, Yamada T.;
UnlEu352, AF050564, uncultured eubacterium WCHB1–43, WCHB1–43, Dojka M.A.
AnrTherm, AB046413, Anaerolinea thermophila, Sekiguchi
UnlHyd25, AF154084, uncultured hydrocarbon seep bacterium BPC110, BPC110, O'Neill K.
Unl003zx, FJ628311, uncultured bacterium, Nit5Au0613_699, Schmidtova
Unl03q89, GQ356984, uncultured bacterium, FeSO4_B_17, Beal E.J.;
UnlB9603, AF419665, uncultured bacterium Green Nonsulfur, Teske A.;
UnlC2677, GQ850583, uncultured Chloroflexi bacterium, d147, Zeng Y.; ;
UnlB9867, AF419667, uncultured bacterium Green Nonsulfur, Teske A.;
Unl03bed, FN436032, uncultured bacterium, HAW–R60–B–609d–Q, Satke K.F.
UnlB1864, AB300116, uncultured bacterium Chloroflexi, KM22B–110, Takeuchi M
CdlAerop, AB067647, Caldilinea aerophila, Sekiguchi
NzgP1150, ARB_CE5FBF7C, denovo192 P1_15004 1..5$ (P1 = 1150)
NzgP4210, ARB_BF19A947, denovo933 P4_25781 1..501
Unl00aks, FJ746192, uncultured bacterium, SPG12_461_471_B65, Durbin A.M
Unl038cs, FJ746231, uncultured bacterium, SPG12_213_223_B78, Durbin A.M
Unl01m3s, EU487927, uncultured bacterium, CK_1C2_25, Green–Garc
Unl014b6, EU181483, uncultured bacterium, 5BAV_A12arb, Harrison B
DhdEthen, AF004928, Dehalococcoides ethenogenes, Maymo–Gate
NzgP3102, ARB_88F000B4, denovo590 P3_10947 1..538
NzgP3132, ARB_9E02FFA, denovo598 P3_13210 1..343
Unl12021, AY093456, uncultured bacterium Green Nonsulfur, MB–A2–101, Reed D.W.;
UnlBa883, AB177135, uncultured bacterium, ODP1230B10.04, Inagaki F.
Unl92858, FJ264678, uncultured bacterium, OrigSedB8, Beal E.J.;
ChfAura6, D38365, Chloroflexus aurantiacus, Hanada S.;
ChfAuran, AJ308500, Chloroflexus aurantiacus, Nuebel U.;
OshTric3, AF093427, Oscillochloris trichoides, Keppen O.I
RsfCaste, AB041226, Roseiflexus castenholzii, Hanada S.;
HrpGeyse, AF039293, Herpetosiphon geysericola, Sly L.I.;
NzgP2725, ARB_8452DD6, denovo502 P2_17387 1..452
NzgP4303, ARB_58FDEC90, denovo432 P4_30123 1..349
NzgP4222, ARB_75588EEE, denovo323 P4_2233 1..512
NzgP2721, ARB_C42BD845, denovo21 P28_18653 1..426
NzgP2726, ARB_47DB85CA, denovo518 P28_25121 1..470
NzgP7255, ARB_D083077E, denovo122 P7_25598 1..397
UnlCal65, HM041955, uncultured Caldiserica bacterium, NRB38, Kobayashi

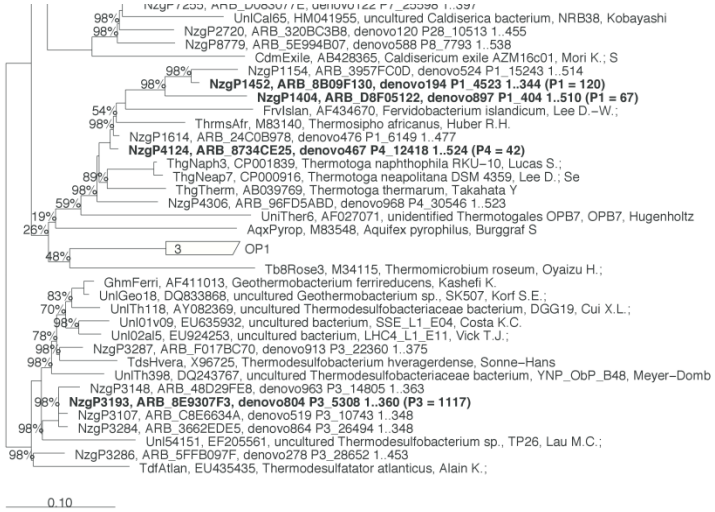

Supplementary Figure S7A, B. Total 16S rRNA phylogeny for Archaea (A) and Bacteria (B) for chapter 3. Trees were generated by the Arb neighbor-joining method with a Jukes-Cantor correction. Bootstrap values indicate the confidence in branch placement after 500 iterations of the tree. OTU from this study are shown in bold and following each OTU name is the associated sample name and number of sequences in that sample separated by an underscore.

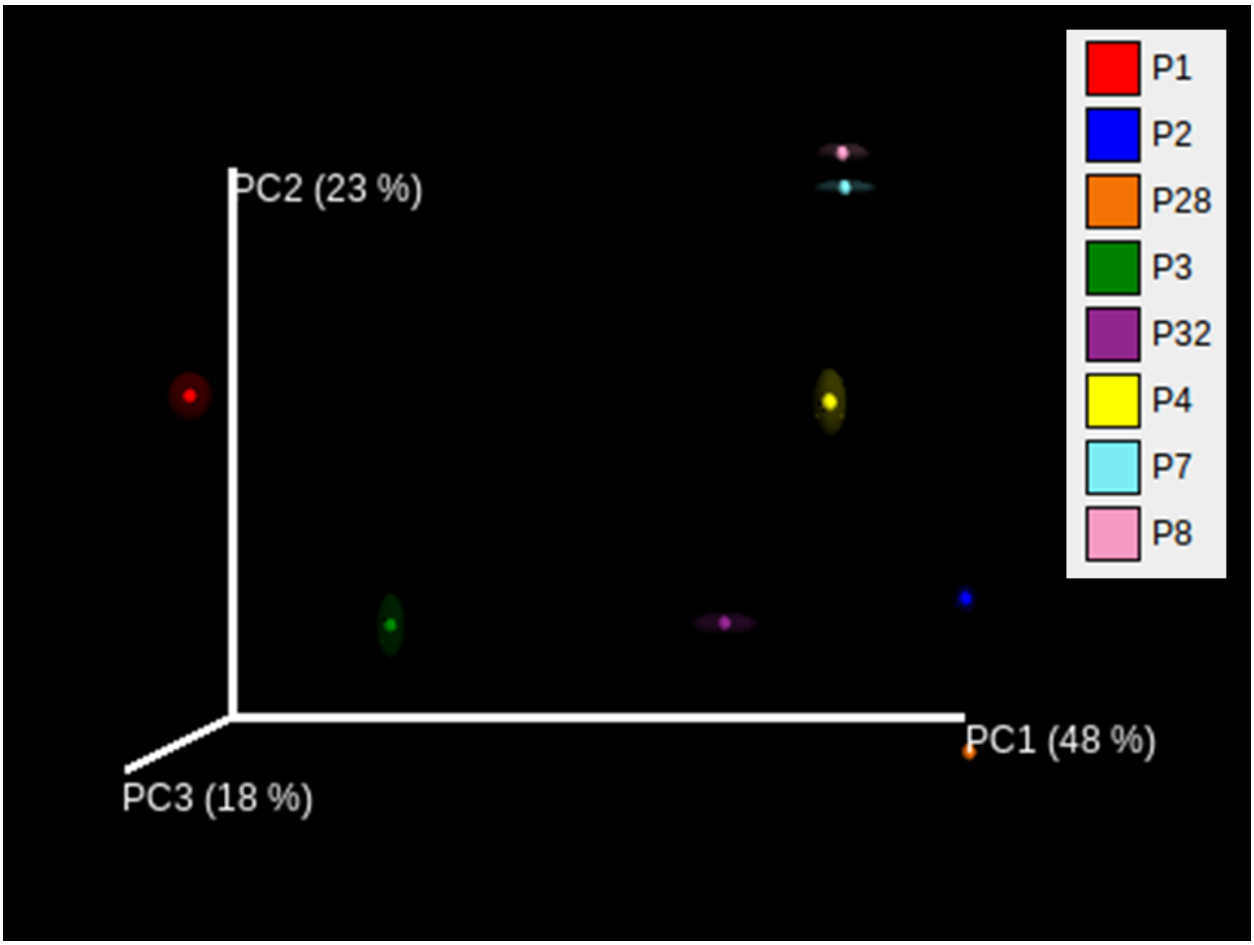

Supplementary Figure S8. Jackknifed beta diversity for weighted, normalized sequence information from collapsed samples. Data is plotted three dimensionally on component axes representing 48%, 23%, and 18% of the total variation in diversity.

REFERENCES

Alm EW, Oerther DB, Larsen N, Stahl DA, Raskin L (1996) The Oligonucleotide Probe Database. *Appl Environ Microbiol* 62: 3557-3559.

Abed RMM, Zein B, Al-Thukair A, de Beer D (2007) Phylogenetic diversity and activity of aerobic heterotrophic bacteria from a hypersaline oil-polluted microbial mat. *Syst Appl Microbiol* 30: 319-330.

Amann RI, Ludwig W, Schleifer K-H (1995) Phylogenetic identification and in situ detection of individual microbial cells without cultivation. *Microbiol. Rev.* 59: 143–69.

Amin SA, Green DH, Hart MC, Kupper FC, Sunda WG, and Carrano CJ (2009) Photolysis of iron-siderophore chelates promotes bacterial-algal mutualism. *Proc Nat Acad Sci* 106,17071-17076.

Beeder J, Nilsen RK, Rosnes JT, Torsvik T, Lien T (1994) *Archaeoglobus fulgidus* isolated from Hot North Sea Oil Field Waters. *Applied and Environmental Microbiology* 60 (4): 1227 – 1231.

Biddle JF, Cardman Z, Mendlovitz H, Albert DB, Lloyd KG, et al. (2012) Anaerobic oxidation of methane at different temperature regimes in Guaymas Basin hydrothermal sediments. *ISME J* 6: 1018-1031.

Blackburn SI, Hallegraeff GM and Bolch CJ (1989) Vegetative reproduction and sexual life cycle of the toxic dinoflagellate *Gymnodinium catenatum* from Tasmania, Australia *J Phycol* 25: 577-590.

Boetius A, Ravenschlag K, Schubert C, Rickert D, Widdel F, et al. (2000) A marine microbial consortium apparently mediating anaerobic oxidation of methane. *Nature* 407: 623 – 626.

Brinkmeyer R, Knittel K, Jurgens J, Weyland H, Amann R, Helmke E (2003) Diversity and Structure of Bacterial Communities in Arctic versus Antarctic Pack Ice. *Applied and Environmental Microbiology* 69 *(11): 6610-6619.*

Burggraf S, Jannasch HW, Nicolaus B, Stetter KO (1990) *Archaeoglobus profundus* sp. nov., represents a new species within the sulfate-reducing archaebacteria. *Syst Appl Microbiol* 13: 24 – 28.

Campbell BJ, Engel AS, Porter ML, Takai K (2006) The versatile epsilon-proteobacteria: key players in sulphidic habitats. *Nat Rev Microbiol* 4: 458 – 468.

Caporaso JG, Kuczynski J, Stombaugh J, Bittinger K, Bushman FD, et al. (2010) QIIME allows analysis of high-throughput community sequencing data. *Nature Methods* doi:10.1038/nmeth.f.303

Cline JD (1969) Spectrophotometric determination of hydrogen sulfide in natural waters. *Limnol Oceanogr* 14: 454 – 458.

Cline MS, Smoot M, Cerami E, Kuchinsky A, et al. (2007) Integration of biological networks and gene expression data using Cytoscape. *Nature Protocols* doi: 10.1038/nprot.2007.324

Cole JR, Wang Q, Cardenas E, Fish J, Chai B, Farris RJ, et al. (2009) The ribosomal database project: improved alignments and new tools for rRNA analysis. Nucleic Acids Research 37: D141-D145.

Daims H, Stoecker K, and Wagner M (2005) Fluorescence in situ hybridization for the detection of prokaryotes. Advanced Methods in Molecular Microbial Ecology. BIOS Scientific Publishers, Abingdon, UK, pp. 213-239.

De la Lanza-Espino G, Soto LA (1999) Sedimentary geochemistry of hydrothermal vents in Guaymas Basin, Gulf of California, Mexico. *Applied Geochemistry* 14: 499 – 510.

Dell'Anno and Danovaro (2005) Extracellular DNA plays a key role in deep-sea ecosystem functioning. *Science* 309 (5744), 2179

DeLong EF (1992) Archaea in coastal marine environments. *Proc Natl Acad Sci* USA 89: 5685 – 5689.

Diercks AR, Highsmith RC, Asper VL, Joung D, Zhou Z, Guo L, et al. (2010) Characterization of subsurface polycyclic aromatic hydrocarbons at the Deepwater Horizon site. *Geophys. Res. Lett.* 37: L20602

Dojka MA, Hugenholtz P, Haack SK, Pace NR (1998) Microbial diversity in a hydrocarbon- and chlorinated-solvent-contaminated aquifer undergoing intrinsic bioremediation. *Appl Environ Microbiol* 64: 3869 – 3877.

Duran R (2010) Marinobacter. In: Timmis KN (ed) *Handbook of hydrocarbon and lipid microbiology*. Springer-Verlag, Berlin, pp. 1726–1735.

Durbin AM, Teske A (2011) Microbial diversity and stratification of South Pacific abyssal marine sediments. *Envrion Microbiol* 13 (12): 3219 – 3234.

Dyksterhouse SE, Gray JP, Herwig RP, Lara JC, Staley JS (1995) *Cycloclasticus pugetii* gen. nov., sp. nov., an aromatic hydrocarbon-degrading bacterium from marine sediments. *Int.*

J. Syst. Bacteriol. 45: 116-123.

Edgar RC (2010) Search and clustering orders of magnitude faster than BLAST. *Bioinformatics* 26(19), 2460-2461. doi: 10.1093/bioinformatics/btq461

Einsele G, Gieskes JM, Curray J, Moore DM, Aguayo E, et al. (1980) Intrusion of basaltic sills into highly porous sediments, and resulting hydrothermal activity. *Nature* 283: 441 – 445.

Engel AS, Lee N, Porter ML, Stern LA, Bennett PC, Wagner M (2003) Filamentous "*Epsilonproteobacteria"* dominate microbial mats from sulfidic cave springs. *Appl Environ Microbiol* 69 (9): 5503 – 5511.

Finster KW, Kjeldsen KU, Kube M, Reinhardt R, Mussmann M, Amann R, and Schreiber L (2013) Complete genome sequence of *Desulfocapsa sulfexigens*, a marine deltaproteobacterium specialized in disproportionating inorganic sulfur compounds. *Stand Genomic Sci*, 8(1): 58-68.

Fuerst JA and Sagulenko E (2011) Beyond the bacterium: planctomycetes challenge our concepts of microbial structure and function. Nature Reviews Microbiology 9: 403 – 413.

Gauthier MJ, Lafay B, Christen R, Fernandez L, Acquaviva M, Bonin P, Bertrand J-C (1992). Marinobacter hydrocarbonoclasticus gen. nov., sp. nov., a new extremely halotolerant, hydrocarbon-degrading marine bacterium. *Int. J. Syst. Bacteriol*. 42*:* 568*–576.*

Girguis PR, Orphan VJ, Hallam SJ, DeLong EF (2003) Growth and Methane Oxidation Rates of Anaerobic Methanotrophic Archaea in a Continuous-Flow Bioreactor. *Appl Environ Microbiol*, 69 (9): 5472 – 5482.

Glöckner FO, Amann R, Alfreider A, Pernthaler J, Psenner R, Trebesius K, Schleiger KH (1996) An in situ hybridization protocol for detection and identification of planktonic bacteria. *Syst Appl Microbiol* 19: 403-406.

Graham WM, Condon RH, Carmichael RH, D'Ambra I, Patterson HK, Linn LJ, Hernandez Jr FJ (2010) Oil carbon entered the coastal planktonic food web during the Deepwater Horizon oil spill. *Environ. Res. Lett.* 5: 045301

Gray ND, Sherry A, Grant RJ, Rowan AK, Huber CRJ, Callbeck CM, Aitken CM, Jones DM, Adams JJ, Larter SR and Head IM (2011) The quantitative significance of Syntrophaceae and syntrophic partnerships in methanogenic degradation of crude oil alkanes. *Environ Microbiol* 13: 2957-2975.

Green DH, Bowman JP, Smith EA, Gutierrez T, and Bolch CJS (2006). *Marinobacter algicola* sp. nov., isolated from laboratory cultures of paralytic shellfish toxin-producing dinoflagellates. Int J Syst Evol Microbiol 56*:* 523–527.

Gundersen JK, Jørgensen BB, Larsen E, Jannasch HW (1992) Mats of giant sulphur bacteria on deep-sea sediments due to fluctuating hydrothermal flow. *Nature* 360: 454 – 456.

Guo B, Jun G, Yu-Guang Y, Yue-Qin T, Kenji K, and Xiao-Lei W (2007) Marinobacter segnicrescens sp. nov., a moderate halophile isolated from benthic sediment of the South China Sea. Int J Syst Evol Microbiol 57: 1970 – 1974.

Hafenbradl D, Keller M, Dirmeier R, Rachel R, Rossnagel P, et al. (1996) *Ferroglobus placidus* gen. nov., a novel hyperthermophilic archaeum that oxidizes Fe2+ at neutral pH under anoxic conditions. *Arch Microbiol* 166: 308 – 314.

Haroon MF, Hu S, Shi Y, Imelfort M, Keller J, Hugenholtz P, Yuan Z, Tyson GW (2013) Anaerobic oxidation of methane coupled to nitrate reduction in a novel archaeal lineage. *Nature* 500: 567–570

Hayworth JS, Clement TP, Valentine JF (2011) Deepwater Horizon oil spill impacts on Alabama beaches. *Hydrol Earth Syst Sci* 15: 3639-3649.

Hazen TC, Dubinsky EA, DeSantis TZ, Andersen GL, Piceno YM, Singh N, et al. (2010) Deep-sea oil plume enriches indigenous oil-degrading bacteria. *Science* 330: 204-208.

Head IM, Jones DM, Röling WFM (2006) Marine microorganisms make a meal of oil. *Nature Microbiol Rev* 4: 173-182.

Holler T, Widdel F, Knittel K, Amann R, Kellermann MY, et al. (2011) Thermophilic anaerobic oxidation of methane by marine microbial consortia. *ISME J* 5: 1946 – 1956.

Hu S, Zeng RJ, Burow LC, Lant P, Keller J, Yuan Z (2009) Enrichment of denitrifying anaerobic methane oxidizing microorganisms. *Environmental Microbiol. Rep.* 1: 377 – 384.

Huber H, Jannasch H, Rachel R, Fuchs T, Stetter KO (1997) *Archaeoglobus veneficus* sp. nov., a novel facultative chemolithoautotrophic hyperthermophilic sulfite reducer, isolated from abyssal black smokers. *Systematic and Applied Microbiology* 20 (3): 374 – 380.

Inagaki F, Suzuki M, Takai K, Oida H, Sakamoto T, Aoki K, Nealson KH, Horikoshi K (2003) Microbial communities associated with geological horizons in coastal subseafloor sediments from the Sea of Okhotsk. *Appl Environ Microbiol* 69: 7224 – 7235.

Jones WJ, Leigh JA, Mayer F, Woese CR, and Wolfe RS (1983). *Methanococcus jannaschii* sp. nov., an extremely thermophilic methanogen from a submarine hydrothermal vent. *Arch. Microbiol*. 136, 254-261.

Jorgensen SL, Hannisdal B, Lanzén A, Baumberger T, Flesland K, et al. (2012) Correlating microbial community profiles with geochemical data in highly stratified sediments from the Arctic Mid-Ocean Ridge. PNAS doi: 10.1073/pnas.1207574109

Kallmeyer J, Boetius A (2004) Effects of temperature and pressure on sulfate reduction and anaerobic oxidation of methane in hydrothermal sediments of Guaymas Basin. *Appl Environ Microbiol* 70: 1231 – 1233.

Kanokratana P, Chanapan S, Pootanakit K, Eurwilaichitr L (2004) Diversity and abundance of *Bacteria* and *Archaea* in the Bor Khlueng Hot Spring in Thailand. *Journal of Basic Microbiology* 44 (6): 430 – 444.

Kelley DS, Karson JA, Fruh-Green GL, Yoerger DR, Shank TM, Butterfield DA, et al. (2005) A serpentinite-hosted ecosystem: the Lost City Hydrothermal Field. *Science* 307: 1428–1434

Kessler JD, Valentine DL, Redmond MC, Du M, Chan EW, Mendes SD, Quiroz EW, Villanueva CJ, Shusta SS, Werra LM, Yvon-Lewis SA, Weber TC (2011) A persistent oxygen anomaly reveals the fate of spilled methane in the deep Gulf of Mexico. *Sci*ence 331: 312-315

Kirchman DL (2002) The ecology of Cytophaga – Flavobacteria in aquatic environments. *FEMS Microbiol Ecol* 39: 91 – 100.

Knittel K, Lösekann T, Boetius A, Kort R, Amann R (2005) Diversity and Distribution of Methanotrophic Archaea at Cold Seeps. *Appl. Environ. Microbiol.* 71(1): 467 – 479.

Knittel K, Boetius A (2009) Anaerobic oxidation of methane: progress with an unknown process. *Annu Rev Microbiol* 63: 311 – 334.

Kostka JE, Prakash O, Overholt WA, Green SJ, Freyer G, Canion A, Delgardio J, Norton N, Hazen TC, Hüttel M (2011) Hydrocarbon-degrading bacteria and the bacterial community response in Gulf of Mexico beach sands impacted by the Deepwater Horizon oil spill. *Appl Environ Microbiol* 77: 7962-7974.

Kurr M, Huber R, König H, Jannasch HW, Fricke H, Trincone A, Kristjansson JK, Stetter KO (1991) *Methanopyrus kandleri*, gen. and sp. nov. represents a novel group of hyperthermophilic methanogens, growing at 110ºC. *Arch. Microbiol.* 156, 239 –247.

Lane DJ, Pace B, Olsen GJ, Stahl DA, Sogin ML, Pace NR (1985) Rapid determination of 16S ribosomal RNA sequences for phylogenetic analyses. *Proc Natl Acad Sci* USA 82:6955–6959.

Lane DL (1991) 16S/23 rRNA sequencing. In: Goodfellow, E. S. (Eds.) *Nucleic Acid Techniques in Bacterial Systematics*. John Wiley & Sons, Chicester, UK, pp. 115–176.

LaRowe DE, Dale AW, Regnier P (2008) A thermodynamic analysis of the anaerobic oxidation of methane in marine sediments. *Geobiol* 6 (5): 436 – 449.

Lau MCY, Aitchison JC, Pointing SB (2009) Bacterial community composition in thermophilic microbial mats from five hot springs in central Tibet. *Extremophiles* 13(1): 139 – 149.

Lin C and Stahl D (1995) Taxon-specific probes for the cullulolytic genus Fibrobacter reveal abundant and novel equine-associated populations. *Appl. Environ. Micriobiol*. 61: 1348 – 1351.

Liu Z, Liu J, Zhu Q, Wu W (2012) The weathering of oil after the *Deepwater Horizon* oil spill: insights from the chemical composition of the oil from the sea surface, salt marshes and sediments. *Environ. Res. Lett.* 7: 035302

Lizarralde D, Axen GJ, Brown HE, Fletcher JM, González-Fernández A, et al. (2007) Variation in styles of rifting in the Gulf of California. *Nature* 448: 466 – 469.

Lloyd KG, Schreiber L, Petersen DG, Kjeldsen KU, Lever MA, et al. (2013) Predominant archaea in marine sediments degrade detrital proteins. *Nature* 496: 215 – 218.

Lloyd KG, Alperin MJ, Teske A (2011) Environmental evidence for net methane production and oxidation in putative ANaerobic MEthanotrophic (ANME) archaea. *Environmental Microbiology* 13 (9): 2548 – 2564.

Lloyd KG, Albert DB, Biddle JF, Chanton JP, Pizarro O, Teske A (2010) Spatial structure and activity of sedimentary microbial communities underlying a *Beggiatoa* spp. Mat in a Gulf of Mexico hydrocarbon seep. *PLOS One* PLoS ONE 5(1): e8738. doi: 10.1371/journal.pone.0008738

Lozupone C, Knight R (2005) UniFrac: a new phylogenetic method for comparing microbial communities. *Appl Environ Microbiol* 71 (12): 8228 – 8235.

Lozupone C, Hamady M, Knight R (2006) UniFrac – an online tool for comparing microbial community diversity in a phylogenetic context. *Bioinformatics* 7: 371

Loy A, Schulz C, Lücker S, Schöpfer-Wendels A, Stoecker K, Baranyi C, et al. (2005) 16S rRNA gene-based oligonucleotide microarray for environmental monitoring of the betaproteobacterial order Rhodocyclales. *Appl Environ Microbiol* 71: 1373-1386.

Loy A, Arnold R, Tischler P, Rattei T, Wagner M, Horn M (2008) probeCheck - a central resource for evaluating oligonucleotide probe coverage and specificity. *Environ Microbiol* 10: 2894-2896.

Ludwig W, Strunk O, Westram R, Richter L, Meier H, et al. (2004) ARB: a software environment for sequence data. *Nucleic Acids Res* 32: 1363 – 1371.

MacGregor B, Moser DP, Alm EW, Nealson KH, Stahl DA (1997) Crenarchaeota in Lake Michigan sediment. *Appl. Environ. Microbiol.* 63: 1178 – 1181.

Manz W, Amann R, Ludwig W, Wagner M, Schleifer KH (1992) Phylogenetic Oligodeoxynucleotide Probes for the Major Subclasses of Proteobacteria: Problems and Solutions. *Systematic and Applied Microbiology* 15: 593-600.

Martens CS, Albert DB, Alperin MJ (1999) Stable isotopic tracing of anaerobic methane oxidation in the gassy sediments of Eckernförde Bay, German Baltic Sea. *Am J Sci* 299: 589 – 610.

Maruyama A, Ishiwata H, Kitamura K, Sunamura M, Fujita T, Matsuo M, Higashihara T (2003) Dynamics of microbial populations and strong selection for *Cycloclasticus pugetii* following the Nakhodka oil spill. *Microb Ecol* 46: 442–453

McIlroy S, Porter K, Seviour RJ, Tillett D (2008) Simple and safe method for simultaneous isolation of microbial RNA and DNA from problematic populations. *Appl. Environ. Microbiol*. 74: 6806 – 6807.

McKay LJ, MacGregor BJ, Biddle JF, Albert DB, Mendlovitz HP, et al. (2012) Spatial heterogeneity and underlying geochemistry of phylogenetically diverse orange and white *Beggiatoa* mats in Guaymas Basin hydrothermal sediments. *Deep-Sea Research I* 67: 21 – 31.

McGowan L, Herbert R, Muyzer G (2004) A comparative study of hydrocarbon degradation by *Marinobacter* sp., *Rhodococcus* sp. and *Corynebacterium* sp. isolated from different mat systems. *Ophelia* 58: 271–281.

Meng J, Xu J, Qin D, He Y, Xiao X, Want F (2014) Genetic and functional properties of uncultivated MCG archaea assessed by metagenome and gene expression analyses. *ISME J* 8: 650-659.

Merkel AY, Huber JA, Chernyh NA, Bonch-Osmolovskaya EA, Lebedinsky AV (2013) Detection of a putatively thermophilic anaerobic methanotrophs in diffuse hydrothermal vent fluids. *Appl Environ Microbiol* 79: 915 – 923.

Meyer S, Wegener G, Lloyd KG, Teske A, Boetius A, Ramette A (2013) Microbial habitat connectivity across spatial scales and hydrothermal temperature gradients at Guaymas Basin. *Frontiers in Microbiology* DOI: 10.3389/fmicb.2013.00207

Mills HJ, Martinez RJ, Story S, Sobecky PA. (2004). Identification of members of the metabolically active microbial populations associated with Beggiatoa species mat communities from Gulf of Mexico cold-seep sediments. *Appl Environ Microbiol* 70: 5447–5458.

Moe WM, Yan J, Nobre MF, da Costa MS, Rainey FA (2009) *Dehalogenimonas lykanthroporepellens* gen. nov., sp. nov., a reductively dehalogenating bacterium isolated

from chlorinated solvent-contaminated groundwater. *Int J Syst Evol Microbiol* 59: 2692 – 2697.

Mori K, Yamaguchi K, Sakiyama Y, Urabe T, Suzuki K (2009) *Caldisericum exile* gen. nov., sp. nov., an anaerobic, thermophilic, filamentous bacterium of a novel bacterial phylum,*Caldiserica* phyl. nov., originally called the candidate phylum OP5, and description of *Caldisericaceae* fam. nov.,*Caldisericales* ord. nov. and *Caldisericia*classis nov. *Int'l Journ. System. Evol. Microbiol.* 59 (11): 2894 – 2898.

Moussard H, Moreira D, Cambon-Bonavita MA, López-Garcia P, Jeanthon C (2006) Uncultured archaea in a hydrothermal microbial assemblage: phylogenetic diversity and characterization of a genome fragment from a euryarchaeote. *FEMS Microbiol Ecol* 57: 452 – 469.

Mußmann M, Ishii K, Rabus R, Amann R (2005) Diversity and vertical distribution of cultured and uncultured *Deltaproteobacteria* in an intertidal mud flat of the Wadden Sea. *Environ Microbiol* 7 (3): 405 – 418.

Muyzer G, Stams AJM (2008) The ecology and biotechnology of sulphate-reducing bacteria. *Nat Rev Microbiol* 6: 441 – 454.

Nguyen BH, Denner E, Ha Dang T, Wanner G, Stan-Lotter H (1999) *Marinobacter aquaeolei* sp. nov., a halophilic bacterium isolated from a Vietnamese oil-producing well. *Int J Syst Bacteriol* 49: 367–375.

Orphan VJ, Hinrichs K-U, Paull CK, Taylor LT, Sylva S, and Delong EF (2001) Comparative analysis of methane-oxidizing archaea and sulfate-reducing bacteria in anoxic marine sediments. *Appl. Environ. Microbiol*. 67: 1922 – 1934.

Pearson A, Seewald JS, Eglinton TI (2005) Bacterial incorporation of relict carbon in the hydrothermal environment of Guaymas Basin. *Geochim Coscochim Acta* 69: 5477 – 5486.

Pernthaler J, Glöckner FO, Schönhuber W, Amann R (2001*) Fluorescence* in situ *hybridization (FISH) with rRNA-targeted oligonucleotide probes.* Methods Microbiol 30: 207-*226.*

Porter KG, Feig YS (1980) The use of DAPI for identifying and counting aquatic microflora. *Limnol Oceanogr* 25: 943–948.

Pruesse E, Quast C, Knittel K, Fuchs BM, Ludwig WG, Peplies J, Glöckner FO (2007) SILVA: a comprehensive online resource for quality checked and aligned ribosomal RNA sequence data compatible with ARB. *Nucleic Acid Res* 35: 7188–7196.

Ravenschlag K, Sahm K, Knoblauch C, Jørgensen BB, Amann R (2000) Community structure, cellular rRNA content, and activity of sulfate-reducing bacteria in marine arctic sediments. *Appl Enviro Microbiol* 66 (8): 3592 – 3602.

Raghoebarsing AA, Pol A, van de Pas-Schoonen KT, Smolders AJP, Ettwig KF, Rijpstra WIC, Schouten S, Damsté JSS, Op den Camp HJM, Jetten MSM, Strous M (2006) A microbial consortium couples anaerobic methane oxidation to denitrification. *Nature* 440: 918 – 921.

Redmond MC, Valentine DL (2012) Natural gas and temperature structured a microbial community response to the Deepwater Horizon oil spill. *Proc. Natl. Acad. Sci.* 109 (50): 20292-20297

Roesch LFW, Fulthorpe RR, Riva A, Casella G, Hadwin AKM, Kent AD, et al. (2007) Pyrosequencing enumerates and contrasts soil microbial diversity. *ISME J* 1:283–290.

Rossel PE, Elvert M, Ramette A, Boetius A, Hinrichs K-U (2011) Factors controlling the distribution of anaerobic methanotrophic communities in marine environments: Evidence from intact polar membrane lipids. *Geochimica et Cosmochimica Acta* 75 (1): 164 – 184.

Schouten S, Wakeham SG, Hopmans EC, Sinninghe Damsté JS (2003) Biogeochemical evidence that thermophilic Archaea mediate the anaerobic oxidation of methane. *Appl Enviro Microbiol* 69 (3): 1680 – 1686.

Seewald JS, Cruse AM, Lilley MD, Olson EJ (1998) Hot-Spring fluid chemistry at Guaymas Basin, Gulf of California: temporal variations and volatile content. *EOS* 79: 46.

Seyler LM, McGuinness LM, and Kerkhoff LJ (2014) Crenarchaeotal heterotrophy in salt marsh sediments. *ISME J*, advance online publication, doi: 10.1038/ismej.2014.15

Sievert SM, Ziebis W, Kuever J, Sahma K (2000) Relative abundance of *Archaea* and *Bacteria* along a thermal gradient of a shallow-water hydrothermal vent quantified by rRNA slot-blot hybridization. *Microbiology* 146 (6): 1287 – 1293.

Sievert SM, Scott KM, Klotz MG, Chain PSG, Hauser LJ, et al. (2008) Genome of the Epsilonproteobacterial chemolithoautotroph *Sulfurimonas denitrificans*. *Appl Environ Microbiol* 74 (4): 1145 – 1156.

Silliman BR, van de Koppel J, McCoy MW, Diller J, Kasozi GN, Earl K, Adams PN, Zimmerman AR (2012) Degradation and resilience in Louisiana salt marshes after the BP-*Deepwater Horizon* oil spill. *Proc. Natl. Acad. Sci.* 109 (28): 11234-11239

Slobodkin AI, Reysenbach A-L, Slobodkina GB, Kolganova TV, Kostrikina NA, Bonch-Osmolovskaya EA (2013) *Dissulfuribacter thermophilus* gen. nov., sp. nov., a thermophilic, autotrophic, sulfur-disproportionating, deeply branching delatproteobacterium from a deep-sea hydrothermal vent. *Int. J. Syst. Evol. Microbiol.* 63: 1967-1971

Stetter KO (1988) *Archaeoglobus fulgidus* gen. nov., sp. nov.: a new taxon of extremely thermophilic Archaebacteria. *System. Appl. Microbiol*. 10: 172–173.

Stewart FJ, Dalsgaard T, Young CR, Thamdrup B, Revsbech NP, et al. (2012) Experimental Incubations Elicit Profound Changes in Community Transcription in OMZ Bacterioplankton. *PLoS ONE* 7(5): e37118. doi:10.1371/journal.pone.0037118

Syutsubo K, Kishira H, Harayama S (2001) Development of specific oligonucleotide probes for the identification and in situ detection of hydrocarbon-degrading Alcanivorax strains. *Environ Microbiol* 3 (6): 371-379.

Takai K, Nakamura K, Toki T, Tsunogai U, Miyazaki M, Miyazaki J, Hirayama H, Nakagawa S, Nunoura T, Horikoshi K (2008) Cell proliferation at 122°C and isotopically heavy CH_4 production by a hyperthermophilic methanogen under high-pressure cultivation. *Proc Natl Acad Sci USA* 105: 10949 – 10954.

Takai K, Horikoshi K (1999) Genetic diversity of Archaea in deep-sea hydrothermal vent environments. *Genetics* 152: 1284 – 1297.

Teske A, Hinrichs KU, Edgcomb V, de Vera Gomez A, Kysela D, et al. (2002) Microbial diversity in hydrothermal sediments in the Guaymas Basin: Evidence for anaerobic methanotrophic communities. *Applied and Environmental Microbiology* 68: 1994 – 2007.

Teske A, Dhillon A, and Sogin M (2003) Genomic Markers of ancient anaerobic microbial pathways: sulfate reduction, methanogenesis, and methane oxidation. *The Biological Bulletin* 204: 186 – 191.

Teske A, Edgcomb V, Rivers AR, Thompson JR, de Vera Gomez A, et al. (2009) A molecular and physiological survey of a diverse collection of hydrothermal vent *Thermococcus* and *Pyrococcus* isolates. *Extremophiles* 13: 917 – 923.

Teske A, Sørensen KB (2008) Uncultured Archaea in deep marine subsurface sediments: have we caught them all? *The ISME Journal* 2: 3 – 18.

Tijhuis L, van Loosdrecht MCM, Heijnen JJ (1993) A thermodynamically based correlation for maintenance Gibbs energy requirements in aerobic and anaerobic chemotrophic growth. *Biotechnology and Bioengineering* 42: 509 – 519.

Vetriani C, Jannasch HW, MacGregor BJ, Stahl DA, Reysenbach AL (1999) Population structure and phylogenetic characterization of marine benthic archaea in deep-sea sediments. *Appl Environ Microbiol* 65: 4375 – 4384

Wade TL, Sweet ST, Sericano JL, Guinasso Jr. NL, Diercks A-R, Highsmith RC, et al. (2011) Analyses of water samples from the Deepwater Horizon Oil spill: Documentation of the Subsurface Plume. pp. 77 – 82. Monitoring and Modeling the Deepwater Horizon Oil Spill: A Record-Breaking Enterprise. Geophysical Monograph Series 195. American

Geophysical Union. 10.1029/2011GM001103.

Webster G, Parkes RJ, Fry JC, Weightman AJ (2004) Widespread occurrence of a novel division of bacteria identified by 16S rRNA gene sequences originally found in deep marine sediments. *Appl Environ Microbiol* 70: 5708 – 5713.

Weber A and Jørgensen BB (2002) Bacterial sulfate reduction in hydrothermal sediments of the Guaymas Basin, Gulf of California, Mexico. *Deep Sea Research Part I* 49 (5): 827 – 841.

Welhan JA, Lupton JE (1987) Light hydrocarbon gases in Guaymas Basin hydrothermal fluids; thermogenic versus abiogenic origin. *AAPB Bull* 71: 215 – 223.

Welhan JA (1988) Origins of Methane in Hydrothermal Systems. Chemical Geology 71: 183 – 198.

Wery N, Moricet JM, Cueff V, Jean J, Pignet P, Lesongeur F, Cambon-Bonavita MA, Barbier G (2001) *Caloranaerobacter azorensis* gen. nov., sp. nov., an anaerobic thermophilic bacterium isolated from a deep-sea hydrothermal vent. Int'l Journ System. Appl. Microbiol. 51 (5): 1789 – 1796 doi:10.1099/00207713-51-5-1789IJSEM

Whitman W, Bowen T, Boone D (2006) The methanogenic bacteria. *Prokaryotes* 3: 165 – 207.

Xiao Y, Roberts DJ, Zuo G, Badruzzaman M, Lehman GS (2010) Characterization of microbial populations in pilot-scale fluidized-bed reactors treating perchlorate- and nitrate-laden brine. Water Research 44: 4029-4036.

Yakimov MM, Timmis KN, Golyshin PN (2007) Obligate oil-degrading marine bacteria. *Current Opinion in Biotechnology* 18: 257-266.

Yanagawa K, Hiruta A, Sunamura M, Ishizaki O, Lever MA, Matsumoto R, Urabe T, Morono Y, Inagaki F (2014) Niche Separation of Methanotrophic Archaea (ANME-1 and -2) in Methane-Seep Sediments of the Eastern Japan Sea Offshore Joetsu. *Geomicrobiology Journal* DOI: 10.1080/01490451003709334

Yang T, Nigro LM, Gutierrez T, D'Ambrosio L, Joye SB, Highsmith R, Teske A (2014) Pulsed blooms and persistent oil-degrading bacterial populations in the water column during and after the Deepwater Horizon blowout. *Deep-Sea Research* Part II Topical Studies, in review

Zhuang DC, Chen YG, Zhang YQ, Tang SK, Wu XL, Tan ZC, et al. (2009) *Marinobacter* zhanjiangensis sp. nov., a marine bacterium isolated from sea water of a tidal flat of the South China Sea. *Antonie van Leeuwenhoek* 96 (3): 295-301.